CIRCULATING MICRORNAS TRIGGER INNATE IMMUNE ACTIVATION IN POLYRAUMATIC INJURY

by

Andrew O. Suen

Submitted in partial fulfilment of the requirements
for the degree of Master of Science

at

Dalhousie University
Halifax, Nova Scotia
August 2020

Dalhousie University is locaked in Mi'kma'ki, the
ancestral and unceded territory of the Mi'kmaq.
We are all Treaty people.

TABLE OF CONTENTS

LIST OF TABLES

LIST OF FIGURES

ABSTRACT

Inflammatory responses frequently follow severe traumatic injury and are, in part, a consequence of innate immune activation by endogenous immune triggers such as extracellular and micro- (mi)RNAs recognized by the pattern recognition receptor Toll-like receptor 7 (TLR7). However, uncontrolled stimulation of the immune response leads to inappropriate systemic inflammation that contributes to the development of multiple organ failure. In this study, we first developed a novel mouse model of polytraumatic injury and evaluated the circulating plasma RNAs and miRNAs found in circulation following trauma. We report that polytrauma causes significant elevations in plasma miRNA as well as distinct patterns of up- and down-regulation of host plasma small miRNAs. Next, we tested the pro-inflammatory function of miRNAs in bone marrow-derived macrophage culture and in a murine air pouch model of inflammation. We found that miRNAs with high uridine (U) contents >40% released into circulation are able to induce a robust TLR7-dependent inflammatory response. Together, these data reveal a pivotal role of circulating U-rich miRNAs as a key damage-associated molecular pattern (DAMP) in polytrauma.

LIST OF ABBREVIATIONS AND SYMBOLS USED

%A	Adenosine content (see %U)
%C	Cytidine content (see %U)
%G	Guanosine content (see %U)
%U	Uridine content (# Uridine nucleobase / miRNA length x 100%)
°C	Degrees Celsius
3'-UTR	Three prime (3'-) untranslated region
A	Adenine
A/P	Air pouch
ALT	Alanine aminotransferase
amol	Attomole
AST	Aspartate transaminase
AU	Absorbance unit
AUC	Area under the curve
BMDM	Bone marrow-derived macrophages
BPM	Beats per minute
BSA	Bovine serum albumin
C	Cytosine
C57BL/6J	C57BL/6 substrain from The Jackson Laboratory
CBC	Complete blood count
cc	Cubic centimeter
CFB	Complement factor B
CI	Confidence interval
cm	Centimeter
cmH_2O	Centimeter of water at 4°C
CO	Cardiac output
CO_2	Carbon dioxide
CpG	Phosphodiester-linked Cytosine-Guanine oligodeoxynucleotides
CT	Clotting time
C-term	Carboxyl-terminus
CV (%)	Coefficient of variation
DAMP	Damage-associated molecular pattern
DE	Differential expression
DEPC	Diethyl pyrocarbonate
DPBS	Dulbecco's phosphate-buffered saline
dsDNA	Double-stranded DNA
dsRNA	Double-stranded RNA
EC_{50}	Half maximal effective concentration
ECD	Ectodomain
ELISA	Enzyme-linked immunosorbent assay
Ex-miRNA	Extracellular microRNA
FACS	Fluorescence-activated cell sorting
FBS	Fetal bovine serum
FC	Fold change
FDR	False discovery rate
FN	False negative
FP	False positive
FPR	False positive rate
FS	Fractional shortening
G	Birmingham needle (wire) gauge
G	Guanosine
GAPDH	Glyceraldehyde 3-phosphate dehydrogenase
H&E	Hematoxylin & eosin
H_2O	Water
HPLC	High performance liquid chromatography
HR	Heart rate
HRP	Horseradish peroxidase
HRPO	Human research protections office
I/R	Ischemia-reperfusion
IACUC	Institutional animal care and use committee
IC_{50}	Half maximal inhibitory concentration
IL	Interleukin
IP	Intraperitoneal
IRAK	Interleukin-1 receptor-associated kinase
IRB	Institutional review board
kg	Kilogram
KIM-1	Kidney injury molecule-1
LAX	Long-axis
LPS	Lipopolysaccharide
LRR	Leucine-rich repeat
LV	Left ventricle
LVIDd / LVIDs	Left ventricular internal diameter at end diastole/systole
MCF	Maximum clot firmness
M-CSF	Macrophage colony stimulating factor
mg	Milligram
MHz	Megahertz
miRNA	microRNA
mL	Milliliter
mm	Millimeter
MO	Monocytes
MOD	Multiple organ dysfunction
MOF	Multiple organ failure
MP	Macrophages
MyD88	Myeloid differentiation primary response 88
NaCit	Sodium citrate

NBF	Neutral buffered formalin
NE	Neutrophils
NF-κB	Nuclear factor kappa-light chain-enhancer of activated B cells
NGAL	Neutrophil gelatinase-associated lipocalin
nM	Nanomolar
nt	Nucleotide
N-term	Amino-terminus
O_2	Oxygen
P/S	Penicillin/Streptomycin
PAGE	Polyacrylamide gel electrophoresis
Pam3Cys	Pam3Cys-Ser-(Lys)4
PAMP	Pathogen-associated molecular pattern
PBS	Phosphate-buffered saline
poly(I:C)	Polyinosinic-polycytodylic acid sodium salt
PRR	Pattern recognition receptor
PVDF	Polyvinylidene difluoride
qPCR	Quantitative real-time polymerase chain reaction
RE	Relative expression
RFC	Relative fold change
RISC	RNA-induced silencing complex
RNA	Ribonucleic acid
RNAseq	RNA sequencing
ROC	Receiver operating characteristic
ROTEM	Rotational thromboelastometry
RT-qPCR	Reverse transcription-qPCR
SAX	Short-axis
SBP	Systolic blood pressure
SD	Standard deviation
SDS-PAGE	Sodium dodecyl sulfate PAGE
SEM	Standard error of the mean
SMA	Superior mesenteric artery
ssDNA	Single-stranded DNA
ssRNA	Single-stranded RNA
SV	Stroke volume
SVR	Systemic vascular resistance
TBST	Tris-buffered saline with Tween 20
TBV	Total blood volume
TIR	Toll-IL-1 receptor
TLR	Toll-like receptor
TMM	Trimmed mean of M-value
TN	True negative
TNF	Tissue necrosis factor
TP	True positive
TPR	True positive rate
TRAF	TNF receptor associated factor
TRIF	TIR-domain containing adapter-inducing interferon-β
TTE	Transthoracic echocardiography
U	Unit(s)
U	Uridine
UTR	Untranslated region
YLL	Years of life lost
α	Alpha
µL	Microliter
µm	Micrometer or micron
µM	Micromolar

ACKNOWLEDGEMENTS

To Charlie MacAdams, Richard Hall, Wei Chao, Lin Zou, and Christian Lehmann: thank you for instilling a sense of curiosity and wonderment as well as the tools and knowledge for lifelong inquisitive pursuits.

To Sheng Wang, Brittney Williams, Briana Shimada, Kerri Lopez, Ping Cui, and all of the members of the Chao Lab: thank you for your mentorship, your friendship, and the unending efforts that underlie this work.

To Janice Chisholm, Jason Berman, Catriona Miller, Andrew Warren, Dalhousie University's Department of Anesthesia, and the University of Maryland: thank you for your wager in providing the means & opportunity for this academic venture.

CHAPTER 1. INTRODUCTION

Despite significant improvements in the care of seriously injured persons, major traumatic injury continues to be a leading cause of death in persons below 50 years of age in North America and Western Europe[1–3]. Immediate effects of trauma include the direct and indirect mechanical forces acting on tissues, which in turn induces local tissue damage, contusions, hemorrhage, fractures, and compromised host defense mechanisms from disrupted barrier defenses[4–6]. Additionally, immunological and inflammatory responses frequently follow severe traumatic injury and are, in part, a consequence of innate immune system activation by endogenous immune triggers[7–9]. While inflammatory processes are essential and integral to host defense and repair, uncontrolled stimulation of the immune response leads to inappropriate systemic inflammation that contributes to the development of multiple organ failure. We hypothesize that microRNA (miRNA), a normally intracellular nucleic acid species, are released into circulation following trauma injury and act as activators of a pro-inflammatory response. In the following pages, an investigation into the role of miRNA as a potent mediator of innate immune system function in the genesis of trauma-induced immune system dysfunction will be presented.

1.1 Broad Overview

Chapter 1 will substantiate the aims of the thesis work by describing the rationale of the experimental study (Section 1.2), provide a brief review of innate immune system activation via Toll-like receptors (TLRs) (Section 1.3), outline the mechanisms of nucleic

acid–e.g. miRNA–recognition by TLRs (Section 1.4), and summarize recent provocative studies highlighting the role of miRNAs in activating the innate immune system (Section 1.5).

Chapter 2 catalogues the methodologies used in generating and validating an experimental murine model of polytraumatic injury (Section 2.2); the techniques used to study RNA and miRNA biology (Section 2.3); and describes the *in vitro* (Section 2.4) and *in vivo* (Section 2.5) methods used throughout the study.

Chapter 3 presents the results of the experiments performed in the development of a murine model of polytraumatic injury (Section 3.1); the characterization of extracellular RNA and miRNA profiles detected in circulation following polytrauma (Section 3.2), and the discovery of specific uridine-rich miRNA motifs responsible for activation of inflammatory immune responses *in vitro* and *in vivo* (Section 3.3-3.4).

1.2 Traumatic Injury, Tissue Damage, and The Host Response

1.2.1 The Impact of Trauma on Health Outcomes

Trauma accounts for a significant burden of disease worldwide; according to the World Health Organization, in 2016 an estimated 477,000 deaths globally were due to homicide, while road traffic injuries accounted for as many as 1.35 million deaths and injured 50 million others[10]. For that year, these two injury modalities alone represented 38% of global deaths due to trauma.

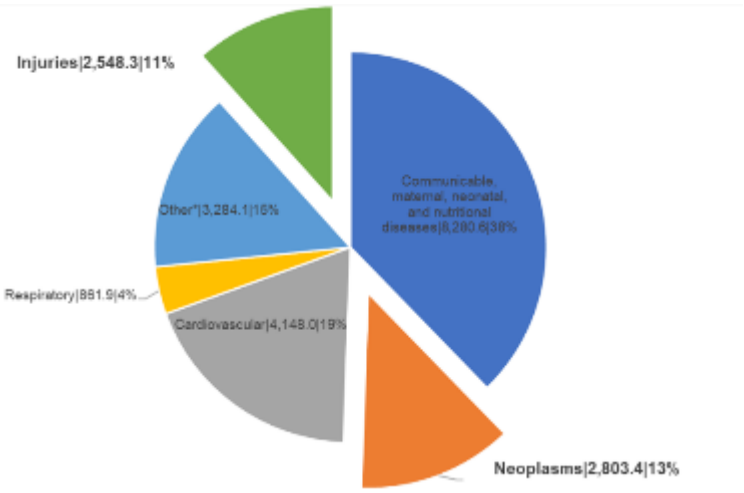

Figure 1. Global burden of disease in Years of Life Lost per 100,000.

Global causes of death by age-standardized Years of Life Lost (YLL) rate per 100,000 | (%). Adapted from the 2017 Global Burden of Disease Study cancer [14]. Detailed breakdown can be found in Table 1, below.

In addition, nonfatal traumatic injury often leads to permanent disability that contributes heavily to morbidity within populations. Damage to body or limb frequently results in direct costs of medical care required to resuscitate, repair, and rehabilitate injured individuals, as well as indirect costs from loss of productivity, burden to caregivers, and all of the medical encumbrances resulting from lasting disability[11].

The chronicity of disability resulting from injury is further compounded due to the fact that trauma disproportionally affects younger individuals: in the United States, trauma is the leading cause of death from ages 1-46[12] and thus contributes nearly 23% of causes of death in potential years of life lost before the age of 65[13]. Consequently, traumatic injury represents nearly the same burden of disease than that attributable to cancer[14] (Figure 1, Table 1; Injuries vs. Neoplasms age-standardized YLL rate: 2,548.3 vs 2,803.4 per 100,000).

More importantly, over the lengthy course of the military excursion in Afghanistan during Operation Enduring Freedom (OEF) between 2001-2014, over 158 Canadian and

2,218 U.S. service-men and -women have been killed, while another 22,162 have been wounded[15,16]. Interestingly, retrospective analyses of cohorts of wounded civilians and military combatants have demonstrated that the development of chronic medical conditions such as hypertension, diabetes mellitus, and coronary artery disease, is strongly correlated with the severity of injury suffered during combat[17,18]. Though causal origin of these chronic diseases directly resulting acute critical illness is not yet established, these chronic conditions are well known to be associated with prominent inflammatory processes, suggesting the hypothesis that combat injury–to wit, any injury–may predispose to chronic inflammatory conditions and diseases.

1.2.2 The Physiological Response to Trauma

The mechanism of injury and the specific involvement of body systems dictate the initial as well as final responses of the body; consequently, any cause of death after sustaining a lethal injury is either a direct consequence of an individual body system failing, a sequential cascading failure of interrelated body systems, multiple body systems failing in unison, or any combination thereof. While it may be desirable to attribute death to the failure of any one particular organ, one must recognize that no physiological body system operates in isolation. Therefore, any trauma will necessarily impact the function of multiple organ systems given their interdependency. Despite this, a few key physiological systems are often studied in isolation to better understand the body's responses, such as the cardiovascular and immune systems. Specifically, failure of either of these systems tautologically precipitates death, thereby highlighting the importance of these systems and their respective roles in being vitally important to an organism's wellbeing.

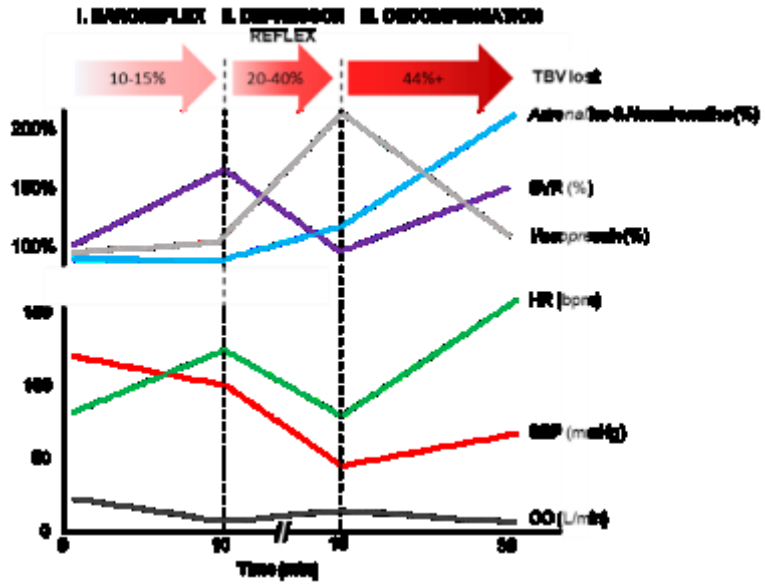

Figure 2. Cardiovascular response to haemorrhage.

Triphasic *neurohormonal* and physiological changes (systemic vascular resistance [SVR], heart rate [HR], systolic blood pressure [SBP], and cardiac output [CO]) in response to mild (10-15% TBV), modest (20-40% TBV), and severe (44%+TBV) haemorrhage induced by venesection in healthy volunteers and a porcine haemorrhage model. Adapted from Barcroft et al. (1944) & Jacobsen et al. (1980).

1.2.3 The Cardiovascular Response to Trauma

The impact of traumatic injury on the cardiovascular system arises principally from the effects of significant blood loss occurring due to major tissue damage leading to either a disruption in the continuity of the integumentary system and thus haemorrhage of blood from exposed blood vessels, or direct damage to central large diameter blood vessels within the circulatory system. Either circumstance results in massive haemorraghic blood loss that is immediately noticeable if it occurs externally; alternatively, haemorrhage happening within enclosed body cavities can be an inconspicuous process.

Studies of the effects of haemorrhage on the cardiovascular system—such as simple isolated haemorrhage wherein a reduction in the total blood volume (TBV) occurs rapidly—have shown a triphasic cardiovascular response[7,19]. In the first stages of a mild haemorrhage of 10-15% of TBV, the loss of blood volume produces a decrease in the

intravascular pressure that is detected by baroreceptors located in the aortic arch and carotid sinuses. Known as the "baroreflex mechanism", these baroreceptors react to a reduction in intravascular pressure by increasing efferent sympathetic tone and decreasing efferent parasympathetic tone, producing the net effect increasing the heart rate and vascular resistance such that blood pressure is maintained, thus maintaining organ perfusion[20,21] (Figure 2, *I. Baroreflex*).

With additional exsanguination and further reduction in blood volume exceeding approximately 20% of TBV, the initial baroreflex response is observed to be overridden by a second cardiovascular response phase, termed the "depressor reflex" [20,22]. In this second phase, though the heart rate drops, an accompanying drop in systemic vascular resistance ultimately leads to a mild increase in cardiac output, albeit with a reduction in perfusion pressure (Figure 2, *II. Depressor Reflex*).

Continuing blood loss beyond 44% TBV results in the third phase of the triphasic cardiovascular response to haemorrhage, characterized by tachycardia, hypotension, and an increased sympathetic activity[19] (Figure 2, *III. Decompensation*). In this last terminal phase of haemorrhage, neither the hormonal compensatory surge nor the baroreflex and depressor reflexes are able to accommodate sufficiently to maintain perfusion pressure to central organs, leading to the development of end-organ failure from hypoperfusion and hypoxia.

Alternatively, traumatic injury can result in tissue injury without haemorrhage. These injuries patterns are observed to produce a considerable sympathetic efferent stimulation classically known as the "fight or flight" response, which overlaps with and is similarly identified as the "pain response." In studies of tissue injury alone, the resultant

sympathetic stimulation is thought to prepare an organism for defense from an injury stimulus: observed are the predominant effects of tachycardia, an increase in cardiac output, and a relative vasodilation to skeletal muscles with a concurrent vasoconstriction of visceral organs.

In most traumatic injury patterns haemorrhage rarely occurs without corresponding tissue damage, and similarly tissue damage rarely occurs without some degree of haemorrhage. Interestingly, in studies of traumatic injury models combining both a component of haemorrhage and an element of tissue injury, the depressor reflex—i.e. a haemorrhage-induced bradycardia—is usually not observed. Some authors have attributed the absence of the second stage of haemorrhage as being due to the tachycardia-inducing tissue injury pathways superseding the bradycardia-inducing depressor reflex[22,23], while others have suggested that this stage is generally overlooked given its rapidity[19]. Ultimately, in most circumstances the fundamental aim of maintaining cardiac output and organ perfusion employs a combination of all the compensatory mechanisms laid out above, producing the net physiological response of a progressive tachycardia and hypotension[7,22].

1.2.4 The Immunological Response to Trauma

Alternatively, trauma-related mortality is frequently an indirect consequence of immune-related responses and dysfunction incited by an inappropriately strong pro- and anti-inflammatory response to injury[4,24]. It has been reported that between 7-17% of traumatically injured patients will develop multiple organ dysfunction and failure (MOD/MOF)[25–27] that may not directly attributable to the original injury but rather as a result of an overwhelming host defense response that occurs in the time after the traumatic insult[28]. While initiation of the complex cascade of the host defense response is

essential in activation of host defense mechanisms, the production of local and systemic inflammatory mediators beyond a homeostatic magnitude (hyper-inflammation) leads to the systemic inflammatory response syndrome (SIRS) which is known to precipitate multiple organ dysfunction and failure[2].

It is clear that an immunological response is a necessary response to traumatic injury. Indeed, induction of a robust local and systemic inflammatory response is needed to preserve an organism's integrity by protecting the body against additional insult and by stimulating reparative mechanisms. However, it is less clear to what magnitude an immunological is considered appropriate. While multiple clinical studies have confirmed the development of SIRS and the presence of raised inflammatory cytokine concentrations following traumatic injury, these studies also demonstrate that the degree of immune system activation as measured by the cytokine levels appears to be associated with a higher mortality rate and an increased incidence of MOD and MOF[29,30].

Furthermore, despite a tacit acknowledgement that traumatic injury precipitates activation of the immune system, the primary initiators of the post-traumatic hyper-inflammatory response are not fully known[24]. While some authors have proposed microbial-causative mechanisms, the observation that inflammatory responses also occur following "sterile" trauma indicates that activation of the immune system may result from the tissue damage itself. In these experimental models, the injury to and destruction of tissues following traumatic injury appears to induce an acute inflammatory response stemming from the release of endogenous molecules, termed "alarmins," that interact with immune cells thus activating an immune response. In essence, as cells are destroyed, molecules normally located intracellularly are expelled into the extracellular environs where they act as

ligands functioning as “danger” or “damage” signals sensed by any of the body’s immune cells. There is now an ever-growing body of evidence that following traumatic injury, several of these normally intracellular molecules—such as HMGB1, nucleosomes, histones, and DNA—are found in the non-native *extracellular* environment. Moreover, subsequent experiments have demonstrated that these molecules are functionally active in that they strongly stimulate immune responses, thereby garnishing them the label of “damage-associated molecular patterns” (DAMPs) or “alarmins” [8].

Table 1. Global causes of death in 2017.

2017	All-age deaths (thousands)	Age-standardised death rate (per 100 000)	All-age YLLs (thousands)	Age-standardised YLL rate (per 100 000)
All causes	**55,945.7**	**737.7**	**1,646,249.6**	**21,926.4**
Communicable, maternal, neonatal, and nutritional diseases	**10,389.9**	**143.8**	**578,416.6**	**8,280.6**
Non-communicable diseases	**41,071.1**	**536.1**	**872,601.8**	**11,097.4**
Neoplasms	9,556.2	121.2	225,738.1	2,803.4
Cardiovascular	17,790.9	233.1	330,172.6	4,148.0
Respiratory	3,914.2	51.4	68,004.9	861.9
Other*	9,809.8	130.4	248,686.2	3,284.1
Injuries	**4,484.7**	**57.9**	**195,231.1**	**2,548.3**

* Digestive, neurological, mental, substance use, diabetes and kidney, skin, MSK, other

YLL (Years of life lost) = $\sum_{Age=0}^{\infty} Deaths_{age} \times Life\ Expectancy_{age}$

Adapted from Roth et al. (2018), Global Burden of Disease Study 2017, Lancet[14].

1.3 Innate Immune Activation By Pattern Recognition Receptors

The innate immune system functions to detect and defend against threats to its host by triggering an immune response against pathogen- or damage-associated alarm signals. As the first line of defense against invading organisms presenting an immense diversity of potential host-pathogen interactions, germline-encoded innate immune cells such as dendritic cells, macrophages, and neutrophils express an evolutionarily conserved system of pattern recognition receptors (PRRs) whose primary purpose is to recognize conserved molecular structures[31,32]. Identification of pathogen- or damage-associated molecular patterns (PAMPs or DAMPs) located on invading pathogens or host-derived endogenous ligands, respectively[33–35], serves to rapidly induce host immune responses. Working towards the fundamental purpose of preserving host survival, these responses occur via various inflammatory pathways and culminate in the elimination of pathogens and the initiation of cellular repair mechanisms.

Several classes of PRRs have been identified in mammals that are classified according to their structural homology, including Toll-like receptors (TLRs), retinoic acid-inducible gene I [RIG-I]-like receptors (RLRs), nucleotide-binding oligomerization domain [NOD]-like receptors (NLRs), AIM2-like receptors (ALRs), C-type lectin receptors[36], and intracellular DNA sensors such as cyclic GMP-AMP Synthase (cGAS). Though each class of PRR serves to recognize distinct molecular patterns in various compartments of the cell, both the diversity and localization of PRRs provides an unprecedented ability for the innate immune system to appropriately shape an effective response that matches the

massive heterogeneity of DAMPs and PAMPs, all while discriminating between host, pathogen, and commensal organisms.

Of the various PRRs that have been identified, one of the most well-studied is the Toll-like receptor. Immunological discoveries around the Toll-like receptor owe their existence to the work of Eric Wieschaus and Christiane Nusslein-Volhard, whose discoveries in 1985 of the role of the Toll gene in *Drosophila* fruitfly embryogenesis provoked the observations of parallel function and mechanisms of the *Toll* gene within the interleukin-NF-κB cell signaling system, which were identified by various investigators examining the *Drosophila* Toll pathway[37,38]. Subsequently, in the early 1990s, these discoveries prompting several laboratory groups to investigate the function of Toll proteins in immune responses[39], eventually leading to the discovery of the human analogue Toll-like proteins[40] and the demonstration of their roles in host innate immunity vis-à-vis fungal[41], bacterial[42], and viral[43] infections. Since then, over ten human TLR proteins have been identified (Table 2), each responsible for recognition of unique pathogen- or damage-associated ligands[44]

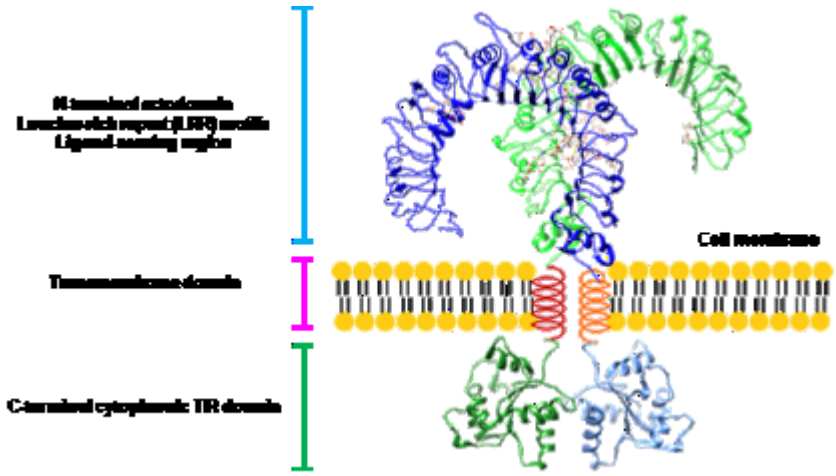

Figure 3. General macro structure of Toll-like receptors (TLRs).

TLRs consist of two protein hetero- or homodimer subunits each with an extracellular or endosomal N-terminal ectodomain responsible for ligand recognition, a transmembrane domain, and a cytoplasmic TIR domain to which adaptor proteins interact with following activation of a TLR unit. Schematic adapted from Gao et al. [129].

1.3.1 General Structural Features of Toll-like receptors (TLRs)

TLRs are membrane-associated glycoproteins localized to either the cell surface or an intracellular compartment such as the endosome, lysosome, or the ER[31,32,45,46]. Each TLR is defined by 3 components: the N-terminal ectodomain is characterized by the presence of multiple leucine-rich repeats (LRR) that serve principally for ligand recognition[47–49], a transmembrane domain, and a C-terminal cytoplasmic region composed of a Toll/interleukin-1 receptor (TIR) domain that mediates downstream intracellular signaling (Figure 3).

In the ectodomain (ECD) of a TLR subunit, tandem copies of LRR motifs are typically found, consisting of a 20-30 amino acid structural motif containing disproportionally more leucine residues. The ectodomain region of a TLR subunit is arranged in a beta strand-turn-alpha helix structure[45,49], which when fully assembled, commonly forms an

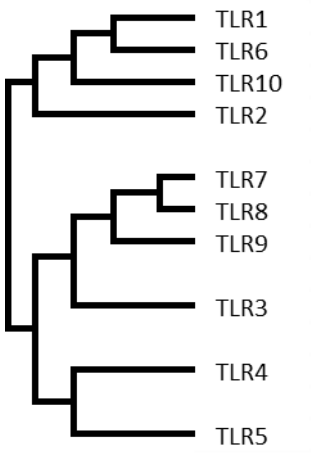

Figure 4. Phylogenetic tree of human Toll-like receptors.

Subfamilies of the ten human TLRs, depicted via the phylogenetic tree derived by amino acid sequence alignment using the neighbor-joining method.

α/β horseshoe-shaped fold[49,50] composed of a ligand-interacting site and the homo- or heterodimerization interface between two interacting dimer subunits[51–55].

TLRs otherwise characteristically contain a TIR (Toll/IL-1 Receptor) domain in the cytoplasmic region, which represents the intracellular docking region to which many adaptor proteins of the IL-1 receptor family are known to interact. These proteins, such as MyD88 (myeloid differentiation factor 88), MAL (MyD88 adaptor-like protein), TRIF (TIR-related adaptor protein inducing IFNβ), and TRAM (TRIF-related adaptor molecule), similarly possess a TIR domain thus allowing a TIR-TIR interaction between an adaptor protein and an activated TLR.

1.3.2 Toll-like Receptor Subfamilies

Among the ten human TLRs, five subfamilies have been described based on the sequence homology of the LRRs found in their N-terminal ectodomains[49,56] (Figure 4, Table 2). While the ectodomains (ECDs) of all TLRs generally take the form of a horseshoe-shaped fold, the specific arrangement and number of LRRs appear to influence the degree of curvature of the ECD solenoid structure as well as the distribution of amino acid

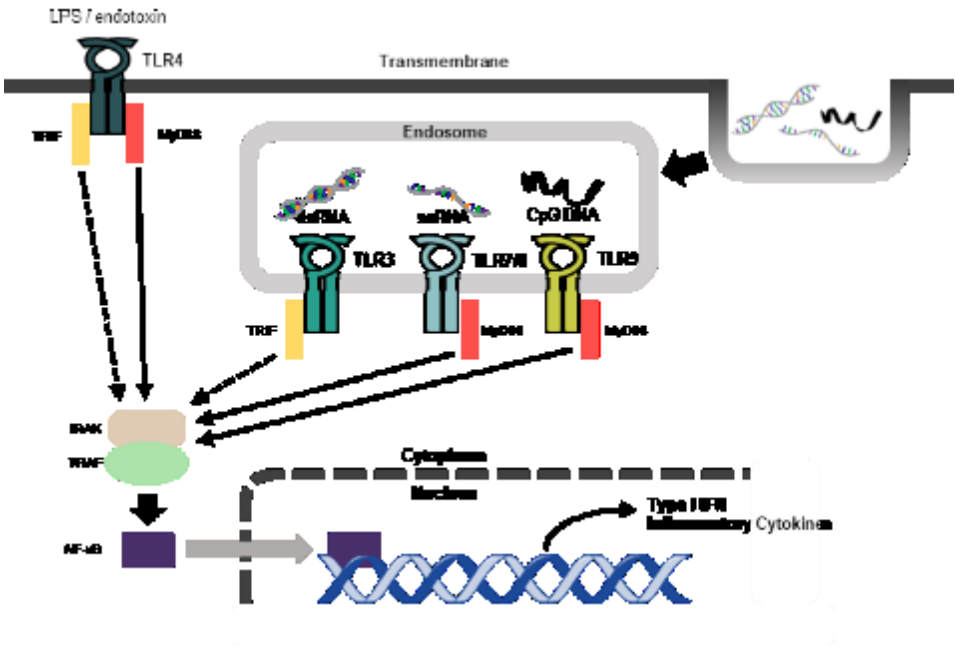

Figure 5. An overview of TLR signaling pathways.

Activation of membrane- or endosomal-bound TLRs by their respective canonical ligands activates TRIF- or MyD88-dependent inflammatory signaling pathways converging on nuclear translocation of transcription factor NF-κB and subsequent upregulation of inflammatory cytokine production.

residues within the ECD ligand binding surfaces of each TLR subunit[56]. Hence, while TLR subfamily are identified on the basis of consensus sequences of their ECD LRRs, it is the arrangement and number of these tandem motifs that generates unique arrangements in ECD structure that ultimately dictate ligand-binding surfaces and thereby govern ligand specificity of each subfamilytake[57]. As a result, the human TLR1/2/6/10, TLR3, TLR4, TLR5, and TLR7/8/9 subfamilies have been described, which serve to detect, respectively, lipid containing PAMPs, dsRNA, lipopolysaccharide, bacterial flagellin, and ssRNA/dsDNA.

1.3.3 Molecular Pathways of Innate Immune Stimulation by TLRs

Upon activation by their respective ligands, a pair of TLR monomers will dimerize and recruit adaptor proteins from the MyD88 family (e.g. MyD88, MAL, TRIF, and TRAM) to their cytosolic TIR domains. Subsequent downstream signaling (Figure 5) is achieved

upon the adaptor proteins' interactions with IRAK-4/1 (IL-1R-associated kinases -4 and -1) which in turn activates TRAF-6 (TNF receptor-associated factor-6).

With the exception of TLR3, all TLRs initiate downstream signaling pathways via the MyD88/IRAK/TRAF6 pathways. On the hand, TLR3 signaling occurs principally via a TRIF/IRAK/TRAF6-dependent signaling pathway, a feature which is also shared by TLR4. Ultimately, convergence of TLR signaling by either the MyD88- or TRIF-dependent pathways on the IRAK/TRAF complex results in the activation of several transcription factors—including NF-κB (nuclear factor-κB)—involved in regulating the transcription of genes involved in immunity and inflammation, thereby leading to the production of multiple inflammatory cytokines, chemokines and Type I interferons.

Table 2. Characteristics of Toll-like receptors and their ligands

Catalogue of ten known human Toll like receptors and their respective activating ligands, key signaling pathway mediators, and structural homology (No. of amino acid residues; LRR, leucine rich repeats); TLRs with an identical number of LRRs indicate similarities in structure, function, and developmental origin, therefore these are grouped into subfamilies.

TLR	Localization	Canonical ligand(s)	Adapter protein(s)	Subfamily	Residues (n=)	LRRs (n=)
1	Cell surface	Triacyl lipopeptides Peptidoglycans	MyD88	1 / 2 / 6 / 10	786	19
2	Cell surface	Triacyl lipopeptides	MyD88	1 / 2 / 6 / 10	784	19
3	Endosome	dsRNA poly-(I:C)	TRIF		904	23
4	Cell surface	LPS	MyD88 TRIF		839	21
5	Cell surface	Flagellin	MyD88		858	20
6	Cell surface	Diacyl lipopeptides	MyD88	1 / 2 / 6 / 10	796	19
7	Endosome	ssRNA Purine analog compounds	MyD88	7 / 8 / 9	1049	25
8	Endosome	ssRNA Purine analog compounds	MyD88	7 / 8 / 9	1041	25
9	Endosome	CpG-DNA motif dsDNA	MyD88	7 / 8 / 9	1032	25
10	Cell surface	Lipopeptides	Undefined	1 / 2 / 6 / 10	811	19

1.4 Mechanisms of Sensing of Nucleic Acids By TLRs

Although TLRs evolutionarily appear to serve as a warning system to detect infectious pathogens of various origins, there exists a peculiar difference in the localization of certain TLR subfamilies. Despite the inclination that positioning of a TLR to the cell surface allows for maximal exposure of a Toll-like receptor's ligand binding region, several TLRs—specifically TLR3 and TLR7/8/9—are found purely associated with endosomal structures rather than the cell membrane (Table 2, above).

Chief among several hypotheses that have been advanced to explain the differences in localization of these two specific subfamilies is a explanation that arises by scrutiny of the ligands known to activate the TLRs among these two subfamilies: nucleic acids[34,58,59]. These ligands include double-stranded (ds) RNAs, such as those produced by many reoviruses during their replicative cycle, are potent agonists of TLR3[43]; single-stranded (ss) RNA, originating from many viruses including the influenza viruses, act as TLR7 and TLR8 ligands[60]; and viral DNA and unmethylated CpG motifs of bacterial DNA[61] recognized by TLR9. Since endogenous nucleic acids are found ubiquitously in cells, an organism must be able to differentiate between self and not-self. Thus, it follows that TLRs within subfamilies that sense (i.e. are activated by) nucleic acids—namely, TLR3 & TLR7/8/9—are located in endosomal compartments such that spatial separation is achieved to prevent or reduce the probability of endogenous nucleic acids inappropriately activating otherwise membrane-mounted TLRs.

1.4.1 TLR7/8/9 and the Recognition of Extracellular Nucleic Acids

Although the overarching focus of this thesis work encompasses an investigation of the profound inflammatory responses observed following traumatic injury, the origins of this inquiry take cues from a parallel interest in the delineation of the mechanisms of TLR immune system activation by viral pathogens. Since the mid-1980s, patterns of TLR activation by nucleic acids have been a focus of many investigators examining the ability of immune cells to initiate antiviral responses by detecting viral (i.e. foreign) nucleic acids. Numerous groups have already demonstrated that TLR3, 7 & 8 constitute a class of virus-sensing receptors on the basis that nucleic acids originating from viral RNA transcripts are detected and recognized by these TLRs. While the localization of immunostimulatory nucleic acids within endosomal comparts is clearly crucial in the immune system's ability to distinguish between nucleic acids of "self" vs. "foreign" origin, additional experimental evidence has suggested that specificity is achieved based on characteristic structural features and sequences unique to foreign RNA transcripts: certain sequence motifs within RNA transcripts are seen to be more apt to stimulate a pro-inflammatory response than others. This unique observation suggests that TLRs may possess the ability to discriminate between self and foreign nucleic acids beyond merely relying on spatial separation of endogenous and exogenous nucleic acids by endosomal compartments. Rather, sequence specific features of ligands appear to represent another feature by which immunostimulatory TLR activation is controlled.

As investigators began elucidating immunostimulatory features of RNA in relation to activation of TLR7 and TLR8, the two single-stranded RNA (ssRNA) sensors, evidence mounted that supported the premise that immunostimulatory features of RNA ligands

depends on factors such as their nucleotide content (e.g. GU-content)[62], as well as the potential existence of immunostimulatory nucleic acid "motifs" within ssRNAs that preferentially function as strong pro-inflammatory ligands[62–65]. However, while many groups have described novel immunostimulatory motifs, unfortunately to this date no consensus sequence or motif has yet been determined, as it is likely that other ligand characteristics contribute to the nucleic acid sequence specificity of TLR sensing such as RNA tertiary structure, base position, or even the composition of flanking sequences.

1.5 The Role of Extracellular miRNA In Innate Immune Activation

Recently, several studies have demonstrated the release of various nucleic acids into circulation following tissue injury, such as during traumatic injury[66–68]. Of the various nucleic acids observed to be in circulation, one subtype has recently been of tremendous focus: microRNAs (miRNAs), a group of small noncoding single stranded RNAs approximately 20-24 nucleotides in length. While miRNAs were once considered to function primarily intracellularly in post-transcriptional gene regulation by binding to the 3'-UTR of target mRNAs, miRNAs have been found in a range of extracellular compartments including a wide range of bodily fluids, such as the circulating blood volume[69]. Unlike their parent RNA molecule, miRNAs are thought to be remarkably stable in bodily fluids such as plasma, serum, and urine[70–72]; a feature that many have espoused in endorsing the analysis of miRNAs as potential biomarkers in a variety of pathological conditions from oncological disease[73], polytraumatic injury[67], sepsis[74], and heart disease[75].

In addition to its potential role as a biomarker of disease, recent findings suggest that miRNAs also act on target tissues and cells in a paracrine or endocrine fashion[76]. Some provocative studies have reported that miRNA found in circulation in circulation are host RNAs released in pathological conditions, such as during sepsis[77] and myocardial ischemia-reperfusion[78] injury. For example, it was demonstrated using a murine model of sepsis that circulating (plasma) cell-free RNA is significantly higher in septic mice than in sham controls, which also correlated with the sepsis severity. More interestingly, various miRNAs were identified from the plasma of septic and IRI mice, which when isolated and seeded within immune cell culture were seen to have an remarkable capability to induce a robust pro-inflammatory response by functioning as DAMPs through a TLR7 dependent mechanism[79].

1.6 Hypothesis

While circulating miRNAs have been implicated in sepsis and cardiac injury in inducing inflammatory responses, the expression patterns of circulating ex-miRNA and their biological roles in trauma is unknown[8,68]. Thus, we hypothesize that traumatic injury induces an acute release of endogenous host miRNAs that are potent activators of damage-induced systemic inflammation.

1.7 Research Objectives

In this study, we use a mouse model of polytraumatic injury to identify the differential expression of miRNAs in circulation after trauma using RNA sequencing (RNAseq)

technology, then evaluate the role of these ex-miRNAs as DAMPs in immune cell culture and in an *in vivo* system of inflammation.

The focus of the work described herein is an investigation of the immunological sequelae after traumatic injury, and seeks to achieve the following two specific aims:

1. First, to investigate the effects of traumatic injury, we set out to create a murine model of polytraumatic injury that represents a common multisystem injury pattern encountered after exposure to blast- or explosion detonation waves. We thoroughly characterize essential parameters of injury severity, such as organ injury markers and physiological markers of organ dysfunction, and then further refine the model by optimizing injury severity to maximize the sensitivity and specificity of the immunological outcomes of interest in ensuing experiments.
2. Second, to examine the impact of traumatic injury on immunological activation and dysfunction, we explore the hypothesis that nucleic acids–specifically, miRNAs, a group of small noncoding RNAs–released from damaged and stressed cells into the extracellular milieu and function as key pro-inflammatory elements in the body's immune response to trauma. We will demonstrate the presence of circulating extracellular miRNAs in circulation following traumatic injury, explore its role in activating various components of the immune system, and finally describe several novel distinguishing characteristics of miRNAs that dictate how they interact with elements of the innate immune system: namely, Toll-like receptor 7.

CHAPTER 2. MATERIALS AND METHODS

2.1 ANIMALS & MOUSE STRAINS

8- to 12-week old sex and age matched wild type (WT) C57BL/6J, TLR3$^{-/-}$ and TLR7$^{-/-}$ mice were purchased from Jackson Laboratories (Bar Harbor, ME) for use in these studies. All animals were housed for at least 1 week before experiments in a conditioned, pathogen-free environment with free access to water and a bacteria free diet at the Animal Veterinary Facilities at the University of Maryland, Baltimore MD. Blinding and randomization was conducted using simple sequential numbering generated manually to determine group assignment for blocks of 5 mice (1 cage). Blinding was maintained throughout all procedures, data collection, and analysis. All animal care and procedures were reviewed and approved by the Institutional Animal Care and Use Committee of the University of Maryland School of Medicine and comply with the "Guide for the Care and Use of Laboratory Animals" published by the National Institutes of Health.

2.2 EXPERIMENTAL ANIMAL MODEL

A polytrauma model was created consisting of 35 min of superior mesenteric artery (SMA) occlusion, tibia fracture, and gastrocnemius muscle crush. Male mice were anaesthetized using isoflurane vapour anaesthetic (Fluriso, VetOne; 3-4% for induction, 1-3% for maintenance) in 100% O_2 at 100mL/min. After midline laparotomy, the SMA was exposed via a peri-hepatic approach and occluded at the aortic origin using a microvascular clip. Ischemia, lasting 35min, was confirmed visually by pallor in the distal bowel, hyperperistalsis, and the absence of distal pulsating flow (Figure 6). To

minimize evaporative losses during ischemia, the abdominal contents were replaced and the abdominal wall temporarily closed using Steri-Strips (3M). After ischemia, the SMA was partially re-exposed and reperfusion initiated by removal of the surgical clip and confirmed by the plethoric appearance of bowel indicating restoration of perfusion. At the onset of ischemia, a unilateral midshaft tibia & fibula fracture was induced by blunt force and the ipsilateral gastrocnemius muscle crushed by application of a Kelly forceps for 30min. Reduction and external fixation of the fracture was performed using tape splinting and a hollow foam boot cast (Figure 7). Sham animals underwent laparotomy and exposure of the SMA without vessel occlusion only. Fascial and skin layers were individually approximated and closed with running 5-0 silk suture (Ethicon) at the termination of the sham or polytrauma procedures, and bupivacaine hydrochloride (3.5mg/kg SC) was infiltrated widely at the incision. All animals were maintained at 37°C using homeothermic heating pad during all procedures and were given preemptive buprenorphine hydrochloride (Hospira) analgesia (0.1mg/kg SC) and fluid supplementation (0.9% saline 5mL/kg SC) prior to instrumentation.

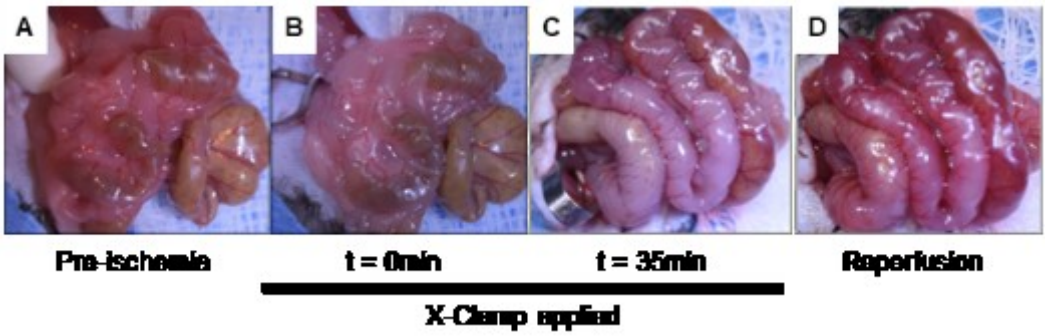

Figure 6. Gross appearance of bowel ischemia & reperfusion injury (IRI).

Bowel IRI is induced by application of a cross-clamp to the aortic origin of the superior mesenteric artery. Temporary occlusion of blood flow to the bowel is achieved (Panel B-C) with restoration of perfusion following removal of the clamp (Panel D). Panel A represents normal healthy bowel.

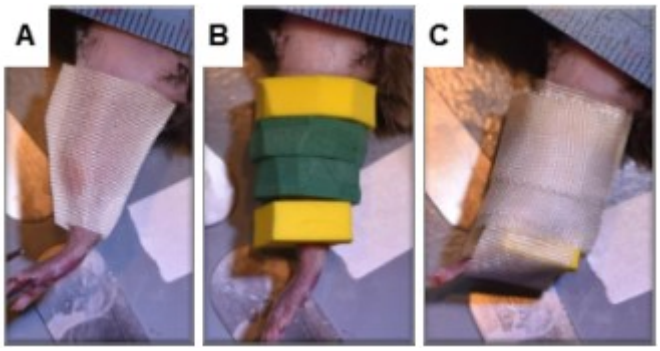

Figure 7. Method of long bone (tibia & fibula) fracture fixation.

External reduction & fixation of a tibia & fibula fracture is achieved using a tape splint to maintain the reduced fracture in anatomical alignment (Panel A) within a rigid foam boot cast (Panel B-C).

2.2.1 Animal Model Blood and Solid Tissue Sample Collection

Animals were euthanized at 6h, 24h, or 14d following polytrauma by cardiac puncture under isoflurane anesthesia (Fluriso, VetOne). Blood samples were collected in K2EDTA phlebotomy collection tubes (MiniCollect, Greiner Bio One) and immediately processed by two-step centrifugation at 1,000g then 10,000g for 10min at 4°C to obtain a cell-free plasma aliquot, which was stored at -80°C until batch analysis.

Tissues, thoracic, and abdominal organ samples were dissected sterilely and rinsed in cold phosphate buffered saline (PBS). Samples destined for analysis using tissue homogenates were immediately snap frozen in liquid nitrogen then stored at -80°C until analysis.

2.2.2 Tissue Histology

Organ specimens for histological analysis were collected at necropsy, rinsed in PBS, and immersed in 10% neutral buffered formalin (NBF) for 24-48h. Uniquely, lung samples were instilled with NBF at 25cmH_2O for 10 minutes via an intratracheal catheter to maintain alveolar recruitment. Small bowel segments were first flushed with PBS to remove all luminal contents prior to immersion in NBF. All specimens were subsequently embedded in paraffin and 4-µm sections were stained with standard hematoxylin & eosin staining, then viewed on an inverted microscope (Nikon Eclipse Ti-E, Nikon Instruments, Inc., NY, USA) using a 20x objective (CFI S Plan Fluor ELWD ADM, numerical aperture 0.45, Nikon Instruments) on a closed circuit digital color camera (DS-Ri2, Nikon Instruments) attached to the base of the inverted microscope. Whole slide imaging was captured were captured using a motorized stage (TI-S-E/R, Nikon) programmed to

obtain images of entire slides using post-processing image stitching completed on NIS-Elements AR v4.6 software (Nikon Instruments).

2.2.3 Measurement of Plasma Cytokines and Serum Markers of Organ Injury

Plasma samples were tested for IL-6 & TNF-α using enzyme-linked immunosorbent assay (ELISA) kits (R&D systems). Myoglobin concentration was detected by ELISA (Life Diagnostics). ALT and AST activity were determined by colorimetric enzyme activity assay kits (Sigma-Aldrich).

2.2.4 Mouse Transthoracic Echocardiography

Transthoracic echocardiography (TTE) was performed on lightly anesthetized mice (ketamine [Zetamine, VetOne], 20mg/kg IP;) at 6h and 24h following procedures. During image acquisition, mice were held supine by hand for passive temperature maintenance. Fur on the chest area of each mouse was removed using depilatory cream and ultrasound gel was applied between the transducer and the skin to maximize picture acquisition quality. Both B- and M-mode images were obtained with parasternal short- (SAX) and long-axis (LAX) views using a 13.0-MHz linear probe (Vivid 7; GE Medical Systems) imaging up to a depth of 10mm (Figure 8). Image analysis was performed offline using Vevo Lab PC software (FUJIFILM VisualSonics). End-diastolic and end-systolic left ventricular inner diameter (LVIDd and LVIDs, respectively) were measured from SAX images obtained at the level of the papillary muscles (Figure 9). Stroke volume (SV) was determined by calculating the change in left ventricular (LV) cavity area between systole and diastole based on LV tracings of SAX and LAX images using Simpson's biplane

method (Figure 9, Equation 1). Cardiac output (CO) and fractional shortening (FS) were calculated as HR x SV, and (LVIDd-LVIDs)/LVIDd x 100%, respectively.

$$Ventricular\ volume = \frac{\pi}{4}\sum_{i=1}^{n} a_i \times b_i \times \frac{L}{n}$$

Equation 1. Calculation of ventricular volume using Simpson's biplane method for the measurement of cardiac output, given by the sum of the volumes of 'n' disks. Each disk volume is calculated by multiplying its length 'L' by ventricular diameters 'a' and 'b' at perpendicular planes.

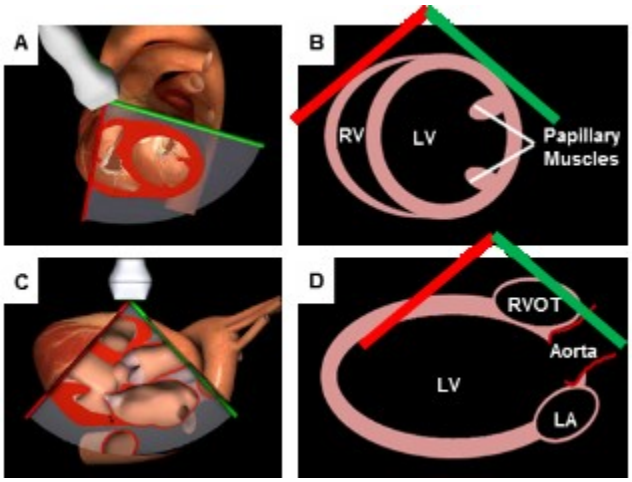

Figure 8. B-mode transthoracic echocardiography imaging.

Transthoracic echocardiography images are obtained using standard parasternal short axis (Panel A-B) and long axis views (Panel C-D). Anatomical cross-sectional areas and views are schematically represented above, demonstrating equivalent orientation and positioning of the major anatomical landmarks; LV: left ventricle, RV: right ventricle, RVOT: right ventricular outflow tract, LA: left atrium.

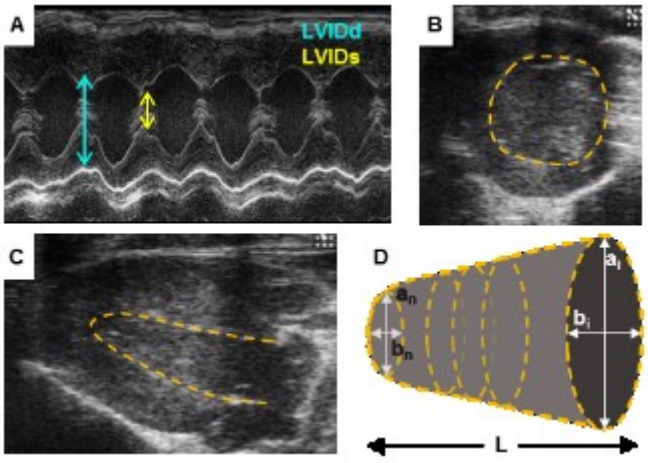

Figure 9. Determination of ventricular volumes by echocardiographic imaging.

LVIDd/s is calculated from both M-Mode images (Panel A) and 2D B-mode images (Panel B-C) of the ventricular cavity. LV tracings of B-mode images (yellow dotted lines) at LV tracings in short axis (Panel B) and long axis (Panel C) images allow calculation of LV cavity volume using a modified Simson's method (Equation 1).

2.2.5 Whole Blood Analysis & Thromboelastometry

Whole blood was collected via cardiac puncture into 0.109M (3.2%) sodium citrate (NaCit) mini phlebotomy tubes. Measurement of hemoglobin concentration, leukocyte counts, and platelet counts was conducted on an AcT diff hematology analyzer (Beckman Coulter, Inc., CA, USA).

The ROTEM Delta system (TEM International, Germany) was used to evaluate changes in viscoelastic properties using the nonactivated rotational thromboelastometric (NATEM) assay. In brief, 300uL of citrated whole blood was mixed with 20uL of 0.2M calcium chloride to reverse NaCit anticoagulation, then the clotting time (CT), maximum clot firmness (MCF), and alpha angle (α°) were determined from the thromboelastogram (Figure 10) generated by measuring the impedance to a rotational force from an oscillating pin suspended inside a small cup of whole blood[80]. These parameters, together, provide information on clot formation kinetics and strength: CT is defined as the time it takes for the thromboelastogram trace to reach an amplitude of 2mm, α is determined by the tangent of the line between the point of clot initiation (CT) and the slope of initial trace, and MCF represents the peak amplitude (strength) reached by the clot.

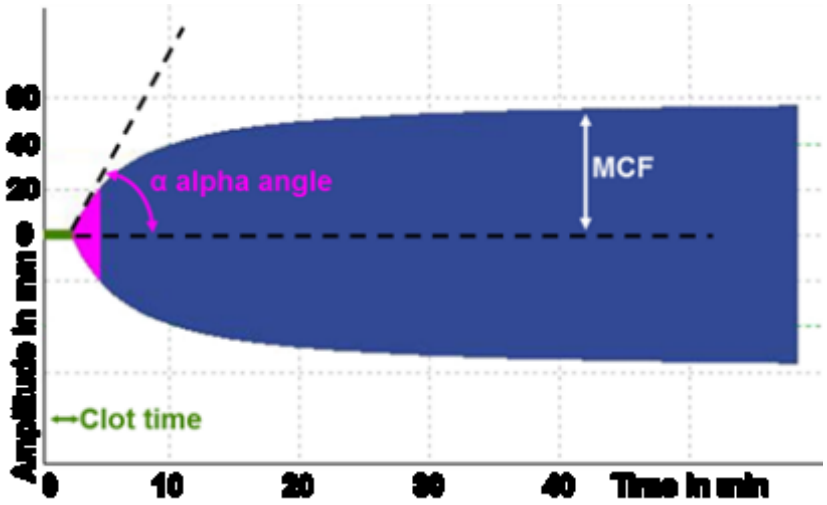

Figure 10. Rotational thromboelastometry (ROTEM) indices of coagulation..

Representative ROTEM thromboelastogram depicting clot initiation, propagation, stabilization, and lysis (not shown). As a clot forms, the viscoelastic strength of a clot increases, generating a resistance to rotational force applied by the oscillating pin within a cup of whole blood. MCF = maximum clot firmness. See text in section 2.2.5 for full description of parameters.

2.3 Isolation and Analysis of RNA and microRNA

2.3.1 Tissue and Cell RNA Extraction.

RNA was isolated from homogenized tissues or cells using TRIzol reagent (Sigma) with alcohol precipitation according to the manufacturer's protocol, then resuspended in diethylpyrocarbonate-treated water (DEPC) for analysis.

2.3.2 Plasma RNA Extraction.

TRIzol LS reagent (InvivoGen) was mixed with 50uL of plasma samples along with 9.9amol of *Caenorhabditis elegans* mir-39 (*cel*-mir-39) as a spike-in control, then processed according to the manufacturer's protocol. To maximize RNA recovery yield, 5µg of glycogen (Invitrogen) was added to samples during alcohol precipitation and chilled at -20°C for 18hours. The purified RNA pellet was then resuspended in DEPC H_2O for analysis.

2.3.3 Quantification of RNA

Total purified RNA concentration was measured in one of several ways. Concentrations of purified RNA in H_2O were initially determined on a Nanodrop One UV spectrophotometer (Thermo Scientific), which calculates nucleic acid concentration using the Beer-Lambert Equation, solved for concentration at a UV absorbance at 260nm (Equation 2):

$$c = A / (\varepsilon \times b)$$

Equation 2. Beer-Lambert equation, solved for concentration, where: c = analyte concentration in ng-cm/µL, A = UV absorbance in absorbance units (AU), ε = extinction coefficient in liter/mol-cm, b = pathlength of light in cm. For ssRNA, a nucleic acid correction factor of 37ng-cm/µL = $(\varepsilon \times b)^{-1}$is applied.

The absorbance peak represents the conjugated double bonds in purine and pyrimidine rings within nucleic acids; the extinction coefficient is the sum of the extinctions of each of their constituent molecules, where generally an average correction factor for ssRNA of 37ng-cm/μL is used[81,82].

Alternatively, a Quant-it RNA Assay Kit (Life Technologies) was used, based on a ribonucleotide-binding fluorescent dye that exhibits >1000-fold fluorescence enhancement upon binding to nucleic acids.

Finally, small RNA and miRNA concentrations–defined as the 0 to 150 nucleotide (nt) and 20 to 24 nt regions, respectively–were determined using a Bioanalyzer 2100 Small RNA Kit (Agilent Technologies), which separates RNA by capillary gel electrophoresis on a microfluidic chip, thereby denoting size based on elution time and deriving concentration based on a laser-induced fluorescent signal produced by a nucleic acid binding dye.

2.3.4 mRNA Gene Expression in Solid Tissues and Cells by Reverse Transcription-quantitative PCR (RT-qPCR)

Moloney Murine Leukemia Virus Reverse Transcriptase (M-MLV, Promega) was used to synthesize complementary DNA (cDNA) from purified template RNA samples. Subsequently, quantitative real-time polymerase chain reaction (qPCR) with GoTaq Master Mix (Promega) was carried out in a QuantStudio 5 PCR thermocycler (Applied Biosystems). Relative expression (RE) of mRNA was calculated using the comparative cycle threshold ($2^{-\Delta\Delta CT}$) method normalized to GAPDH expression. Sequences for the primers can be found in the supplemental materials.

2.3.5 miRNA Detection by RT-qPCR

RT-PCR using the miScript SYBR Green PCR kit (Qiagen) was performed on cDNA generated from purified RNA samples using the miScript II Reverse Transcriptase kit according to the manufacturer's instructions. RE was calculated using the $2^{-\Delta\Delta CT}$ method normalized to spike-in *cel*-miR-*39*. Primer sequences can be found in the supplemental materials.

2.3.6 RNAseq

Purified samples of RNA extracted from plasma were sequenced by Norgen Biotek (Thorold ON, Canada) on the Illumina NextSeq500 platform (Figure 11). In brief, small RNA libraries were prepared using the Norgen Biotek Small RNA Library Preparation Kit (Norgen), and the resultant cDNA was subjected to PCR amplification then purified and size selected by PAGE to enrich the miRNA fraction. The library was then analyzed on NextSeq500 (Illumina) sequencer with a total of 20M raw reads per sample.

2.3.7 miRNA Differential Expression Analysis

Bioinformatic analysis of RNAseq (Figure 12) performed using the exceRpt Small RNA-seq Pipeline (Genboree). First, adapter sequences and low-quality reads were removed from raw reads. The remaining high-quality reads were aligned to the following reference databases: mouse miRNA (miRbase.org v.21), mouse genome (C57BL/6J:mm9), tRNA (gtRNAdb), and piRNA (RNAdb). miRNAs with a minimum read count of 5 were used to perform statistical analysis and determine differentially expressed miRNAs in subsequent bioinformatics analysis. Using the edgeR package in the R programming environment, read counts were normalized using the trimmed mean of M-value (TMM)

method for differential expression (DE) analysis between sham and polytrauma groups with the Benjamini-Hochberg procedure for adjusting the false discovery rate (FDR). Statistically significant differentially expressed miRNAS is defined as a fold change (FC) $\geq$ or ≤ 2 of sham vs. trauma at *p*-value and FDR <0.05. Volcano plot analysis was constructed by plotting $-\log_{10}$(FDR) against $\log_2$FC to identify the most highly statistically significant differentially expressed miRNAs, while the most variably expressed (i.e. largest %CV of DE) 50 miRNAs were selected for hierarchical cluster analysis.

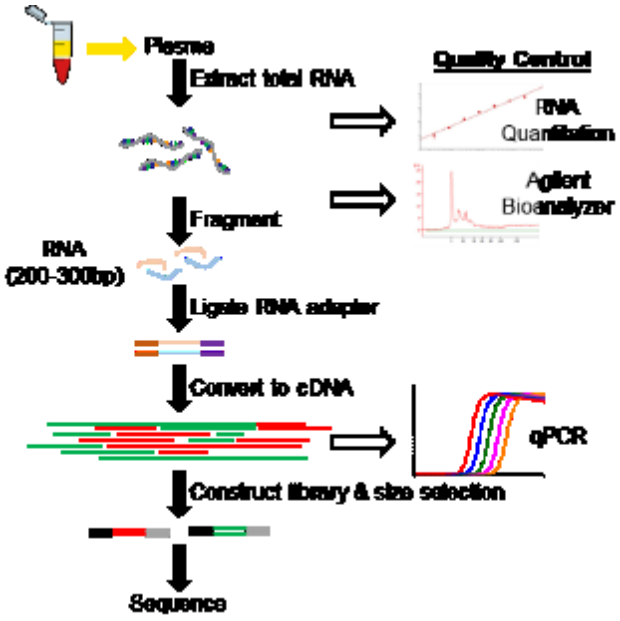

Figure 11. Overview of RNA sequencing workflow.

RNA is first isolated and extracted from plasma samples. Secondly, RNA is quantified and assessed for sample purity and quality. Third, RNA adapters are ligated to RNA fragments then converted to cDNA by reverse transcription to preserve strand orientation. Next, primers and/or barcodes are ligated to cDNA with subsequent PCR amplification and size selection to generate a full cDNA library that is ready for sequencing.

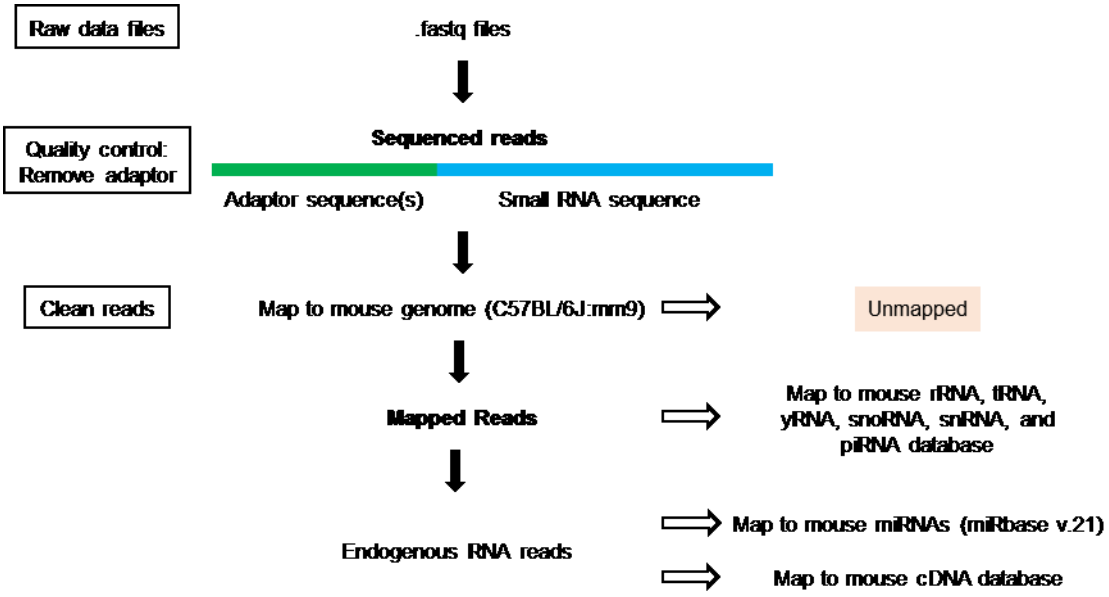

Figure 12. Overview of RNAseq analysis.

The conventional approach uses raw reads generated by the NGS Illumina sequencer platform in .fastq file format. Before mapping to reference genome(s), adaptor sequences introduced during cDNA library preparation and for multiplexing are identified to abstract sample information. Resulting small RNA sequence reads are then aligned and mapped to the mouse reference genome (C57BL/6J:mm9), then to the miRNA database (miRbase v.21). The mapped reads are then assembled into transcripts which can be quantified.

2.4 Cell Culture and Reagents

2.4.1 Bone Marrow-derived Macrophages (BMDMs)

Myeloid progenitor cells were isolated from bone marrow flushed from the femurs and tibias of 8- to 12-week old male or female mice and resuspended in RPMI-1640 growth medium (Gibco) supplemented with 10ng/mL macrophage colony-stimulating factor (M-CSF, R&D Systems), 10% fetal bovine serum (FBS), 5% horse serum, and penicillin & streptomycin (P/S; 100U/mL & 100µg/mL). Cells were seeded at a density of $2x10^6$ cells/mL on 6-well, 12-well, 24-well, or 96-well plates (5mL, 2mL, 0.5mL, or 0.1mL/well, respectively) in an incubator at 37°C with 5% CO_2. Growth medium was exchanged 48h after initial plating, and at 72h the BMDMs were approximately 70-80% confluent and ready for experiments.

2.4.2 Synthetic miRNAs

miRNA mimics were ordered from Integrated DNA Technologies (IDT) as synthetically synthesized single strand RNA (ssRNAs) with phosphorothioate internucleotidic linkages, purified by high-pressure liquid chromatography (HPLC) and supplied in lyophilized form. ssRNAs were resuspended in sterile DNase/RNase-free DEPC-treated H_2O and diluted to working concentrations. A complete list of the miRNAs used in this study and their sequences is included in Table 6 and Table 8.

2.4.3 Cell Transfection, Stimulation, and Cytokine Measurement

BMDMs were serum starved at 1h prior to cell treatment by replacing growth medium with RPMI-1640 + 0.05% BSA. Synthetic miRNA mimics (various, 0-5000nM) were

complexed with Lipofectamine 3000 transfection reagent (1.5µL/mL; Invitrogen) and incubated for 5 min at room temperature prior to addition of the RNA-lipid complex to cells. Lipofectamine (1.5µL/mL), poly(I:C) (10µg /mL; Enzo Life Sciences), R837 (1µg/mL; InvivoGen), or Pam3Cys (1µg/mL; Enzo Life Sciences) were added directly to wells. Culture medium was collected 18h after treatment for analysis by ELISA or Western blot.

2.4.4 SDS-PAGE and Western Immunoblot Analysis

Secreted proteins from equal volumes of cell culture medium were separated in a 4-20% gradient Tris-HCl SDS-PAGE, transferred to polyvinylidene difluoride (PVDF) membranes, and immunoblotted overnight at 4°C with goat anti-human CFB antibody (1:2,500 dilution, Complement Technology) in TBST (25mM Tris-HCl, pH 8.8, 190mM NaCl, 0.1% Tween 20) + 5% nonfat dry milk. The blot was subsequently probed 24h later with HRP-conjugated rabbit anti-goat IgG secondary antibody (1:10,000 dilution, Sigma-Aldrich) in TBST + 5% nonfat dry milk, then visualized using Luminata Forte Western HRP substrate (Millipore).

2.5 *IN VIVO* RNA ADMINISTRATION

2.5.1 Murine Air Pouch Model.

A dorsal subcutaneous air cavity was created in anesthetized mice based on previously published protocols[83–85] (Figure 13). In brief, under sterile conditions, 3cc of air was injected via a 30G needle and 0.22µm syringe filter into the subcutaneous space between the scapula on day 0 and 3. On day 6, inflammation was initiated by using 1mL of test solutions of either saline or lipofectamine-complexed synthetic miRNAs (0-20ug) were

injected into the air pouch. 24h later, the pouch was washed twice with 2.5mL of PBS to collect the pouch exudates. This lavage fluid was centrifuged at 1000*g* at 4°C, then the supernatant was collected and stored for ELISA analysis, while the cell pellet was resuspended in PBS. Cells were counted using a hemocytometer to determine the total number of pouch cells, then reserved for flow cytometry analysis

2.5.2 Flow Cytometry Analysis

To characterize leukocyte population and subpopulations, $5x10^5$ cells were incubated at 4°C for 30 min (light protected) with anti-mouse CD-45, Ly-6G, F4/80, and Ly-6C cell surface marker antibodies directed against murine leukocytes, neutrophils, monocytes, and macrophages. Flow cytometric analysis (20,000 events) was then performed on a LSR II flow cytometer (BD Biosciences). Data was abstracted using FlowJo (Tree Star, Inc.) according the depicted gating strategy (Figure 14).

Figure 13. *In vivo* dorsal subcutaneous air pouch (A/P) experimental workflow.

In A/P experiments, an air-filled space was created in the dorsal subcutaneous space by injecting 3cc of sterile filtered air on day 1 and 3. At day 6, the air pouch was ready for use and injected with test substances. On day 7, the exudates within the air pouch were collected for analysis by flow cytometry cell sorting. Figure adapted from Vandooren et al.[130]

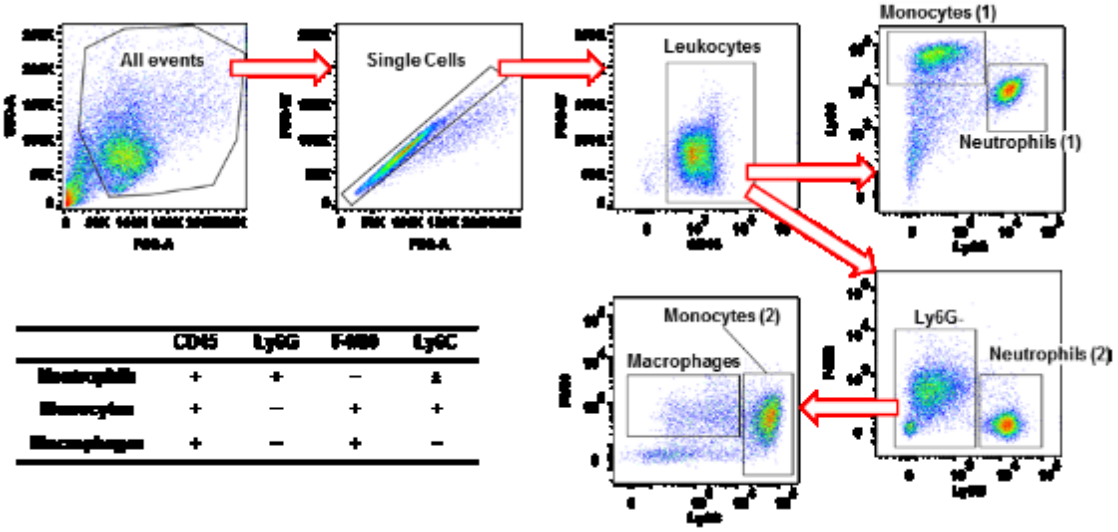

Figure 14. Flow cytometry immunostaining and gating analysis strategy.

Gating strategy used during flow cytometry analysis to identify leukocyte ($CD45^+$) populations. Subgating within the leukocyte population allowed for identification of neutrophil ($Ly6G^+$ / $F4/80^-$ or $Ly6G^+$ / $Ly6C^+$), and monocyte ($Ly6G^-$ / $Ly6C^+$) populations. Additional subgating of $Ly6G^-$ cells further characterized monocyte ($F4/80^+$ / $Ly6C^+$) and macrophage ($F4/80^+$ / $Ly6C^-$) populations.

2.6 Receiver Operating Characteristic Curve Analysis

To facilitate statistical analysis of the immunostimulatory properties of miRNAs, a binary classification system was predefined: miRNAs capable of inducing cytokine responses at 50nM concentrations in BMDMs were defined as “pro-” inflammatory, whereas miRNAs that did not induce cytokine responses at 50nM concentrations were defined as “non-” inflammatory. This classification schemata, thus, permitted evaluation of the ability of prediction models to correctly classify miRNAs according to their immunostimulatory properties.

Arrangement of the binary classification schemata into a 2x2 contingency table (Figure 15) results in four possible combinations: true positives (TP, correct positive prediction), true negatives (TN, correct negative prediction), false positives (FP, incorrect positive prediction), false negatives (FN, incorrect negative prediction). Hence, testing of successive classification queries, such as nucleobase content, is applied to empirical data obtained from miRNA-treated BMDM experiments.

To evaluate the performance of the binary classification system, sensitivity and specificity of nucleobase content (ranging from 1-100%) was calculated, from which true positive rates (TPR) and false positive rates were determined (Figure 15). Plotting of the TPR (y-axis) against FPR (x-axis) generates a receiver operating characteristic (ROC) curve, thus yielding a quantitative assessment of performance of various classification schemata based on the area under the curve (AUC) of the ROC.

		Observation: YES	Observation: NO
Test: YES		True Positive	False Positive
Test: NO		False Negative	True Negative

$$\text{True Positive Rate (TPR) / Sensitivity} = \frac{TP}{TP + FN}$$

$$\text{False Positive Rate (FPR)} = (1 - Specificity) = \frac{FP}{TN + FP}$$

$$\text{Specificity} = \frac{TN}{TN + FP}$$

$$\text{Matthew's correlation coefficient (MCC)} = \frac{(TP \times TN - FP \times FN)}{\sqrt{(TP + FN)(TP + FN)(TN + FP)(TN + FN)}}$$

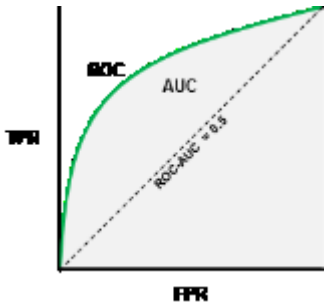

Figure 15. Definition of terms used in AUC and ROC curve analysis.

The Receiver Operating Characteristics (ROC) is a probability curve created by plotting the True Positive Rate (TPR, y-axis) against the False Positive Rate (FPR, x-axis). The Area Under the Curve (AUC) represents the degree of separability for a model to distinguish between two binary classifications. An AUC of 1.0 means that there is a 100% chance of distinguishing between a positive and negative class, while a model with an AUC of 0.5 has no discrimination capacity.

2.7 Statistical Analysis

Continuous variables were expressed as mean+SEM [95% confidence interval (CI)] for normally distributed data and median (25^{th}, 75^{th} percentile for non-normal distributions). Categorical data are described or presented as n (%). Results depicted are representative data obtained in two to three independent experiments using a minimum of animals per endpoint. Statistical comparisons between groups were performed by ANOVA, while Student's *t* test or Mann-Whitney *U*-test was used for paired continuous data. Analyses were performed using GraphPad Prism 6 (GraphPad, San Diego, CA). A p value <0.05 was considered statistically significant.

2.8 Study Approvals

Animal study protocols were reviewed and approved by the University of Maryland IACUC.

CHAPTER 3. RESULTS

3.1 Generation of a Murine Polytrauma Model

To assess the effect of polytraumatic injury on the release of miRNAs, we developed a novel model of polytraumatic injury. Notably, as traumatic injury is highly heterogeneous, to appropriately approximate key components of polytrauma and shock, four methodological considerations were necessary. First, the ideal model must simulate a multisystem traumatic insult pattern observed in encounters with high energy explosions–blast injury; it must reproducibly approximate a clinical and physiological scenario–shock; and cause a post-injury inflammatory state–i.e. induce innate immune system activation. Finally, it was necessary to balance the goal of inducing a robust post-injury state with goal of producing a sublethal polytrauma, as a combination of injuries may aggravate the severity of each individual insult and increase lethality.

To wit, we combined three distinct iatrogenic injuries–muscle crush, tibia fracture, and bowel ischemia-reperfusion–which represent blast injury patterns observed following exposure to explosive devices[86]. These are: soft tissue injury suffered from direct exposure to high energy forces, bone fracture from mechanical forces exerted by a blast wave or subsequent tertiary displacement, and hollow viscus injury (bowel) from mesenteric vessel disruption caused by a blast wave transmitted intraabdominally.

Optimizing the severity of the polytrauma model was initially necessary so that both antithetical goals of a hyperinflammatory response and sub-lethality were achieved. The strategy used to determine the optimal severity in polytrauma model was to adjust the

bowel ischemia time prior to reperfusion, since it is known that increasing ischemia times worsens bowel epithelial loss and enhances the likelihood that all bowel segments will be affected[87].

Preliminary studies demonstrated successful interruption of mesenteric blood flow to the duodenum, jejunum, and ileum, achieved by occlusion of the superior mesenteric artery by placement of a vascular clip (Methods, Figure 6). Next, prolonging ischemia time from 30min to 35min resulted in increases in inflammatory response at 6h and 24h, as measured by IL-6 production (Figure 16A); and a higher degree of I/R-induced systemic shock, manifested as exacerbated decreases in core body temperature at 2h and 6h post-reperfusion (Figure 16B). The effect of increasing ischemia time was also apparent in the gross morphology of bowel immediately at reperfusion: following 35min ischemia, the affected ischemic bowel segments were significantly more plethoric, swollen and edematous as compared to either 30min-I/R or the mice that received a laparotomy only (Figure 16C).

Subsequently, the additional injury elements of tibia fracture and muscle crush were added to the experimental model to complete the polytrauma injury pattern. Quantification of the lethality of the resultant animal model using Kaplan-Meier analysis demonstrated that overall survival of this polytrauma model was approximately 80% at 28d (Figure 17). Notably, the only deaths observed were within the first 48h following polytrauma, which appears to reflect the acute nature of traumatic injury. Furthermore, there was no intraoperative mortality, and no sham animals perished in any of our studies. These data demonstrate that the polytrauma model was generally sublethal and provided a suitable platform to investigate the effects of polytrauma on innate immune activation.

3.1.1 Polytrauma Induces a Massive Inflammatory Response

The innate immune response to traumatic injury was subsequently examined by quantifying the production of inflammatory cytokines IL-6 and TNF-α. As shown in Figure 18, polytrauma resulted in significant elevations in systemic IL-6 (Sham vs Trauma, 6h: 84±17 vs 24184±5790 pg/mL, $p<0.0001$; 24h: 47±15 vs 1945±765pg/mL, $p<0.001$) and TNF-α (6h: 1.7±0.6 vs 9.7±5.0 pg/mL, $p<0.05$; 24h: 2.7±0.4 vs 15.5 ±7.0pg/mL, $p<0.01$).

Changes in local tissue inflammatory markers was also evaluated by measurement of *IL-1B*, *IL-6*, and *TNF-α* gene expression in muscle tissue of the hind leg subjected to muscle crush injury and tibia fracture, revealing an upregulation of these cytokine genes (Figure 19A) known to function heavily in pro-inflammatory signaling pathways.

3.1.2 Polytrauma Results in Direct Tissue & Organ Injury

In addition to local upregulation of inflammatory gene pathways, soft tissue injury to the muscle subjected to crush injury was evaluated histologically. Significant muscle injury and necrosis was observed in mice subjected to polytrauma, as evidenced by the loss of organized muscle fascicle architecture, severe intracellular vacuolization, and global disruptions in muscle fibre cell membrane (Figure 19B). To further illustrate the development of traumatic rhabdomyolysis directly caused by the crush injury and its immediate sequelae, we observed that myoglobin, a typically intracellular protein, was considerably elevated in the plasma of polytrauma mice (Figure 19C).

As previously established, gross morphological differences in bowel appearance are perceptible upon reperfusion of small bowel after a period of ischemia (Figure 16C).

Upon necropsy 6h after reperfusion, these differences were steadily amplified: compared with sham, polytrauma mice developed massively dilated, distended, and edematous bowel loops (Figure 20A). Microscopic evaluation of bowel segments confirmed exhaustive intestinal ischemia reperfusion injury. This was based on the presence or absence of varying degrees of mucosal damage, such as inflammatory cell infiltrates, the development of the subepithelial Gruenhagen's space, separation of the epithelium and the luminal basal layers (lamina propria), villous blunting, and disintegration of epithelial layers beyond the muscle layers[88].

Representative images of the duodenum, jejunum, and ileum, polytrauma mice display some degree of mucosal injury in all three at-risk zones, ranging from inflammatory cell infiltration and villous blunting in the duodenum and jejunum (Figure 20B, panel iv-v), to segmental disintegration and denudation of the villi down to the submucosal level in the jejunum (Figure 20B, panel vi). In contrast, the sham operated mice have no observable mucosal damage (Figure 20B, panel i-iii). These data align well with the gross morphological differences in the appearance of the bowel (Figure 20A), and confirm that the polytrauma injury–specifically, bowel I/R–induce significant local tissue injury.

3.1.3 Polytrauma Produces Remote End Organ Injury & Dysfunction

Although morbidity from trauma is largely due to the initial injurious insult, patients may develop multiorgan dysfunction sometime after the initial injury[28,89]. For example, a peripheral crush injury may primarily affect the integumentary system, yet the resultant rhabdomyolysis may lead to the synchronous multisystem dysfunction in both the kidney and heart due to, respectively, myoglobinuria-induced AKI and hyperkalemia[90–92]. Hence, to establish the association of organ injury in our experimental polytrauma model,

we assessed the development of organ injury in the kidney, liver, lung, heart, and coagulation systems.

We observed that polytrauma induced significant elevations in the kidney injury markers *KIM-1* and *NGAL* genes at the 6h and 24h timepoints (Figure 21A; Trauma, 24h, RFC: 12.4±5.6, $p<0.01$ and 43.5±14.0 $p<0.0001$, respectively), with mild persistent elevation in *NGAL* at 14d. Consequently, kidney injury resulted in an impairment of kidney function as demonstrated by an increase in plasma creatinine levels (Figure 21A), which indicates a reduced glomerular filtration rate and hence impairment of renal creatinine clearance. These findings were also supported by histological findings of acute tubular necrosis and the presence of renal tubular casts at 24h (Figure 21B), that was mainly resolved by 14d.

The liver exhibited evidence of acute liver injury following polytrauma, with mild elevations in plasma aspartate (AST) and alanine (ALT) aminotransferases (Figure 22A). Elevations in plasma activity of these two markers suggest the presence of hepatocellular injury[93]. However, it must be noted that AST is also found in muscle cells thus the muscle crush injury may reduce the specificity of the marker alone[93,94]. Additional evidence of mild hepatic injury following polytrauma was observed on histological examination which demonstrated bile duct proliferation (Figure 22B, green arrows), a nonspecific but sensitive marker of liver injury[95,96]. Interestingly, despite the findings of bile duct proliferation, elevations in direct (conjugated) bilirubin were largely unremarkable, suggesting an absence of a significant cholestatic process. However, there were modest increases in total and indirect (unconjugated) bilirubin (Figure 22C). Given the concurrent traumatic rhabdomyolysis, these increases likely originate from the

unconjugated bilirubin derived from heme proteins produced from the metabolism of myoglobin.

To assess trauma-related changes in the lungs, whole intact lung samples were prepared and examined under microscope for evidence of inflammatory changes and alveolar damage. Uniquely, an intratracheal catheter was placed prior to dissection of specimens through which NBF was instilled at a steady pressure of 25cmH_2O. This resulted in an inflation of the lungs to fill the chest cavity and was performed to standardize and maintain alveolar recruitment (inflation) during sample collection and preparation, as atelectatic lungs grossly overestimate significant findings in the interstitium[97]. Histological examination of lung samples from polytrauma mice at 24h revealed no obvious pulmonary changes as compared to sham mice (Figure 23A). Moreover, there was no evidence of alveolar inflammation such as hemorrhage, leukocyte infiltration, or wall thickening (Figure 23B), which are histological features of diffuse alveolar damage associated with lung injury[98].

Trauma is also associated with significant cardiac dysfunction, through direct and indirect mechanisms. Though our experimental model did not directly induce a state of shock via hemorrhagic means (such as the withdrawal of blood volume), it has been previously established that innate immune activation plays a crucial role in cardiac dysfunction[17,78,99]. Hence, we set out to assess the impact of polytrauma using *in vivo* direct observation of the heart via transthoracic echocardiography. As previously described (Section 2.2.4), 2-dimensional images were captured from sham and polytrauma mice, revealing that polytrauma causes a significant decrease in LVIDd, LVIDs at 6h (Figure 24AB). In keeping with the reduced dimensional volumes and lower

heart rate, we observed decreases in stroke volume and cardiac output parameters derived from dimensional measurements, illustrating that the polytrauma mice show markedly decreased cardiac function at 6h (Figure 24B). Strangely, despite a strikingly decreased SV (Sham v. Trauma, 6h: 31.7 vs 12.7uL) there were no compensatory increases in HR nor EF as would be expected in hypovolemic or shock states, implying poor compensation of cardiac dysfunction (Table 3, Figure 24B). Interestingly, at 24h there was partial and near complete recovery of HR and SV, respectively, resulting in a normalization of cardiac output. These data suggest that trauma is strongly associated with early cardiac dysfunction that ameliorates by 24h.

Finally, to study trauma-associated non-hemorrhagic coagulopathy, viscoelastic testing was completed using rotational thromboelastometry (ROTEM) at 6h. Assessment of CT, α° , and MCF revealed no statistically significant differences in polytrauma mice (Figure 25A). However, close examination of representative thromboelastograms from polytrauma mice suggests that trauma may indeed induce a spectrum of hyper- or hypo-coagulable states as compared with sham mice (Figure 26). Additionally, polytrauma appears equally associated with thrombocytopenia as well as a mild thrombocytosis (Figure 25B). Together, these findings imply that neither ROTEM parameters nor platelet count, two commonly used indices of coagulation function, are reliably associated with polytraumatic injury. Our observations nevertheless reflect the variability in the development of trauma-associated coagulopathy and suggest that the polytrauma model–while able to induce coagulopathic states–may not be a suitable platform for hypothesis testing of the coagulation system.

3.1.4 Summary of Section 3.1

In summary, the highly variable nature of trauma poses unique challenges in studying its pathologies. In spite of this, we have chosen to generate a novel polytrauma experimental model that simulates a blast injury by choosing elements of bowel I/R, tibia fracture, and muscle crush injuries. This experimental model reproducibly simulates the pathophysiological processes of a polytrauma, precipitates a robust inflammatory response, and approximates the clinically relevant development of multiorgan injury and dysfunction in the integumentary, gastrointestinal, renal, hepatic, cardiac, and coagulation systems. The findings validate the use of this methodology in investigating the role and function of miRNAs in innate immune activation following polytrauma.

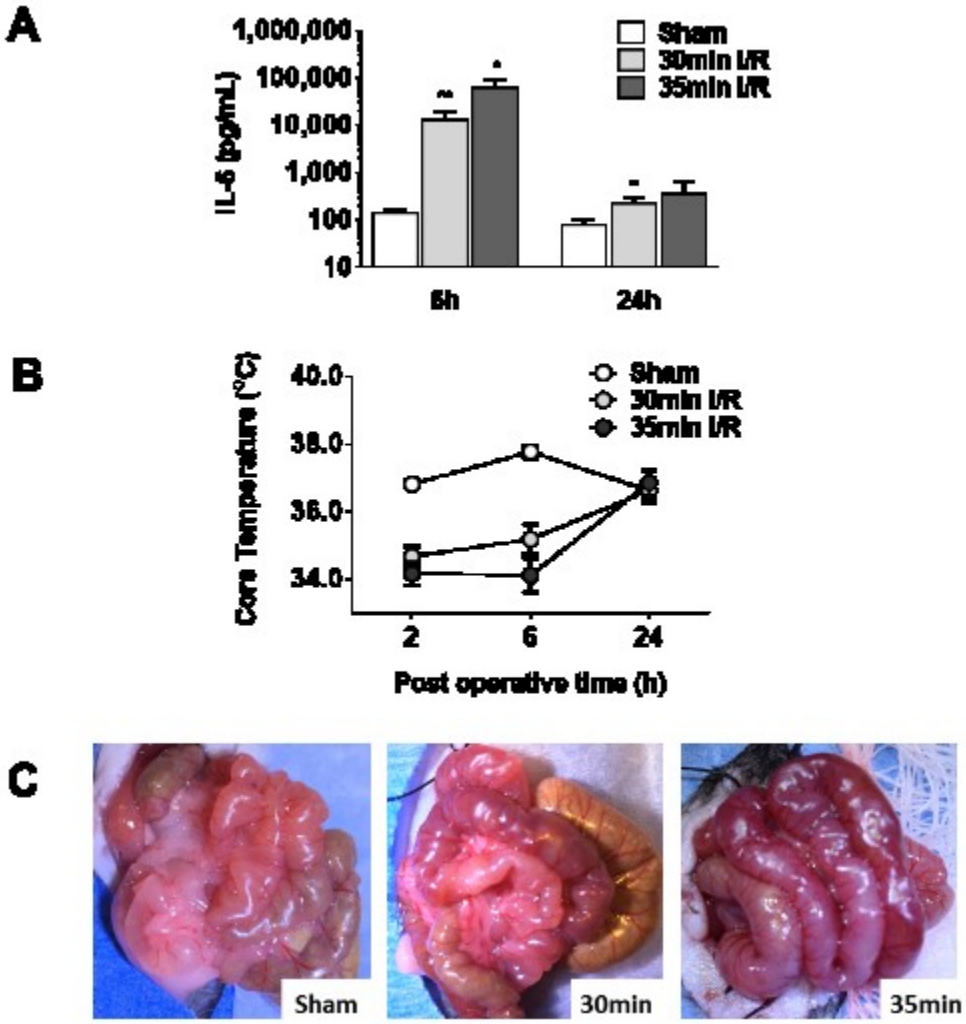

Figure 16. Optimization of bowel ischemia reperfusion injury.

Increasing ischemia time from 30min to 35min (A) exacerbates inflammatory responses at 6h and 24h and (B) worsens ischemia-reperfusion injury-induced systemic shock as manifested through core body temperature. (C) Gross morphological comparison of the appearance of normal healthy bowel (Sham) demonstrates that incremental increases of ischemia time leads to exacerbated bowel edema and dilation suggesting injury, compared with deflated and contracted appearance of sham bowel suggestive of healthy and functional peristaltic processes.

*P<0.05, **P<0.01, Student's t test or nonparametric analysis Mann-Whitney test

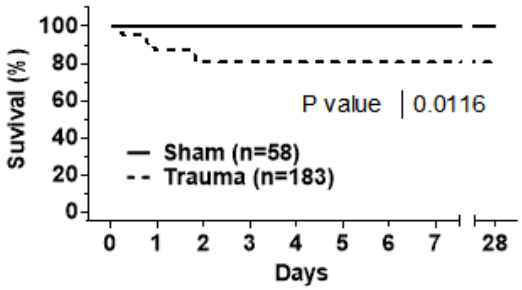

Figure 17. Kaplan-Meir survival curve analysis.

Polytrauma in this mouse model is generally nonlethal. Mice that were used for experiments (e.g. euthanized at 6h or 24h) were included in the analysis as censored data. Survival proportions were compared using a log-rank (Mantel-Cox) test. Mean follow-up duration: days, sham vs. trauma: 5.82 vs 3.4).

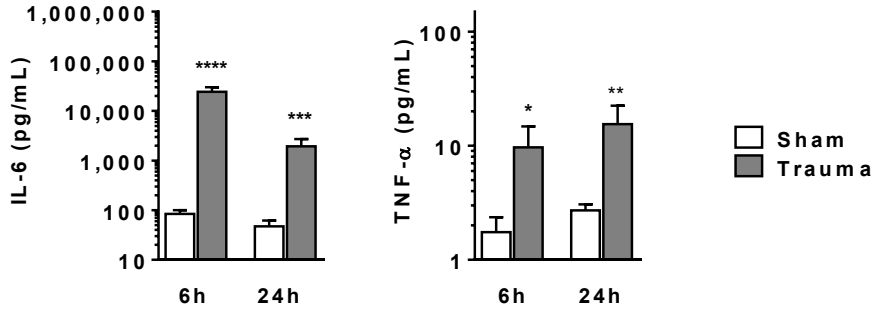

Figure 18. Polytrauma in mice produces significant inflammatory responses.

Elevations of pro-inflammatory cytokines IL-6 and TNF-α measured in plasma is observed at 6h and 24h after Trauma, as measured by ELISA.

*P<0.05, **P<0.01, ***P<0.001, ****P<0.0001, Student's t test or nonparametric analysis Mann-Whitney test

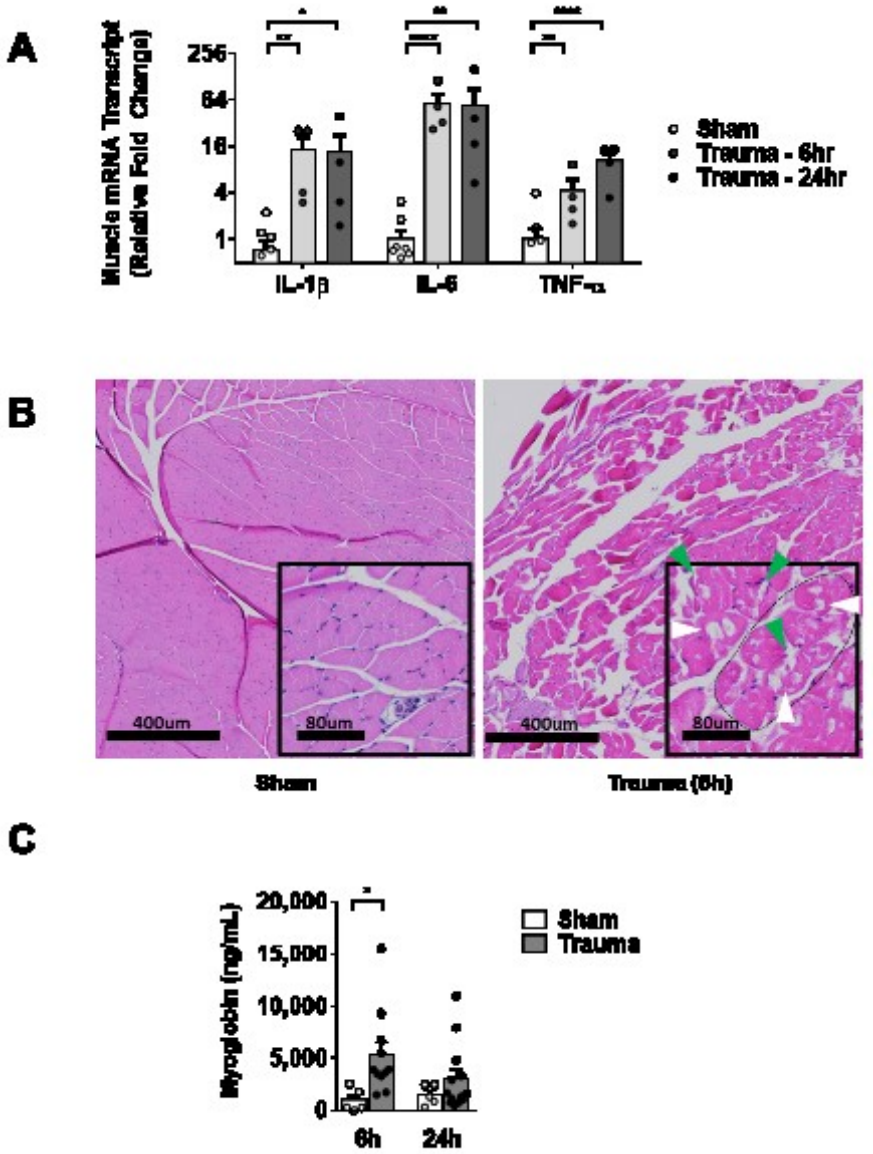

Figure 19. Gastrocnemius muscle crush causes local and systemic injury.

(A) Muscle crush injury induces a significant local inflammatory response; data are normalized to control GAPDH expression and compared with sham. (B) Haemotoxylin & Eosin staining demonstrates loss of organized muscle fascicle architecture (dotted line), severe intracellular vacuolization (black arrows), and global disruptions in muscle fibre cell membrane (green arrows). (C) Plasma myoglobin levels increase following trauma as a consequence of traumatic rhabdomyolysis and is largely cleared at 24h

*P<0.05, **P<0.01, ***P<0.001, ****P<0.0001, Student's t test or nonparametric analysis Mann-Whitney test

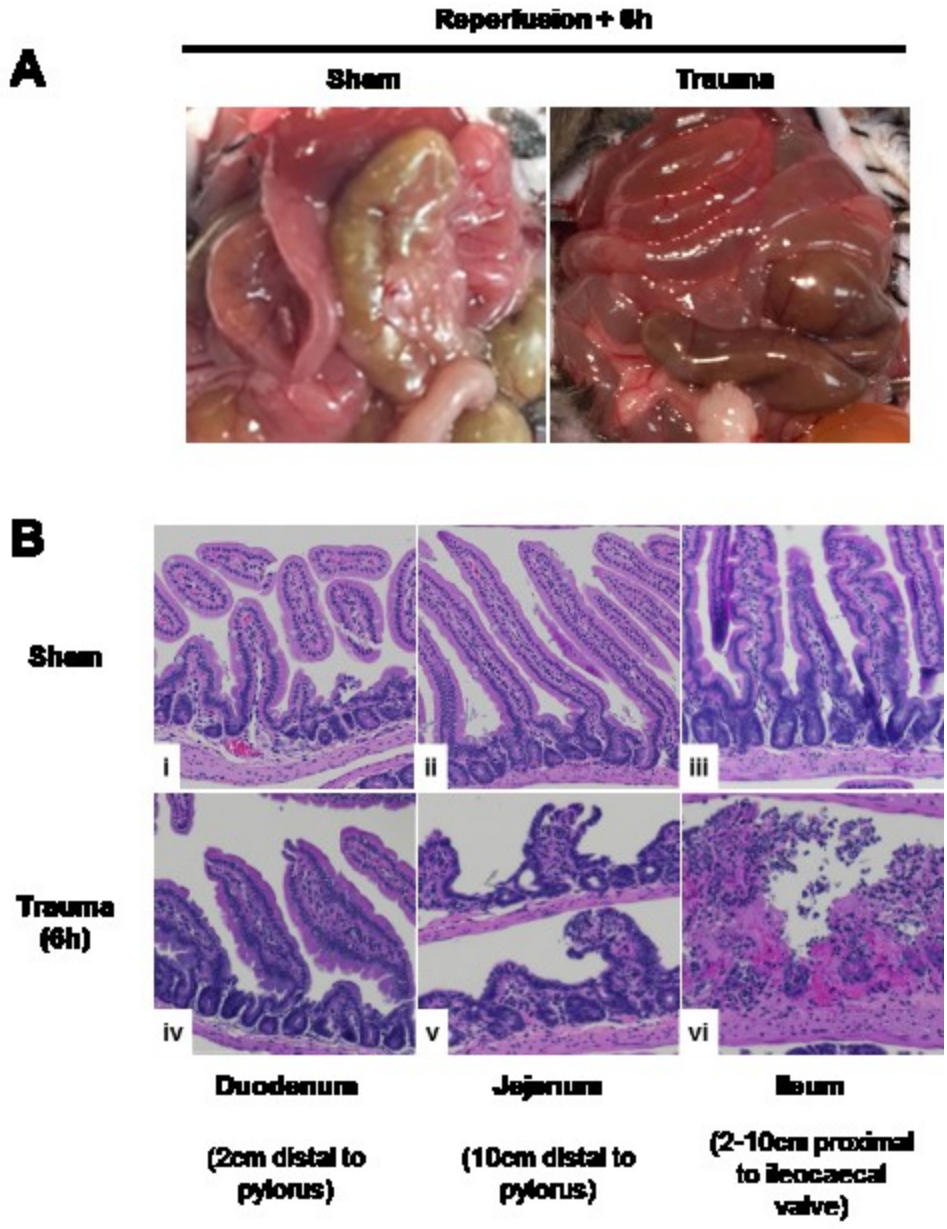

Figure 20. Polytrauma induces significant bowel injury.

(A) Compared to normal healthy bowel before (Sham), markedly edematous and dilated bowel is seen (Trauma) at necropsy at 6h, corresponding to (B) histological changes through the small bowel ranging from inflammatory cell infiltration, separation of the epithelium and the luminal basal layers, villous blunting, and near-complete disintegration of epithelial layers (Panel iv-vi); sham mice (Panel i-iii) display no observable mucosal damage; H&E staining.

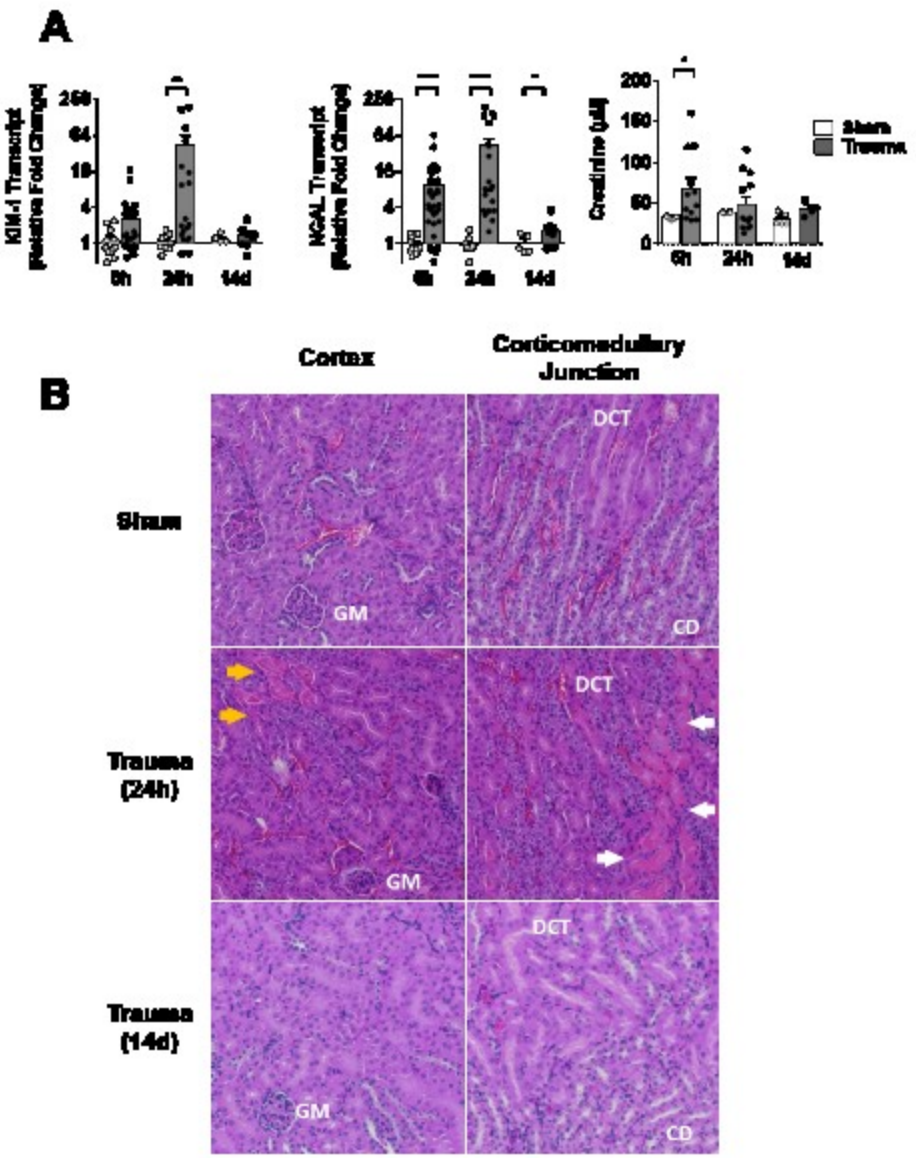

Figure 21. Polytrauma causes acute kidney injury in mice.

(A) Kidney injury markers KIM-1 and NGAL; data are normalized to control GAPDH expression and compared with sham. Mild increases in plasma creatinine levels suggests functional kidney impairment from decreased kidney creatinine clearance. (B) Histological examination by H&E staining demonstrates acute tubular necrosis (white arrows) and the presence of renal tubular casts (yellow arrows) at 24h.

GM=glomerulus, DCT=distal convoluted tubule, CD=collecting duct; *P<0.05, **P<0.01, ****P<0.0001, Student's t test

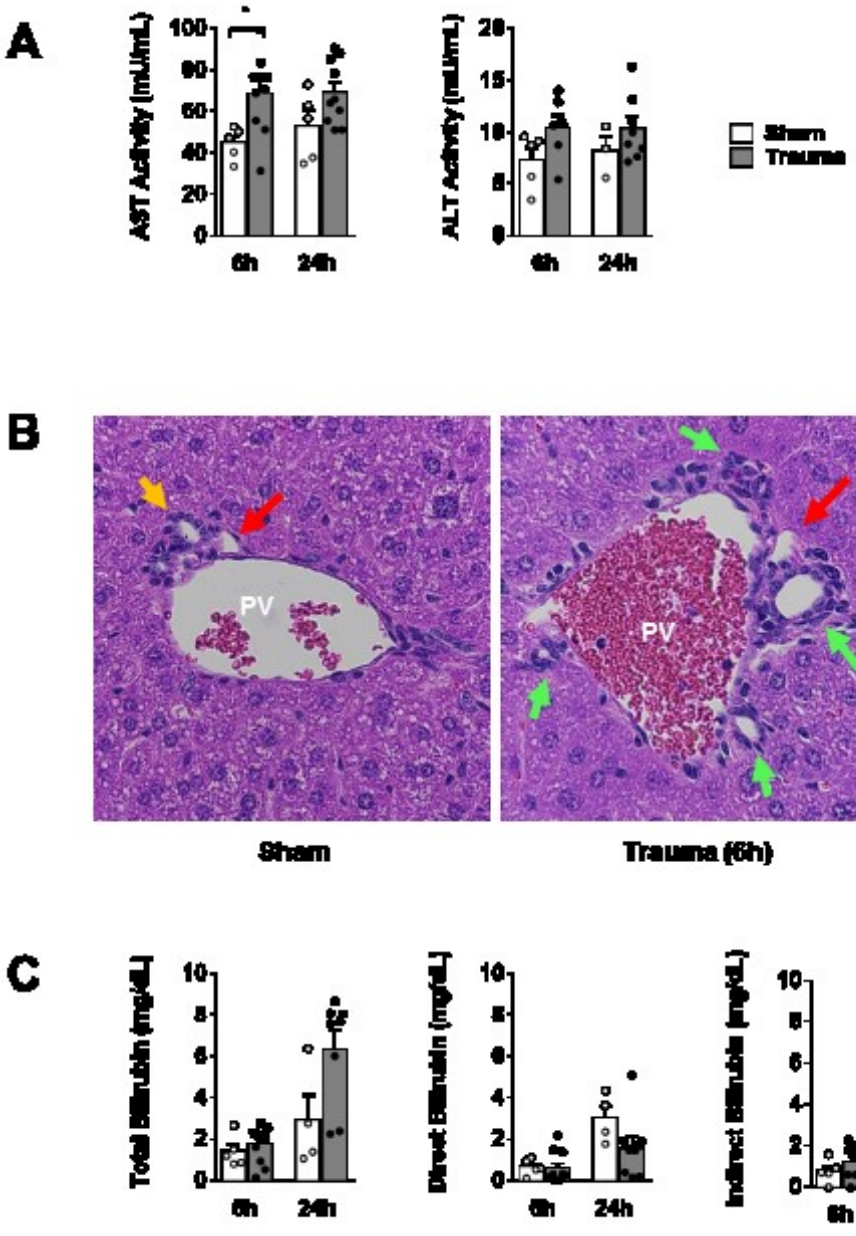

Figure 22. Polytrauma causes mild liver injury.

(A) Mild hepatic injury following trauma is evinced by elevations in plasma aspartate (AST) and alanine (ALT) aminotransferases. (B)Histological analysis by H&E demonstrates portal triad bile duct proliferation (Sham vs Trauma, 1:1:1 vs 4:1:1, bile duct:hepatic artery:portal vein). (B) Mild elevations in total and indirect bilirubin at 24h suggests mild hepatic functional impairment from decreased conversion of conjugated to unconjugated bilirubin by the liver.

PV = portal vein, yellow = bile duct, red = hepatic artery, green = supernumerary bile ducts. *P<0.05, Student's t test

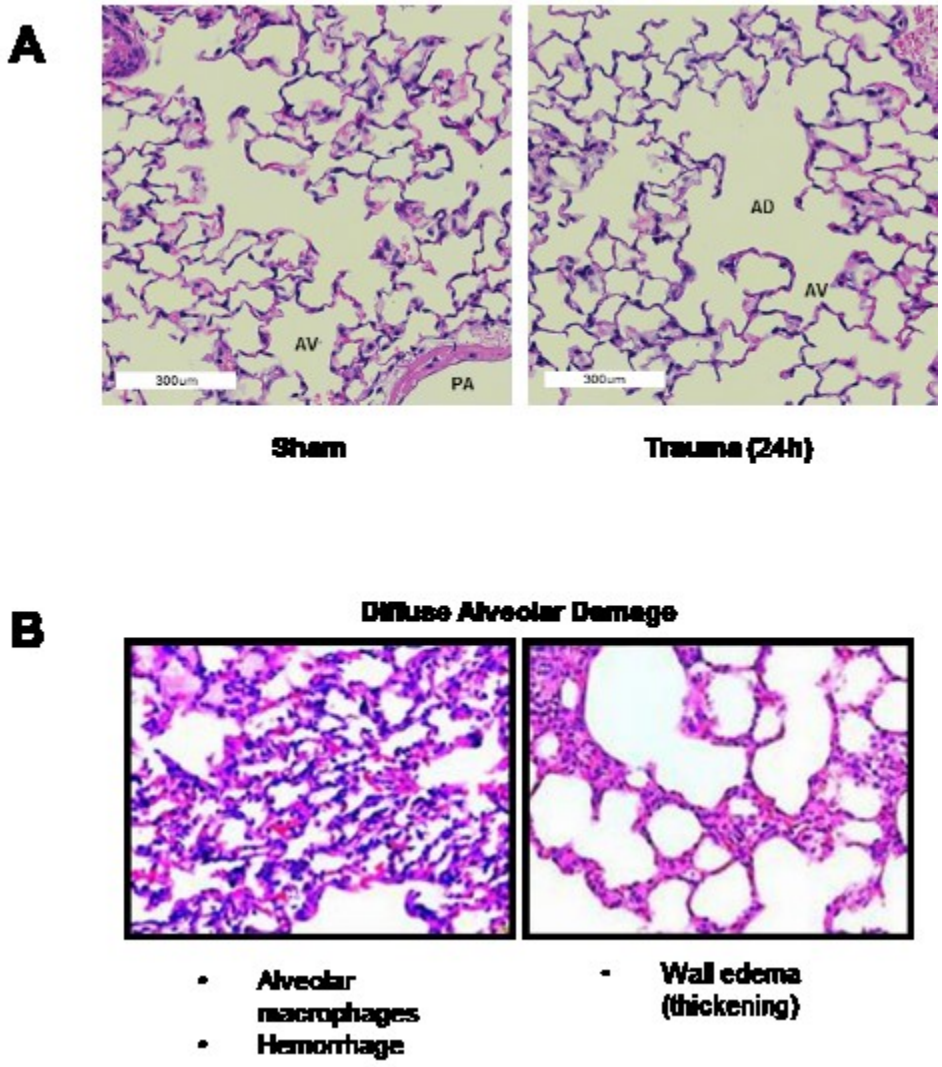

Figure 23. No significant lung injury is observed following polytrauma.

(A) H&E images of aerated lung histological sections collected at 24h demonstrates no significant differences and no evidence of diffuse alveolar damage, as shown in (B) representative images of immune cell infiltration, hemorrhage, or alveolar edema.

B=bronchus, AD=alveolar duct, AV=alveolus, PA=pulmonary arteriole

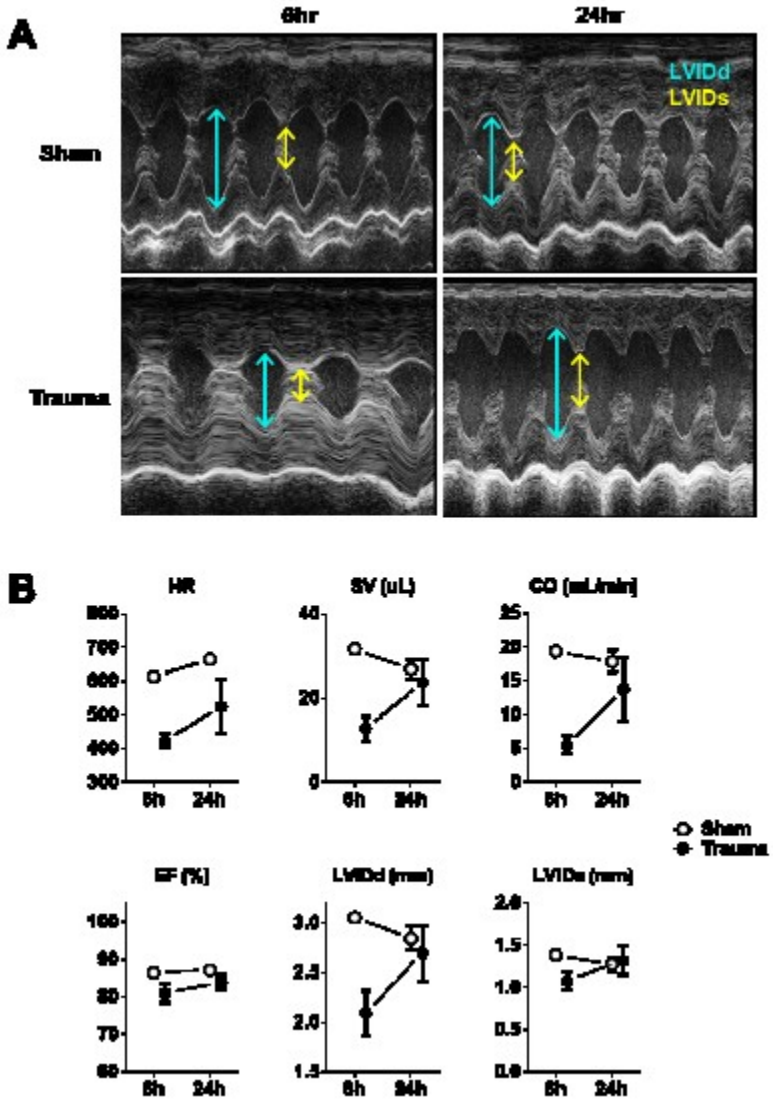

Figure 24. Polytrauma causes hypovolemic changes and moderate cardiac dysfunction.

(A) Dimensional representation of LV volume measurements captured by M-mode transthoracic echocardiographic imaging of the parasternal short-axis views at the level of the papillary muscles. Overt decreases in contractile function is evident at 6h in Trauma mice as compared to Sham mice, evidenced by reduced LVIDd/s and a marked decrease in heart rate. (B) Quantification of echocardiographic parameters.

HR=heart rate, SV=stroke volume, CO=cardiac output, EF=ejection fraction, LVIDd/LVIDs=left ventricular inner diameter in diastole/systole.

Table 3. Summary of transthoracic echocardiographic measurements.

HR=heart rate, LVIDd/LVIDs=left ventricular inner diameter in diastole/systole, SV=stroke volume, EF=ejection fraction, CO=cardiac output, FS=fractional shortening.

	6h		24h	
	Sham	**Trauma**	**Sham**	**Trauma**
HR (bpm)	614±15	422±20	666±14	525±81
LVIDd (mm)	3.06±0.01	2.09±0.23	2.85±0.12	2.70±0.28
LVIDs (mm)	1.39±0.05	1.08±0.1	1.28±0.09	1.32±0.16
SV (μL)	31.7±0.7	12.7±3.1	26.9±2.5	23.8±5.5
EF (%)	86±1	81±3	87±1	84±2
CO (mL/min)	19.4±0.5	5.5±1.4	17.9±1.7	13.8±4.8
FS (%)	55±2	47±3	55±1	51±2
n	3	5	3	4

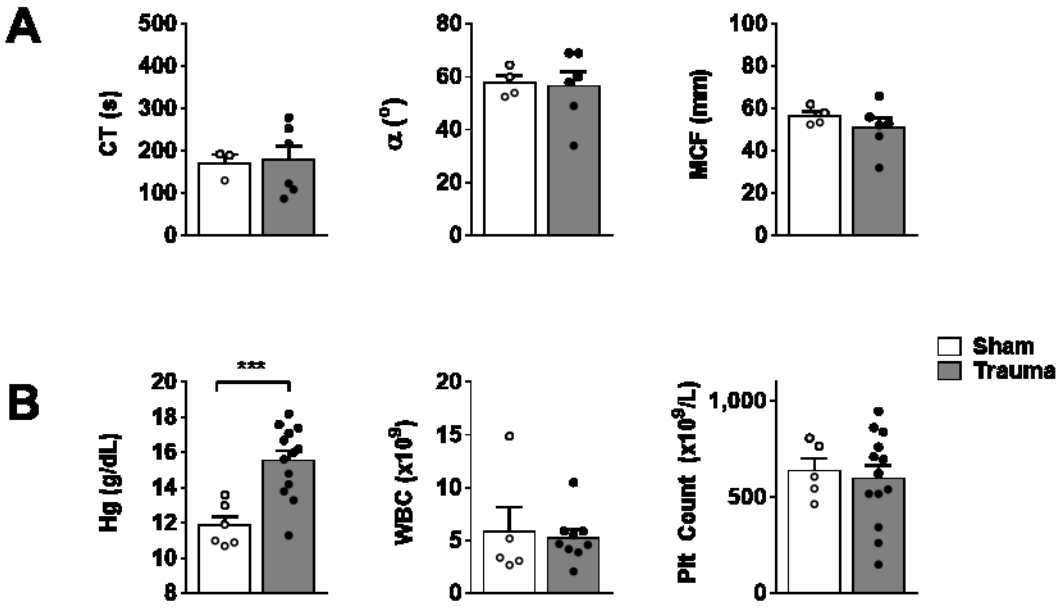

Figure 25. Polytrauma is variably associated with non-hemorrhagic hypovolemia and coagulation changes.

(A) No statistically significant differences in CT (clotting time), α (alpha angle), and MCF (maximum clot firmness) is observed following polytrauma. (B) Complete blood count determined by automatic coulter counter demonstrates significant haemoglobinemia as well as varying degrees of thrombocytopenia thrombocytosis.

[Hg=haemoglobin, WBC=white blood cell, Plt=platelet; ***P<0.001, Student's t test] ROTEM & Coagulation. CT=clotting time, α=alpha angle, MCF=maximum clot firmness.

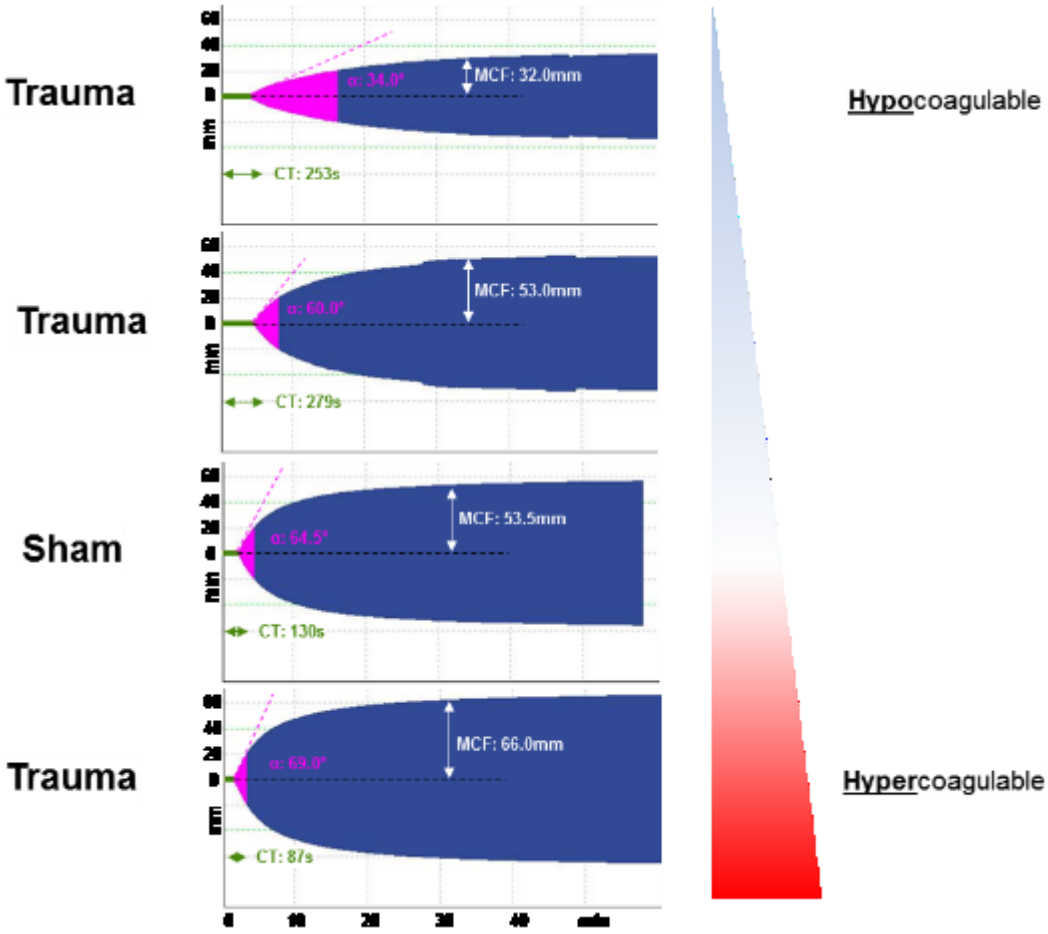

Figure 26. Polytrauma is variably associated with non-hemorrhagic coagulation dysfunction.

Representative ROTEM thromboelastograms demonstrate a spectrum of hypo- or hyper-coagulable states in Trauma mice at 6h as compared with Sham mice.

CT=clotting time, α=alpha angle, MCF=maximum clot firmness

3.2 Extracellular Circulating RNA and miRNA After Polytrauma

3.2.1 Polytrauma Increases Circulating RNA and miRNA Levels

Previous studies have established that extracellular RNA released from cells are potently immunostimulatory[76,77,79]. Based on these findings, we hypothesized that tissue and cellular damage experienced during polytrauma catalyzes the release of RNA, including a constituent miRNA fraction, into circulation.

Thus, we sought to quantify circulating host RNA isolated from the plasma of sham and polytrauma mice. Using a Trizol-alcohol precipitation method, total RNA was isolated from 50μL of plasma of mice subjected to sham or polytrauma procedures and resuspended in DEPC H_2O. Plasma used in these experiments underwent a 2-step centrifugation and was therefore, for all intents and purposes, cell-free. RNA suspensions were then analyzed via microcapillary gel electrophoresis which separates RNA fragments based on nucleotide length whose sizes are then identified based on comparison with a RNA ladder. Subsequently, the concentration of RNA is calculated by integrating the area under the curve which is compared to the RNA ladder of known concentration.

We observed that polytrauma induces significant increases of plasma small RNA at 6h, illustrated by electropherogram as more intense (darker) bands or larger peaks (Figure 27AB). Of note, there were several prominent bands at approximately the 10 and 20nt regions, the latter corresponding to the miRNA fraction. In contrast, sham operated mice displayed low levels of circulating RNA (minimal band density). For quantification, RNA concentration of the RNA suspensions was normalized to the volume of input

plasma (50µL) to generate an estimate of the extracellular RNA concentration in circulation. Besides an increase in extracellular small RNA following polytrauma (Figure 27C, 6h: 112±27 vs 399±45ng/mL plasma, $p<0.001$), a concurrent increase in the ex-miRNA fraction was observed (7±1ng vs 40±5ng/mL, $p<0.0001$). Interestingly, plasma RNA tended to return to basal levels by 24h, approximating sham plasma RNA concentrations.

Next, we examined the correlation between RNA concentration and the degree of cytokine response and organ injury. This revealed that polytrauma mice that there was a positive correlation (RNA v. IL-6: $R^2=0.5658$, $p<0.0001$) between cytokine production and circulating plasma RNA (Figure 28A). In addition to inflammatory outcomes, RNA also correlated positively with markers of kidney injury (Figure 28B, RNA v. NGAL: $R^2=0.3336$, $p<0.01$). These findings are consistent with previous observations in a CLP sepsis model demonstrating a correlation between circulating RNA and sepsis severity[77], and generally support the notion that the RNA is released following polytrauma[68] and can serve as a marker of inflammatory outcomes and organ injury.[100–103].

3.2.2 RNA Sequencing Reveals an Abundance of miRNA Species

We subsequently sought to characterize and identify the miRNAs present in circulation following polytrauma. Small RNA from the plasma of sham (n=6) and polytrauma (n=9) mice were sent for RNA sequencing and analysis, as described previously (Section 2.3.6-2.3.7).

A total of 233,954,936 raw reads were generated, and 166,357,230 were mapped to the mouse genome (Table 4). Of these, 154,201,830 (92.7%) were miRNAs, 3,296,314

(2.0%) mRNA, and 1,495,747 (0.9%) tRNA. Remarkably, rRNA and unmapped RNAs (e.g. small RNAs of bacterial origin), constitute only 17,108,222 (8.4%) and 9,343,661 (4.0%), respectively, of all plasma small RNAs detected (Figure 29A). We also observed that polytrauma tended towards an increase in the rRNA fraction (Figure 29B), supporting the notion that polytrauma increases the release of intracellular nucleic acid—where rRNA is typically localized) into circulation. Ultimately, these data demonstrate that of all the ex-RNA isolated from plasma, the majority are indeed miRNAs, though other small RNA species are also detectable albeit at drastically lower levels. Thus, it follows that there is an abundance of ex-miRNAs in circulation following polytrauma.

3.2.3 Unique Circulating miRNA Expression Patterns are Observed Following Polytrauma

miRNAs mapped to the miRbase reference genome were evaluated using differential expression (DE) analysis. DE analysis assessed relative miRNA expression levels between sham and polytrauma mice by comparing normalized read counts. The trimmed mean of M-value (TMM) method of normalization was performed, which scales read counts across samples based on library size per sample to correct for technical differences in total amount of starting RNA, which otherwise may generate a composition bias. To determine statistical significance, the Benjamini and Hochberg[104] approach for multiple testing was applied. Production of an adjusted *p*-value is accomplished using this method such that the effect of oversampling—which otherwise generates excessive false positives[104]—is eliminated by applying a statistical correction that minimizes the overall false discovery rate (FDR) rather than synchronously testing multiple null hypotheses.

DE analysis identified a total of 142 significantly differentially expressed miRNA species: 80 up- and 62 down-regulated (Table 5, Figure 30A).

In addition, principle component analysis of the 50 most variable miRNAs demonstrated dominant patterns of miRNA differential expression that distinctly identified the sham and polytrauma groups (data not shown). Subsequent hierarchical clustering, which arranges the DE miRNA according to their similarities, illustrated that polytrauma induced the down and upregulation of groups of miRNAs in a way that was distinctly unique (Figure 30B). Together, these data suggest that miRNAs in circulation is non-random, and thus we can infer that polytrauma induces changes in dominant miRNA expression patterns.

3.2.4 Summary of Section 3.2

Consistent with prior studies demonstrating that extracellular RNA and miRNA are found in circulation following traumatic injury, we have also observed an abundance of RNA, consisting primarily of miRNA, in the plasma of mice that have suffered from severe polytraumatic injury. Additionally, RNAseq revealed differential expression of various miRNAs following polytrauma, suggesting that mice exhibit varying patterns of extracellular miRNA expression in response to traumatic injury—that is to say, certain species of miRNA predominate and are found in circulation as a result of polytraumatic injury.

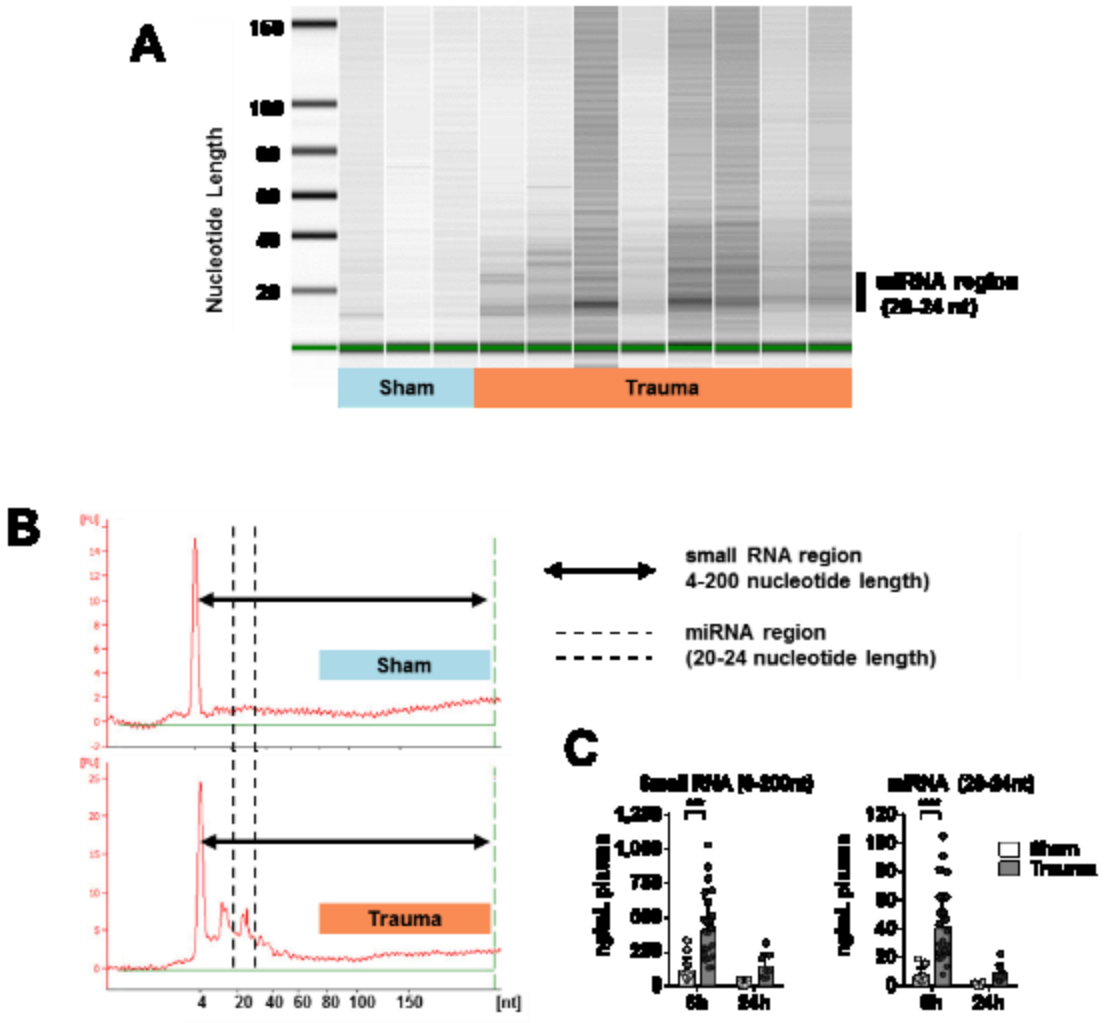

Figure 27. Plasma RNA and miRNAs are significantly increased following polytrauma in mice.

(A) Representative microfluidic electropherograms demonstrate increases in plasma RNA and miRNA subjected to trauma (lanes 4-11) as compared to sham mice (lanes 1-3). (B) Schematic depiction of definitions of small RNA and miRNA regions used in Bioanalyzer quantification. Nucleotide ladder denotes oligonucleotide fragments of known size. (C) Quantification of small RNA (0-200nt) and miRNA (20-24nt). Bioanalyzer 2100 Small RNA chip.

***P<0.001, ****P<0.0001, Student's t test

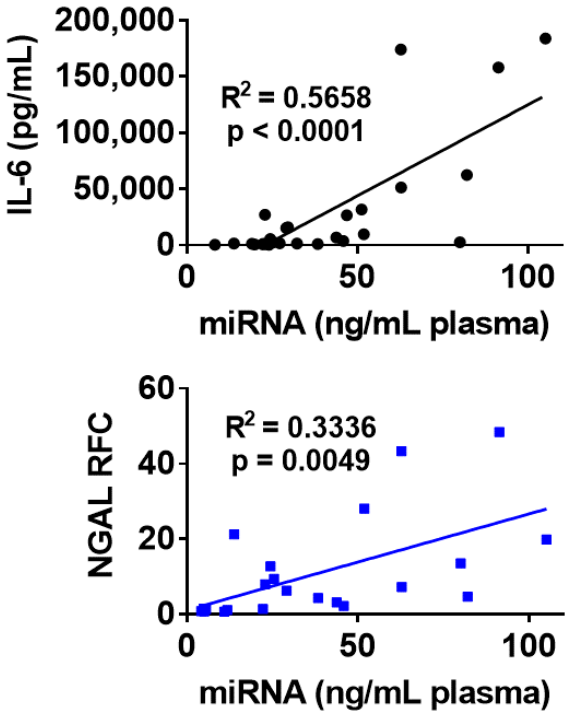

Figure 28. Relationship between circulating RNA and Traumatic injury.

Plasma miRNA levels correlate with markers of trauma severity, such as inflammatory cytokine IL-6 and kidney injury marker NGAL at 6h following polytraumatic injury

Pearson correlation, (IL-6, n=28) and (NGAL, n=22) X-Y pairs.

Table 4. RNAsequencing biotype distribution.

RNAsequencing raw read biotype distribution, by thousands of reads. rRNA=ribosomal RNA, miRNA=microRNA, tRNA=transfer RNA, piRNA=piwi-interacting RNA, mRNA=messenger RNA.

	Reads (Thousands)															
		Sham						Trauma								
	Total	**S1**	**S2**	**S3**	**S4**	**S5**	**S6**	**T1**	**T2**	**T3**	**T4**	**T5**	**T6**	**T7**	**T8**	**T9**
Total Raw Reads	**233,955**	13,545	13,689	13,182	17,250	17,679	12,498	12,917	18,250	19,625	15,324	13,603	15,172	19,034	16,355	15,832
rRNA	**17,108**	553	628	560	805	738	1,067	669	3,628	2,763	1,539	787	799	971	934	667
miRNA	**154,202**	7,919	6,689	8,937	11,155	11,732	6,728	8,459	11,126	12,585	9,862	9,081	11,690	13,655	12,502	12,083
tRNA	**1,496**	65	87	83	136	117	115	129	91	56	92	103	84	140	81	117
piRNA	**612**	11	15	39	26	27	15	95	33	26	67	50	50	56	45	58
mRNA	**3,296**	75	106	93	173	121	78	201	534	680	176	146	159	264	286	205

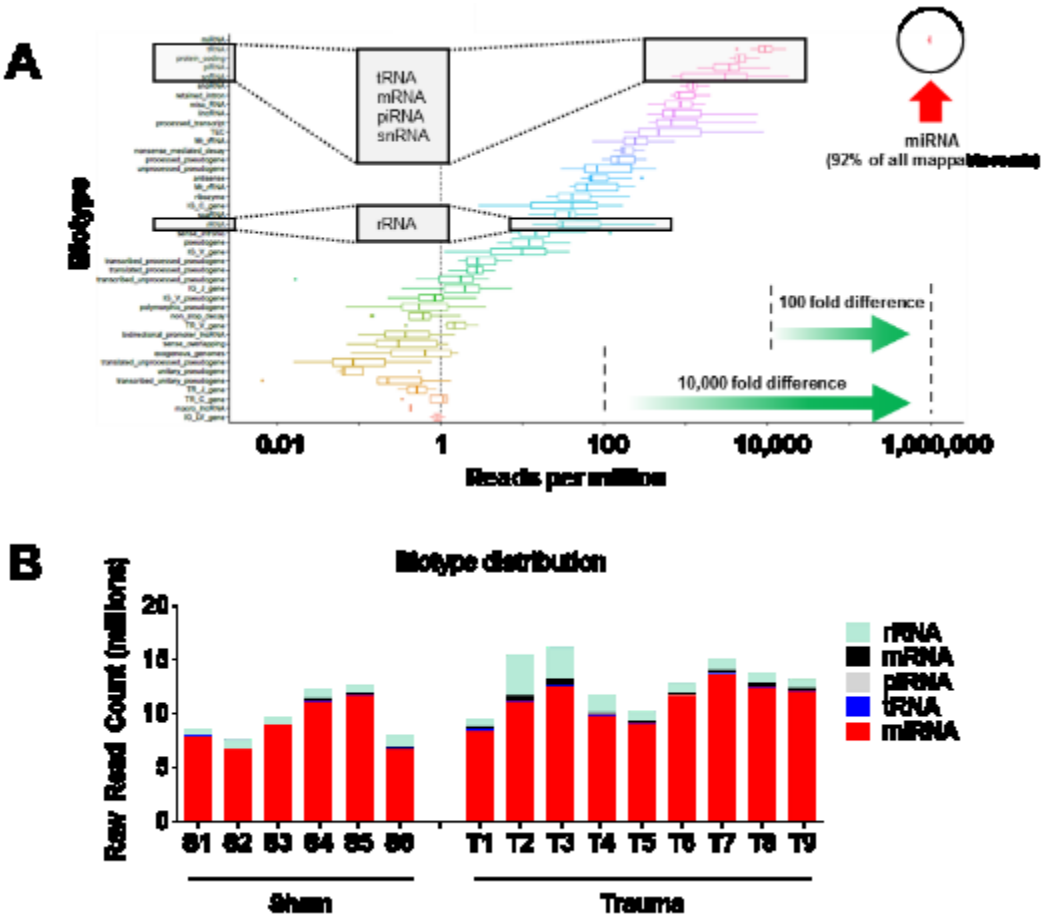

Figure 29. RNAseq reveals that much of circulating RNA is miRNA.

(A) Overall biotype distribution based on normalized read counts demonstrates that of mappable reads are miRNA (>92%) are more than 100-fold or more abundant than other RNA species. (B) Biotype distribution according to raw read count.

miRNA=microRNA, tRNA=transfer RNA, mRNA=messenger RNA, piRNA=piwi-interacting RNA, snRNA=small nuclear RNA, rRNA=ribosomal RNA.

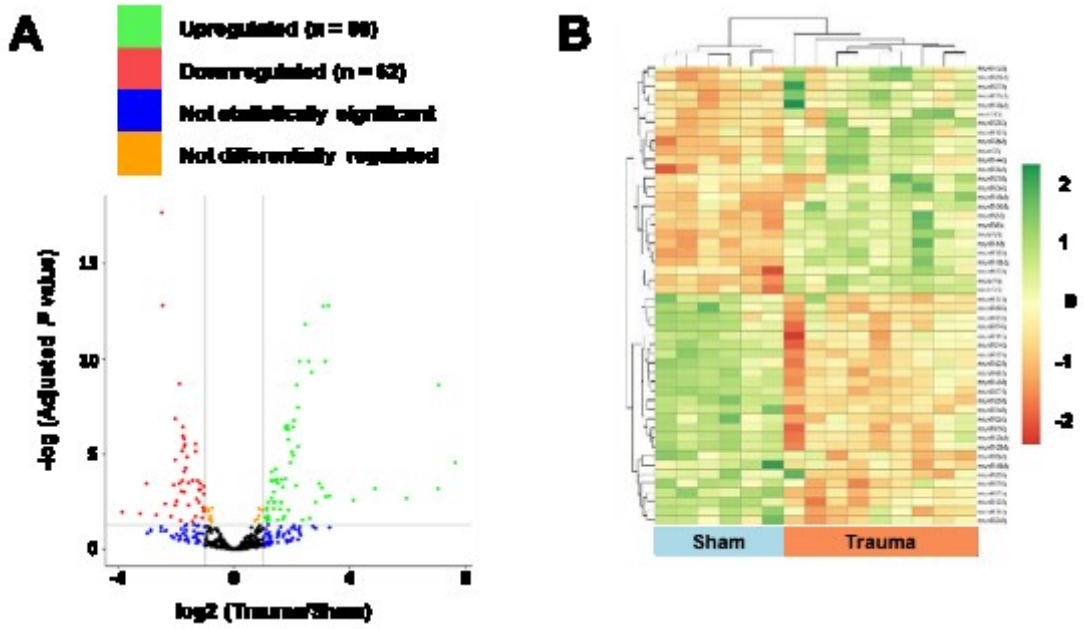

Figure 30. Polytrauma causes differential expression of circulating miRNA.

(A) Volcano plot illustration of DE analysis of miRNAs detected in the plasma following polytrauma identified 80- and 62- statistically significantly up- and down-regulated miRNAs, respectively. Statistical significance was defined as a fold change ≥ or ≤ 2 of Sham vs. Trauma at *p*-value and FDR ≤ 0.05. (B) Dendrogram representation of hierarchical clustering analysis of the top 50 variable (most highly differentially expressed) miRNAs illustrates that polytrauma induces distinct patterns of circulating miRNAs. The color scale indicates the relative expression level of a miRNA to the mean.

$-\log_{10}$(Adjusted P value) = $-\log_{10}(0.05)$ = 1.301 = "FDR" = False Discovery Rate

Table 5. List of miRNA identified as up- (green) or down-regulated (red) by RNAseq analysis.

[FC=relative fold change of Trauma vs. Sham, CPM=(read) counts per million, FDR = False Discovery Rate]

Differential Expression	miRNA	log2 FC	log10 CPM	P Value	FDR
UP	miR-31-5p	7.636	0.710	1.91E-06	2.70E-05
(n=66)	miR-374b-5p	7.054	2.008	5.97E-11	2.46E-09
	miR-1224-5p	7.015	0.173	7.72E-05	6.26E-04
	miR-28a-5p	5.936	-0.654	3.14E-04	2.16E-03
	miR-7236-3p	4.858	0.471	8.38E-05	6.69E-04
	miR-194-1-3p	4.104	0.277	4.12E-04	2.75E-03
	miR-16-1-3p	3.299	3.186	2.24E-04	1.61E-03
	let-7d-5p	3.237	7.357	7.35E-16	1.56E-13
	miR-1968-5p	3.166	2.016	2.57E-04	1.82E-03
	miR-3535	3.152	10.174	1.86E-12	1.39E-10
	let-7i-5p	3.075	10.481	1.39E-15	1.72E-13
	miR-107-3p	3.028	2.589	6.97E-05	5.75E-04
	miR-144-5p	2.942	4.402	3.77E-05	3.47E-04
	miR-217-5p	2.809	9.602	5.20E-04	3.39E-03
	miR-103-3p	2.678	5.589	9.41E-12	5.18E-10
	miR-145b	2.630	-0.118	5.46E-03	2.41E-02
	miR-106b-3p	2.568	9.941	2.12E-12	1.39E-10
	let-7f-5p	2.451	10.119	1.58E-14	1.56E-12
	miR-17-3p	2.351	2.015	7.10E-03	2.93E-02
	let-7c-5p	2.268	10.795	2.24E-12	1.39E-10
	miR-7a-5p	2.203	6.279	9.10E-10	3.46E-08
	miR-374b-5p	2.203	5.864	2.31E-07	4.08E-06
	miR-374c-5p	2.203	5.864	2.31E-07	4.08E-06
	miR-186-5p	2.158	11.001	5.27E-11	2.37E-09
	miR-421-3p	2.139	3.985	5.25E-05	4.56E-04
	miR-215-3p	2.065	7.900	5.37E-09	1.77E-07
	let-7j	2.048	6.938	7.67E-07	1.19E-05
	miR-26b-5p	2.042	5.587	1.50E-08	3.92E-07
	miR-194-5p	1.997	6.442	5.00E-07	7.98E-06
	miR-23b-3p	1.952	6.783	2.09E-06	2.87E-05
	let-7g-5p	1.888	9.068	2.31E-08	5.45E-07
	miR-15b-5p	1.880	4.519	1.63E-03	8.47E-03
	miR-25-3p	1.869	13.188	8.23E-08	1.70E-06
	miR-451a	1.853	11.258	1.04E-08	3.23E-07
	let-7a-5p	1.800	8.825	1.98E-08	4.89E-07
	miR-26a-5p	1.782	11.361	1.46E-08	3.92E-07
	miR-145a-5p	1.776	12.746	1.59E-05	1.92E-04
	miR-141-3p	1.730	5.699	3.94E-03	1.87E-02
	miR-143-5p	1.690	6.443	6.35E-05	5.32E-04
	miR-200a-5p	1.681	3.247	6.40E-03	2.75E-02
	miR-148a-3p	1.634	12.420	5.89E-04	3.57E-03
	miR-145a-3p	1.630	12.726	1.78E-05	2.05E-04
	miR-144-3p	1.603	10.306	5.47E-04	3.47E-03
	miR-802-5p	1.593	4.104	1.55E-03	8.23E-03
	miR-505-5p	1.507	3.893	6.52E-03	2.78E-02
	miR-206-3p	1.505	10.001	3.99E-05	3.59E-04
	miR-93-5p	1.470	5.796	1.77E-05	2.05E-04
	miR-148b-3p	1.439	7.121	2.30E-05	2.59E-04
	miR-16-5p	1.431	9.351	4.61E-06	6.00E-05
	miR-200a-3p	1.426	10.491	5.45E-04	3.47E-03
	miR-132-3p	1.376	4.333	1.30E-03	7.21E-03
	miR-193b-3p	1.374	4.171	5.92E-04	3.57E-03
	miR-23a-3p	1.366	12.309	1.33E-04	9.81E-04
	miR-652-3p	1.345	6.392	2.44E-05	2.60E-04
	miR-181d-5p	1.307	5.526	6.53E-06	8.19E-05
	miR-20a-5p	1.297	4.595	3.10E-04	2.16E-03
	miR-28a-3p	1.283	7.281	2.57E-05	2.60E-04
	miR-30e-5p	1.200	11.713	6.16E-03	2.70E-02
	miR-215-5p	1.194	13.600	7.11E-03	2.93E-02
	miR-382-5p	1.189	5.445	5.55E-04	3.48E-03
	miR-345-3p	1.174	3.608	3.81E-03	1.83E-02
	miR-25-5p	1.165	4.435	6.79E-03	2.85E-02
	miR-192-5p	1.136	15.373	1.61E-03	8.47E-03
	miR-1839-5p	1.133	7.704	1.20E-03	6.85E-03
	miR-490-3p	1.118	4.483	7.85E-03	3.15E-02
	miR-1947-5p	1.087	4.044	4.70E-03	2.13E-02

Differential Expression	miRNA	log2 FC	log10 CPM	P Value	FDR
DOWN	miR-409-3p	-1.028	7.870	5.95E-05	5.08E-04
(n=46)	miR-423-5p	-1.045	13.260	1.77E-04	1.29E-03
	miR-187-5p	-1.045	6.815	1.94E-03	9.88E-03
	miR-673-5p	-1.054	4.874	1.13E-03	6.50E-03
	miR-326-3p	-1.074	3.952	4.90E-03	2.19E-02
	miR-182-5p	-1.145	9.042	3.79E-05	3.47E-04
	miR-330-3p	-1.147	6.217	9.54E-05	7.38E-04
	miR-455-3p	-1.196	5.377	5.90E-04	3.57E-03
	miR-874-3p	-1.203	4.824	9.52E-05	7.38E-04
	miR-29b-3p	-1.250	6.776	2.50E-05	2.60E-04
	miR-871-3p	-1.283	3.581	3.34E-04	2.26E-03
	miR-322-3p	-1.317	8.536	1.49E-07	2.96E-06
	miR-130b-5p	-1.318	3.715	4.00E-03	1.87E-02
	miR-541-5p	-1.325	9.378	4.54E-07	7.49E-06
	miR-668-3p	-1.424	3.568	8.77E-03	3.45E-02
	miR-184-3p	-1.427	6.017	2.54E-05	2.60E-04
	miR-365-2-5p	-1.566	2.609	7.94E-04	4.68E-03
	miR-92b-3p	-1.573	7.439	3.39E-05	3.36E-04
	miR-674-3p	-1.621	7.860	9.76E-07	1.46E-05
	miR-7068-3p	-1.663	4.559	4.21E-06	5.63E-05
	miR-214-3p	-1.698	9.312	1.60E-07	3.05E-06
	miR-125a-5p	-1.700	14.362	6.61E-06	8.19E-05
	miR-671-3p	-1.702	5.769	2.23E-07	4.08E-06
	miR-485-5p	-1.704	6.786	7.64E-08	1.65E-06
	miR-146b-3p	-1.716	2.754	1.33E-04	9.81E-04
	miR-139-3p	-1.764	5.877	4.96E-08	1.12E-06
	miR-125b-5p	-1.769	13.730	1.28E-08	3.73E-07
	miR-23b-5p	-1.777	4.913	3.95E-07	6.74E-06
	miR-615-3p	-1.781	9.019	2.57E-05	2.60E-04
	miR-5107-5p	-1.802	3.068	1.23E-04	9.38E-04
	miR-193b-5p	-1.840	2.127	7.82E-03	3.15E-02
	miR-483-5p	-1.880	3.383	3.52E-05	3.41E-04
	miR-149-5p	-1.887	7.940	4.10E-11	2.03E-09
	miR-485-3p	-1.986	3.257	4.41E-04	2.91E-03
	miR-3102-5p	-2.023	3.346	1.39E-06	2.02E-05
	miR-511-5p	-2.025	5.200	3.78E-09	1.34E-07
	miR-124-3p	-2.027	2.897	8.24E-04	4.80E-03
	miR-344d-3p	-2.062	2.609	4.84E-05	4.28E-04
	miR-6948-3p	-2.166	1.337	4.05E-03	1.87E-02
	miR-1941-5p	-2.357	1.773	6.70E-04	4.00E-03
	miR-877-5p	-2.459	6.091	9.44E-16	1.56E-13
	miR-205-5p	-2.477	9.042	4.08E-21	2.02E-18
	miR-196b-5p	-2.683	2.152	3.16E-03	1.55E-02
	miR-7007-5p	-3.009	2.028	3.69E-05	3.47E-04
	miR-741-3p	-3.226	1.284	2.60E-03	1.29E-02
	miR-7007-3p	-3.847	0.666	2.28E-03	1.14E-02

3.3 URIDINE-RICH miRNAs TRIGGER INFLAMMATION VIA A TLR7 DEPENDENT MECHANISM

3.3.1 Synthetic miRNAs Trigger Pro-inflammatory Responses in Macrophages

To test the innate immune activity of miRNAs upregulated following trauma, we sought to test the miRNAs' ability to generate an innate immune response. Due to the economic impracticality of testing all 66 upregulated miRNAs that were identified by RNAseq, only n=18 target miRNAs (Table 6) were chosen for further testing based on a composite score using the following 3 equally weighted criteria: differential expression (RFC), abundance (read counts), and statistically significant (FDR and *p*-value <0.05).

Synthetic ssRNAs were tested in WT bone marrow-derived macrophage (BMDMs) culture by delivering RNA into BMDMs using Lipofectamine transfection agent. Construction of dose-response curves demonstrated that several miRNAs (let-7b-5p, -7j; miR-7a-5p, -34a-5p, -122-5p, -142a-3p, -145a-3p, -146a-5p, and -802-5p) induced the production of the chemokine MIP-2 and the cytokine IL-6 in a concentration dependent matter (Figure 31). On the other hand, several (miR-22, -126a, 192, -193b, -210, -345, -374, -451, -1947) were apparently nonimmunogenic at doses of up to 5000nM. These data suggest that miRNAs possess varying capacities in inducing an immune response that are seemingly unique. Interestingly, these data also indicate that immunostimulatory miRNAs appear to possess characteristic threshold and ceiling doses, which evince the idea that miRNAs may vary uniquely in their interactions with target receptors within BMDMs.

Indeed, in exploring the relationship between miRNAs and their downstream effect in BMDMs, we note that there exist divergences in the magnitude of response, or maximal attainable response (Figure 31). In addition, it is noteworthy that these data demonstrate that the nine (9) immunostimulatory miRNAs used in this study display significant differences in their immunostimulatory potency, maximal efficacy, and slope; as reflected by dramatic variation in their respective median effective concentrations (EC_{50}) (Figure 32, Table 7). Surprisingly, even let-7b-5p and let-7j, two highly homologous miRNA isoforms (88.24% similar[105]), vary greatly in their biological activity.

To further link circulating RNA found in polytrauma to the inflammatory responses induced by specific upregulated miRNAs, BMDMs were treated with RNA isolated from the plasma of sham or polytrauma mice (Figure 33). We observed that effective doses of 0.25ug/mL of total (endogenous) RNA from Trauma mice induced significant cytokine production in BMDMs, whereas equivalent amounts of RNA from sham mice did not. These data suggest that RNA that are released into plasma are intrinsically pro-inflammatory.

3.3.2 Recognition of miRNA Depends on its Uridine Ribonucleotide Content

In view of the fact that we and others have previously observed that that certain uridine-rich miRNAs mimics induce cytokine and FB production[76,77,106] and that mutation of uridine to adenine (U→A) can abolish a miRNA's immunogenicity[77], we hypothesized that uridine content (%U) alone is a strong predictor of a miRNA's immunogenicity. Furthermore, structural analyses have intimated the critical role of uridine moieties in the

activation of TLR7[51,107]. Thus, we sought next to assess the inflammatory properties of circulating miRNAs in polytrauma based on their uridine content.

To address this question, we initially investigated the relationship between %U and our empirically derived EC_{50} values. In comparing drug agonist effects, increases in EC_{50} are interpreted as denoting that higher effective concentrations are required to achieve the same median effect, i.e. EC_{50} reflects potency. Based on correlation analysis (Figure 34), we did not observe a relationship between the %U and EC_{50}, which suggests that %U are not associated with a miRNA's immunostimulatory potency.

In total, we investigated the immunostimulatory properties in BMDM culture of a total of 33 miRNAs (Table 8) during our studies. Relative to nonimmunogenic miRNAs, we discovered that those miRNAs capable of inducing cytokine responses at 50nM concentrations were statistically more likely to contain more uridines (Figure 35A, pro- vs non-inflammatory, 40±2% vs 23±2%, $p<0.0001$). Next, to assess the ability of using uridine content (%U) content in estimating a miRNA's immunostimulatory properties, a receiver operating characteristic was constructed. *In vitro* test data was input into a binary classification model of "non-" or "pro-" inflammatory, from which the true positive rates (TPR) and false positive rates (FPR) of using %U cutoffs ranging from 1-100% were calculated from sensitivity and specificity determinations (Figure 15), then repeated for each of the other ribonucleobases (% [A]denine, [C]ytosine, and [G]uanosine). Plotting of TPR (*y*-axis) against FPR (*x*-axis) generated the receiver operating characteristic (ROC) (Figure 35B) revealing that %U was the best discriminator of inflammatory properties with an AUC of 0.844 (Table 9). Interestingly, %A was similarly a good discriminator (AUC=0.769), while %C and %G provided no statistically significant

discriminatory power (95%CI 0.43-0.81 and 0.38-0.77, respectively). These data, interpreted as a whole, suggest that %U is powerful predictor of pro-inflammatory properties, while %A negatively predicts immunostimulatory properties.

Next, cross-validation of the discriminatory ability of %U was performed. The miRNAs identified by RNAseq were chosen as the test set and arranged in rank order by %U (Table 6), then divided by quartiles into three strata representing the bottom 25th percentile, the midspread, and the top 75th percentile: low (<20%), moderate (≥20 to <40%), and high (≥40 %U), respectively.

Testing of these stratified miRNAs mimics in BMDM culture at doses of 50nM revealed that all miRNAs with high %U (≥40) all induce cytokine and complement factor B (FB) production; in contrast, those with low %U (<20) failed to do so (Figure 36).

Together, these findings indicate that miRNAs containing high uridine content exhibit greater immunostimulatory potential compared to miRNAs lacking uridine. While it is difficult to ascertain precisely which uridines contribute determine a miRNA's pro-inflammatory function, these observations suggest that the presence of uridine nucleobases is a key element in the immune recognition of RNA. Thus, it follows that the presence of certain U-rich miRNAs in circulation–such as those released following polytrauma and identified in our study–may function as triggers of innate immune activation.

3.3.3 Production of Inflammatory Cytokines and Activation of the Complement System by miRNAs in BMDMs is TLR7 Dependent

We next performed studies to identify the cellular sensor responsible for miRNA-induced inflammation. Among TLRs known to sense nucleic acids in mice, TLR7 has been implicated sequence-dependent detection of single-stranded RNA oligonucleotides in functional[60,108–110] as well as structural studies[51,107,111]. Taking cues from earlier studies demonstrating the critical role of TLR7 in miRNA-induced inflammatory responses[77,79], BMDMs from WT, TLR3$^{-/-}$ & TLR7$^{-/-}$ mice were isolated and treated with several miRNAs and TLR ligands to demonstrate that miRNA-induced inflammatory responses are indeed TLR7-dependent.

Genetic deletion of TLR7 singularly resulted in complete abolishment of complement factor B (FB) and cytokine production in response to all miRNAs and R837, a TLR7-specific ligand (Figure 37). In contrast, WT and TLR3$^{-/-}$ macrophages—which both retain TLR7—responded to R837 and miRNA of high-%U (≥40) by augmenting CFB and MIP-2 production as expected. Furthermore, in agreement with previous experiments described above, miRNAs of low- and moderate-%U did not induce either cytokine or FB production. Additionally, as expected, genetic deletion of TLR3, the ds-RNA sensor, resulted in a mild suppression of FB production (Figure 37A) and an abrogation of cytokine production (Figure 37B) when treated with polyinosine-polycytidylic acid [Poly-(I:C), a synthetic ds-RNA]; these cells nevertheless responded to other miRNAs and other TLR ligands, as described above. Finally, preservation of inflammatory responses to Pam3Cys (TLR2 ligand) and Poly-(I:C) (TLR3 ligand) affirmed the vitality of macrophages in all cell lines.

Hence, this *in vitro* loss-of-function study demonstrates that innate immune activation—as measured by cytokine and FB production—provoked by miRNA with high %U is TLR7 dependent.

3.3.4 miRNA-induced Inflammation is Competitively Inhibited by a Novel Ribonucleotide-based TLR7 Antagonist

Based on our empirical data and structural studies describing the purported binding mechanism of oligonucleotides to TLR7, we developed a novel ribonucleoside-based antagonist of TLR7. Termed MD1, this molecule was designed to annul miRNA/TLR7-mediated immune activation by binding to but failing to activate the receptor.

To first establish its inhibitory capacity, MD1 was tested in BMDM culture alongside miRNA previously shown in this study to be highly immunostimulatory. To wit, coadministration of 500nM of MD1 potently reduced the cytokine production in BMDMs induced by let-7j, miR-145a-5p, and -146a-5p (Figure 38), while itself having no immunostimulatory property. The robust suppression of a cytokine response by MD1 to multiple ss-miRNAs of varying sequences suggested that this was unlikely to be a complementary-strand effect; rather that MD1 was acting at the confluence of the ligand-receptor interface.

As MD1 displayed characteristics of competitive antagonism suggesting direct binding to TLR7, we sought to further establish MD1 functionality in immune cell culture. Creation of median inhibitory concentration (IC_{50}) curves was accomplished by cotreatment of increasing doses of MD1 with several immunostimulatory oligonucleotides (50nM: let-7j, miR-146a-5p & “miR-combo”). Indeed, MD1 reduced–and in some cases nearly

abolished–the induction of IL-6 production in macrophage culture, demonstrating unambiguously that MD1 acts as a potent antagonist of miRNA-induced inflammatory responses (Figure 39). Indeed, even at a 5-fold lower molar concentration (50nM vs. 10nM), MD1 achieved over 50% suppression of IL-6 induced by let-7j, Trauma-combo, and Sepsis-combo.

Finally, to demonstrate the specificity of action at TLR7, MD1 was coadministered in BMDMs alongside several TLR agonists. As expected, MD1 only inhibited the response provoked by R837, a well-defined TLR7 agonist, while the cytokine production by Pam3Cys, LPS, and CpG was not disrupted by MD1 (Figure 40). Secondarily, appropriate cytokine responses of BMDMs to other TLR agonists but not R837 indicates that MD1 provides specific and potent inhibition without causing cellular dysfunction or death.

Together, these data demonstrate the effectiveness and potency of MD1 as a novel TLR7-specific antagonist, capable of suppressing and eliminating RNA- and miRNA-induced immune responses *in vitro*.

3.3.5 Summary of Section 3.3

From a list of various miRNAs identified as being either highly upregulated or abundant, we found that certain miRNA species trigger potent pro-inflammatory responses in *in vitro* macrophage culture. Additionally, miRNA isolated from plasma samples derived from polytrauma mice were observed to be intrinsically pro-inflammatory. Characteristic properties of these pro-inflammatory miRNAs, such as potency, were noted to be related to their nucleotide composition to the extent that miRNAs with a high uridine content

(%U > 40) were all immunostimulatory. Furthermore, using a loss-of-function approach, we confirmed that miRNA induce pro-inflammatory responses via the single-stranded ribonucleotide sensor TLR7. Finally, we investigated the specificity of miRNA-induced pro-inflammatory responses via TLR7 by demonstrating the abrogation of miRNA-induced proinflammatory responses using a novel ribonucleotide-based TLR7 antagonist (MD1) specifically designed to block miRNA-TLR7 specific ribonucleotide interactions.

Table 6. Single-stranded miRNA mimics used in this study.

Rank list ordered by uridine residue content per miRNA.

% = #uridine / # of total nucleotides in miRNA x 100%

miRNA	Sequence (5' - 3')	Length (nt)	Uridine # (%)	Stratify by %U
let-7j	UGAGGUAUUAGUUUGUGCUGUUAU	24	12 (50)	High (≥40)
mir-142a-3p	UGUAGUGUUUCCUACUUUAUGGA	23	11 (48)	
mir-7a-5p	UGGAAGACUAGUGAUUUUGUUGU	23	10 (43)	
let-7b	UGAGGUAGUAGGUUGUGUGGUU	22	9 (41)	
mir-34a-5p	UGGCAGUGUCUUAGCUGGUUGU	22	9 (41)	
mir-145a-3p	AUUCCUGGAAAUACUGUUCUUG	22	9 (41)	
mir-122-5p	UGGAGUGUGACAAUGGUGUUUG	22	8 (36)	Moderate (≥20 to <40)
mir-146a-5p	UGAGAACUGAAUUCCAUGGGUU	22	7 (32)	
mir-802-5p	UCAGUAACAAAGAUUCAUCCUU	22	7 (32)	
mir-451a	AAACCGUUACCAUUACUGAGUU	22	7 (32)	
mir-126a-3p	UCGUACCGUGAGUAAUAAUGCG	22	6 (27)	
mir-374b-5p	AUAUAAUACAACCUGCUAAGUG	22	6 (27)	
mir-192-5p	CUGACCUAUGAAUUGACAGCC	21	5 (24)	
mir-22-3p	AAGCUGCCAGUUGAAGAACUGU	22	5 (23)	
mir-210-3p	CUGUGCGUGUGACAGCGGCUGA	22	5 (23)	
mir-345-3p	CCUGAACUAGGGGUCUGGAGAC	22	4 (18)	Low (<20)
mir-1947-5p	AGGACGAGCUAGCUGAGUGCUG	22	4 (18)	
mir-193b-3p	AACUGGCCCACAAAGUCCCGCU	22	3 (14)	

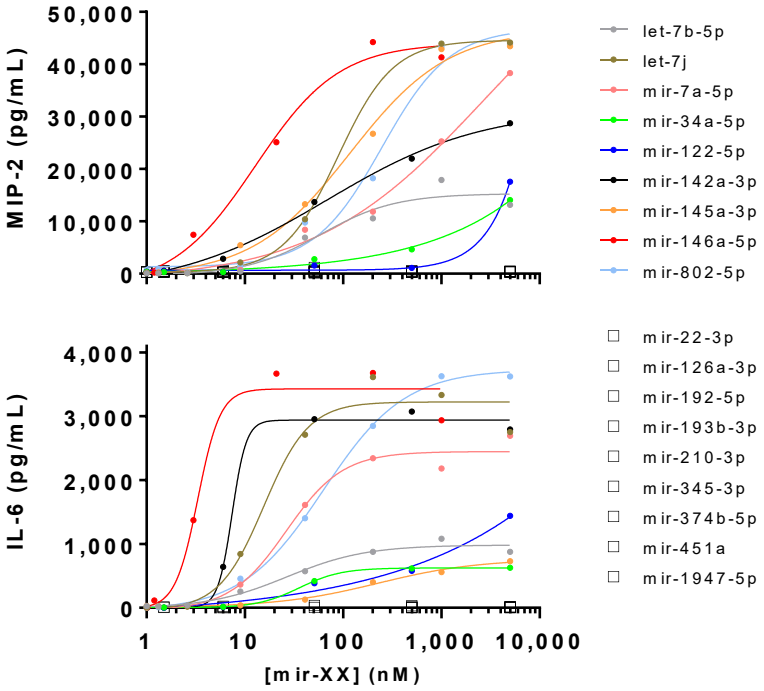

Figure 31. Uridine-rich miRNAs differentially induce cytokine and inflammatory responses in BMDMs.

Treatment of bone marrow-derived macrophages (BMDMs) with single stranded synthetic miRNAs induces variable dose-dependent production of MIP-2 and IL6; □ = no cytokine production up to 5000nM.

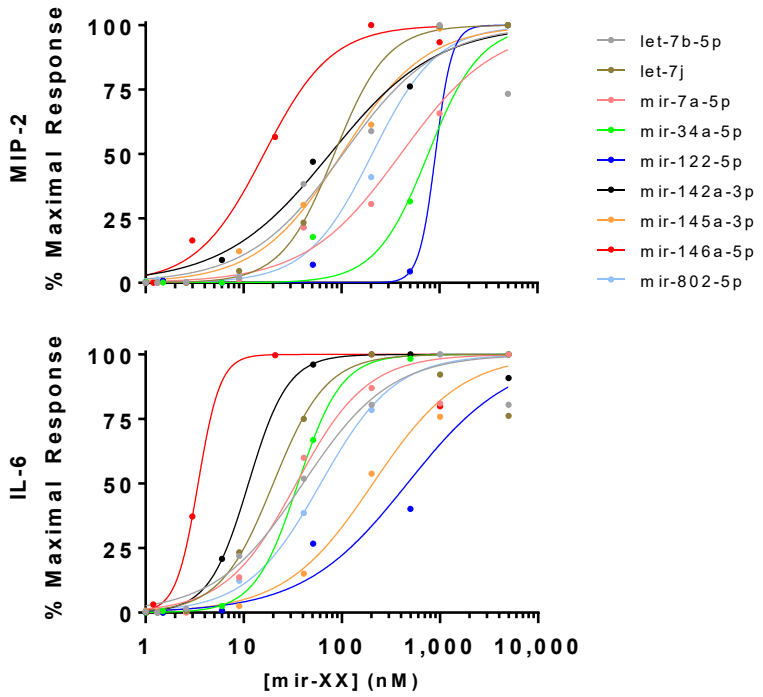

Figure 32. Estimation of miRNA EC_{50} from normalized dose response curves in BMDMs.

Illustration of MIP-2 and IL-6 normalized dose response curves used to determine relative miRNA EC_{50} (median effective concentration) of immunostimulatory miRNAs. An estimate of 0% is defined as Lipofectamine only (no miRNA) and 100% defined as the maximal achievable response. Each curve represents a minimum of 5 concentrations performed in triplicate wells.

Table 7. Relative miRNA EC_{50} for immunostimulatory miRNAs

miRNA	% Uridine	EC_{50}	95% CI
let-7j	50	84.4	68.9 - 103.3
mir-142a-3p	48	76.4	44.0 - 132.6
mir-7a-5p	43	402.0	227.7 - 710.0
let-7b	41	103.3	39.9 - 267.7
mir-34a-5p	41	767.0	336.0 - 1751.0
mir-145a-3p	41	100.7	72.1 - 140.6
mir-122-5p	36	912.5	0.0 - 3E+16
mir-146a-5p	32	16.2	11.2 - 23.4
mir-802-5p	32	205.5	130.7 - 323.1

Relative EC_{50} was calculated using a 4-parameter logistic model (4PL) solved for parameter *c*, presented as estimated EC_{50} and 95% confidence interval.

[%U = #uridine / miRNA sequence length x 100%]

EC_{50} = 4PL curve, solved for parameter *c*, given: $Y = \frac{a-d}{1+(X/c)^b} + d$, where Y is the response and X is the concentration.

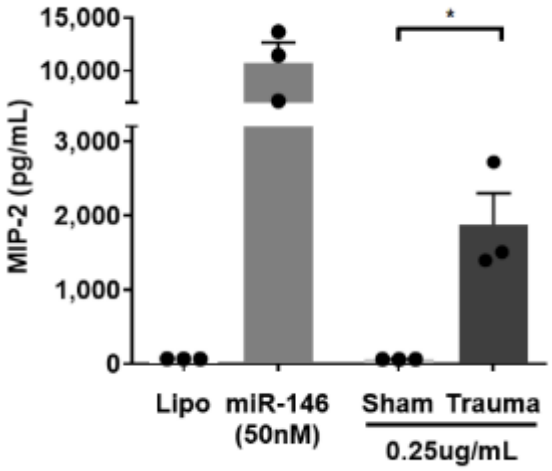

Figure 33. RNA released into circulation following polytrauma is immunostimulatory.

Endogenous RNA isolated from plasma of Trauma mice induces cytokine production but equivalent doses of RNA from sham mice does not.

Lipo=lipofectamine transfection agent, miR-146=positive control. *P<0.05

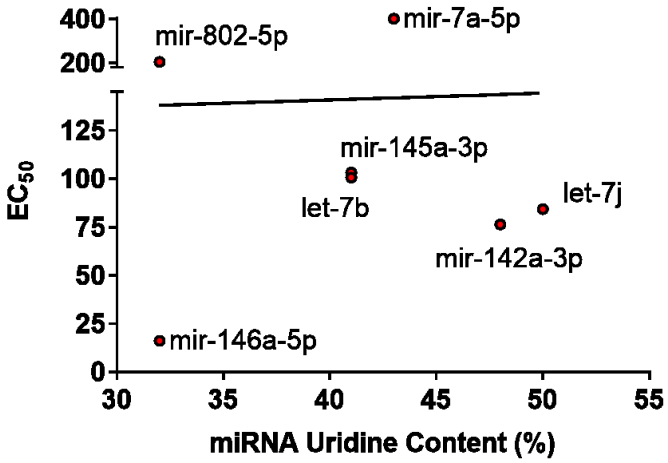

Figure 34. Uridine content of miRNAs is unrelated to its immunostimulatory potency (EC_{50})

Correlation analysis between %U and the median effective concentration (EC_{50}, as determined by dose-response curves) demonstrates no relationship (R^2= 0, p=0.9676).

Table 8. Binary classification schemata for miRNAs used in %U analyses.

Synthetic ss-miRNAs, rank list-ordered by % uridine below, were tested at effective doses of 50nM in BMDM culture. miRNAs capable of inducing both MIP-2 and IL-6 were classified as "inflammatory" (left, n=18) while the absence of a cytokine response were classified as "non-inflammatory" (right, n=15).

Uridine content = (#Uridine nucleobase / miRNA length x 100%)

miRNA	Uridine (%)	Inflammatory?
let-7j	50	Y
mir-142a-3p	48	Y
miR-7a-5p	43	Y
miR-145a-3p	41	Y
let-7b	41	Y
mir-34a-5p	41	Y
miR-181d-5p	39	Y
miR-215-3p	38	Y
mir-122-5p	36	Y
miR-186-5p	36	Y
miR-25-3p	36	Y
miR-382-5p	36	Y
miR-26b-5p	33	Y
miR-802-5p	32	Y
mir-145a-5p	32	Y
miR-133a-3p	32	Y
miR-146a-5p	30	Y
miR-208a-3p	18	Y
		n=18

miRNA	Uridine (%)	Inflammatory?
mir-499-5p	43	N
miR-144-3p	35	N
miR-144-5p	35	N
miR-451a	32	N
mir-1a-3p	32	N
miR-374b-5p	27	N
miR-126a-3p	27	N
mir-150-5p	27	N
mir-26a-5p	27	N
miR-192-5p	24	N
mir-210-3p	23	N
miR-22-3p	23	N
miR-345-3p	18	N
miR-1947-5p	18	N
miR-193b-3p	14	N
		n=15

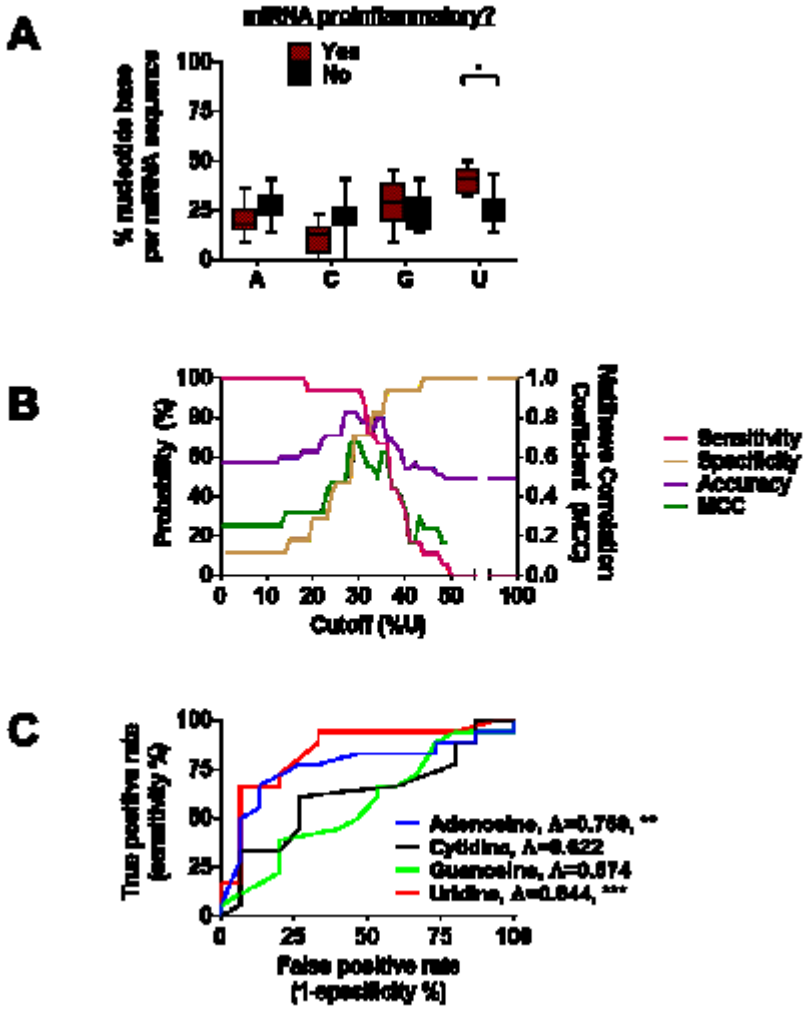

Figure 35. Uridine-rich miRNAs differentially induce cytokine responses in BMDMs.

(A) miRNAs that induce pro-inflammatory cytokine responses at 50nM in BMDMs contain more uridines per sequence length than non immunostimulatory miRNAs. (B) Graphical representation of probability densities of sensitivity, specificity, accuracy, and Matthew's correlation coefficient calculated at each %U cutoff. (C) Receiver operating characteristic (ROC) evaluating discriminatory power of %nucleobase, corresponding to values in Table 9.

%nucleotide = #nucleotide / miRNA sequence length x 100%; A = Adenine, C = Cytosine, G = Guanine, U = Uracil; Λ=Area under the curve (AUROC); **P<0.01, ***P<0.001, ****P<0.0001

Table 9. AUROC (Area under the receiver operating characteristic) curve analysis.

	Adenosine	Cytidine	Guanosine	Uridine
Area under the curve (AUC)	0.769	0.622	0.574	0.844
95% CI	0.597-0.940	0.427-0.818	0.375-0.773	0.701-0.988
P value	0.0088	0.2328	0.4696	0.0008
Non-inflammatory (n=)	15	15	15	15
Pro-inflammatory (n=)	18	18	18	18

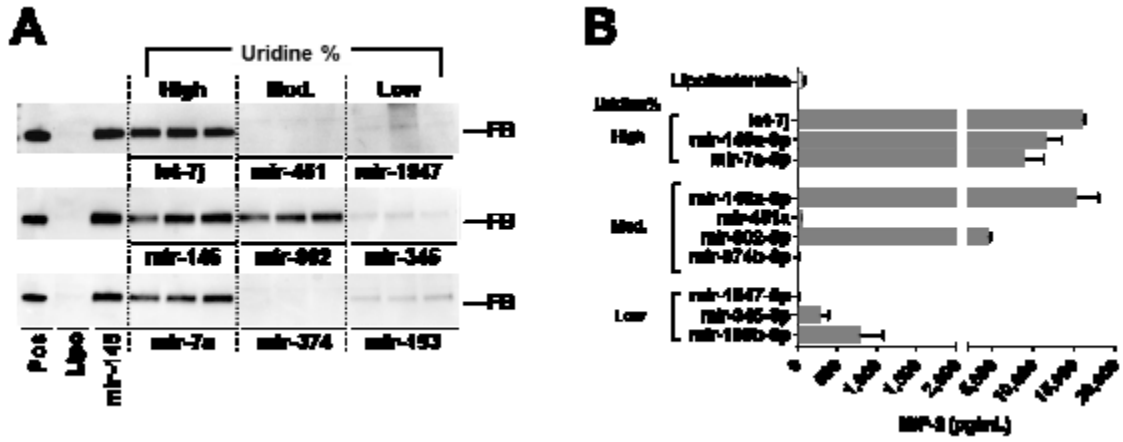

Figure 36. Uridine rich miRNAs induce pro-inflammatory responses in BMDMs

(A) Medium cfB protein (95kDa) detected by Western blot and (B) MIP-2 by ELISA following treatment of BMDMs with lipofectamine or ss-miRNA (50nM) for 16h

FB=complement factor B, Lipo=lipofectamine, Pos=plasma; High, %U≥40, Mod 40<%U≥20-39, Low %U<20.

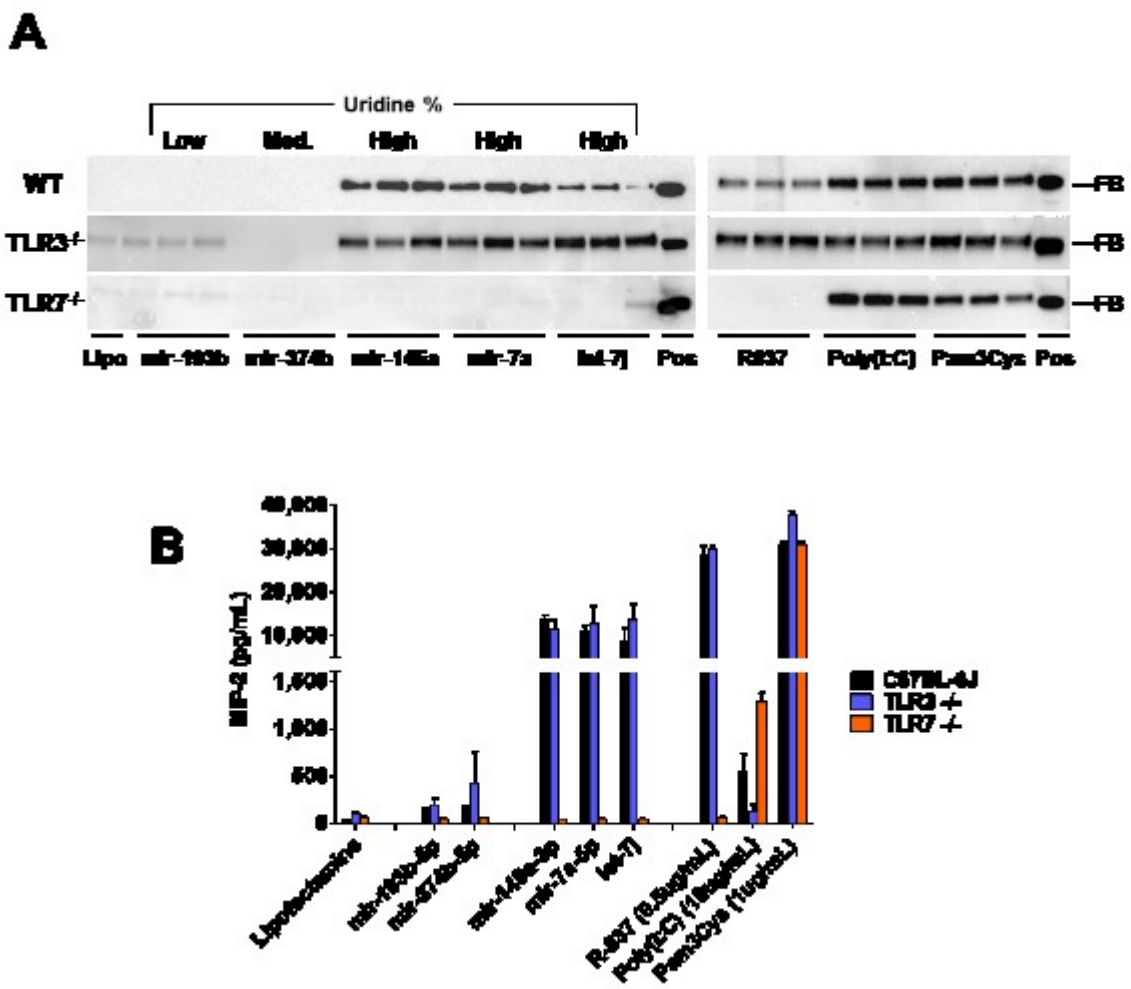

Figure 37. Uridine rich miRNAs induce pro-inflammatory responses via a TLR7 dependent mechanism

(A) Effect of miRNA and TLR ligands on cFB protein production in WT, TLR3-/-, and TLR7-/- BMDMs. Cells were treated with miRNA mimics (50nM), R837 (0.5µg/mL, TLR7 ligand), Poly(I:C) (10µg/mL, TLR3 ligand) or Pam3Cys (1µg/mL) for 16h and medium proteins immunoblotted for cfB and (B) MIP-2 concentration measured from the medium.

FB=complement factor B, Lipo=lipofectamine, Pos=plasma; High, %U≥40, Mod 40<%U≥20-39, Low %U<20

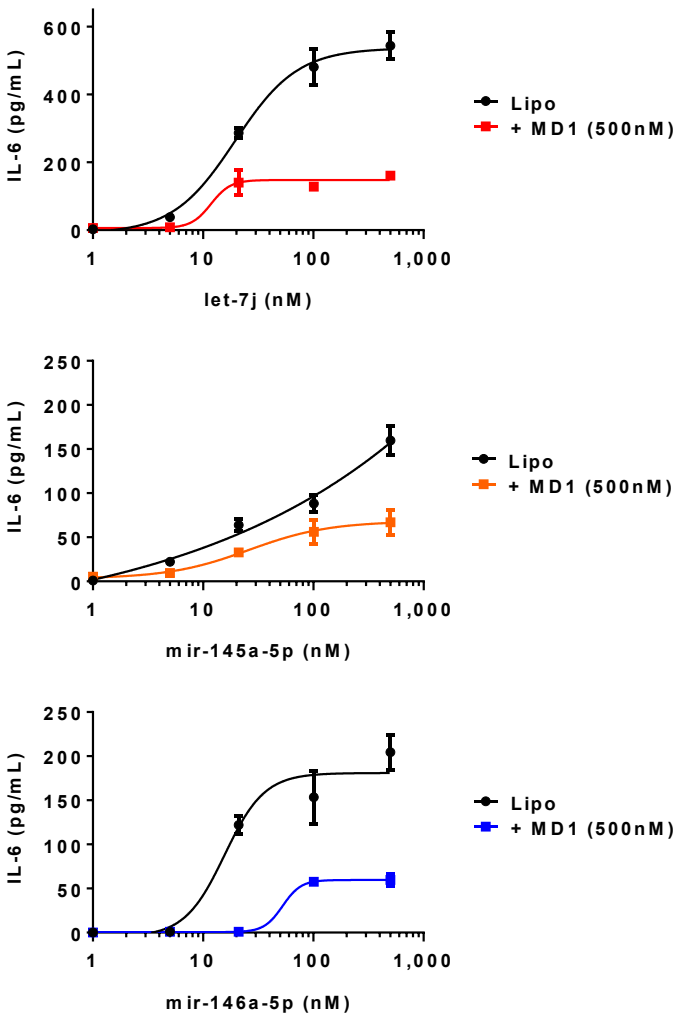

Figure 38. MD1 suppresses miRNA-induced inflammatory responses.

Cotreatment of let-7j, mir-146a-5p, and mir-145a-5p with a fixed 500nM dose of MD1 produces a rightward EC_{50} curve shift and decrease in maximal cytokine response.

Lipo=lipofectamine

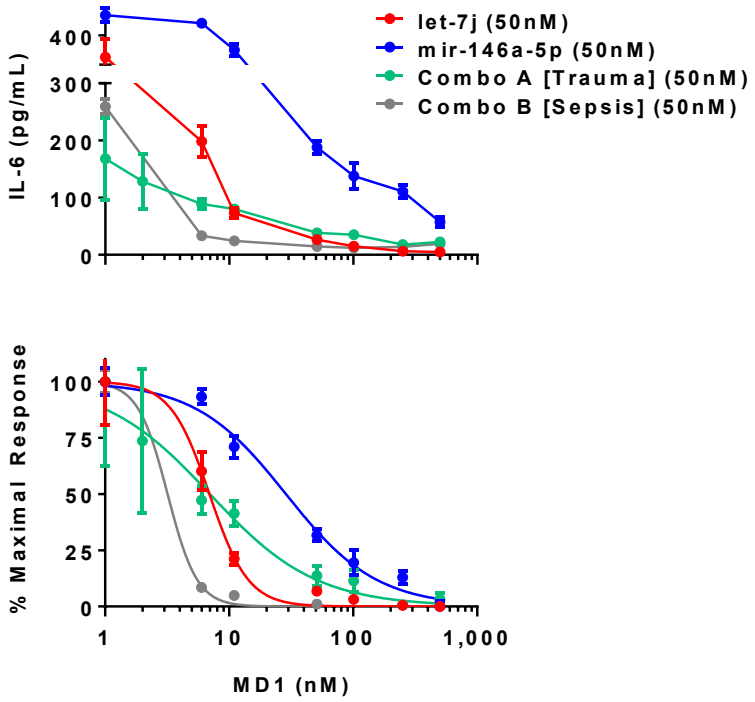

Figure 39. MD1 competitively inhibits miRNA-induced inflammatory responses

IC_{50} dose response curves demonstrate MD1 inverse agonist activity (inhibition) on fixed doses of miRNAs: increasing the concentration of the inhibitor reduces cytokine production induced by 50nM of various pro-inflammatory miRNAs

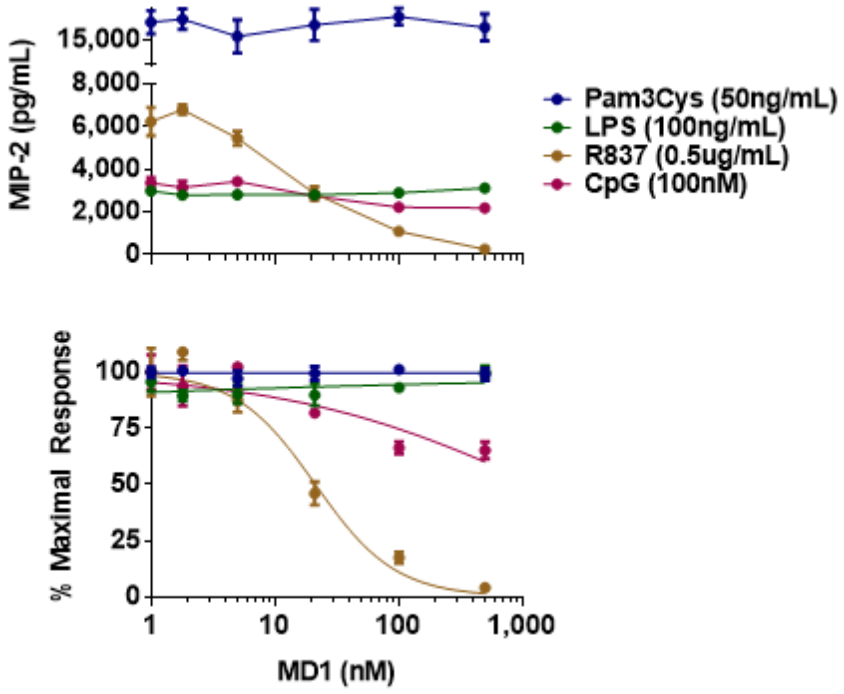

Figure 40. MD1, a novel TLR7 antagonist, competitively inhibits miRNA-induced inflammatory responses.

MD1 selectively inhibits R837 (TLR7 agonist) but does not significantly alter nor inhibit Pam3Cys- (TLR2 agonist), LPS-(TLR4 agonist), or CpG-(TLR9) induced cytokine production.

3.4 miRNA Induces an Immune Response *in vivo* Through TLR7

To demonstrate the *in vivo* effects of miRNA on the innate immune system, miRNA mimics were administered into a subcutaneous air pouch generated on the dorsum of a mouse. This model, created originally as a model of synovial inflammation, was chosen as it provides a simple method of testing injectates within an *in vivo* environment, thus allowing the evaluation of *in vivo* responses to miRNAs. The air pouch, lined primarily with macrophage- and fibroblast-like cells, behaves similarly to a synovial cavity in response to injection of irritants[112], and has an ability to generate a large enough volume of exudate to enable the measurement of multiple inflammatory endpoints[83]. Upon injection of varying substances into the pouch, the resultant *in vivo* inflammatory reactions—or absence thereof—can be assessed by characterizing the resultant infiltration of cells and the production of pro-inflammatory markers.

In the following experiments, the *in vivo* response to exogenously administered miRNAs was determined by collecting the contents of pouch by lavage and aspiration twenty-four hours following injection of a miRNA or saline test solution, which was subsequently analyzed by fluorescence activated cell sorting (FACS) flow cytometry.

3.4.1 miRNA Induces a Dose-dependent Recruitment of Immune Cells Into an Air Pouch

Injection of increasing amounts of let-7j miRNA induces a marked dose-dependent increase of cells within the air pouch. As compared to the vehicle control (Lipofectamine), both 5ug and 20ug of miRNA produce an increase in cell infiltration to the air pouch at 24h of nearly two- and three-fold higher, respectively (Figure 41A).

FACS analysis of the composition of the immune cell populations ($CD45^+$) cells demonstrated that as compared to lipofectamine injections alone, miRNA produces a marked increase in the proportions of neutrophils ($Ly6G^+$ / $F4/80^-$ cells) and a mild increase in macrophages ($Ly6G^-$ / $F4/80^+$ / $Ly6C^-$ cells), while a corresponding decrease in the proportion of monocytes is observed. Additionally, the absolute number of monocytes ($Ly6G^-$ / $F4/80^+$ / $Ly6C^+$ cells) tended not to differ significantly (Figure 41AB), suggesting that while the proportion of monocytes appears to decrease, no significant recruitment of monocytes is observed at 24h.

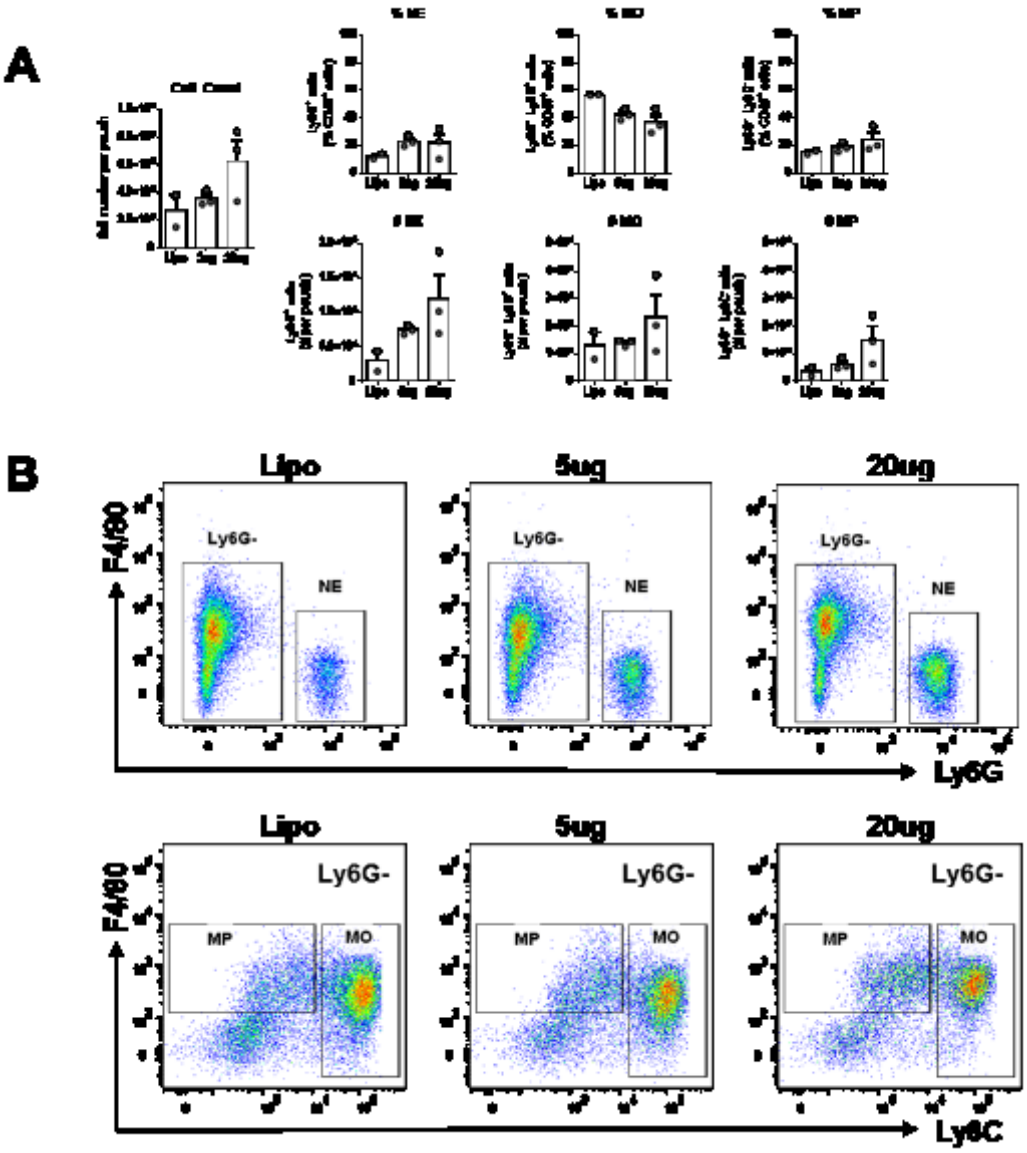

Figure 41. Immune cell recruitment into the air pouch following let-7j is dose dependent

CHAPTER 4. DISCUSSION

4.1 FROM TRAUMATIC INJURY TO TLR7-DEPENDENT IMMUNE ACTIVATION BY CIRCULATING EXTRACELLULAR MIRNAS

4.1.1 Modelling Acute Traumatic Injury and Shock

This study comprehensively evaluated the role of host miRNAs released into circulation during severe traumatic injury. We first sought to generate a model of severe polytraumatic injury that simulated massive tissue and cellular injury that reflects real-world trauma situations. To do so, a murine polytrauma model of traumatic shock was developed to produce a multisystem injury pattern that reflects combat situations with casualties from explosive devices: of note, in addition to direct tissue and bone injury to extremities from direct exposure to high energy explosives and fragmentation, victims of blast injuries present with non-penetrating injury to hollow viscera. Injury to bowel is chiefly characterized by ischemic injury from either hypotension or direct disruption of mesenteric vessels and tissues resulting from blast overpressure waves that propagate through the abdominal wall and solid organs[86], with or without reperfusion following resuscitation to correct systemic hypotension.

Our polytrauma model achieved the goal of approximating this clinical situation using a combination of bowel I/R, long bone fracture, and tissue injury. This effectively produced a reproducible clinical state of shock, significant direct organ injury, and remote end-organ injury to the kidney, liver, and lungs.

4.1.2 Traumatic Injury Can be Defined by Patterns of Nucleic Acid and miRNA Release Into Circulation

Using our novel animal model, we next identified that polytrauma can produce unique circulating miRNA expression profiles. This is an observation that is consistent with numerous other studies that have documented the roles of circulating miRNAs as circulating biomarkers to define various disease states such as myocardial infarction[106], SIRS,[74] and sepsis[100,113]. For example, in a study of experimental sepsis induced by CLP, levels of many miRNA such as miR-145-5p, -122-5p, -146a-5p, -34a-5p, and -210-3p are clearly elevated in septic mice compared to controls[77], suggesting that expression profiles of miRNAs are potentially indicators of an increasingly complex pathology.

Similarly, patterns of miRNA differential expression have been studied in severely injured patients, suggesting potential correlations between miRNAs and key clinical outcomes such as survival, acidosis, and transfusion requirements[67,68,114]. However, as these studies are largely descriptive and simply provide observations about the relative presence of individual miRNAs–i.e. expression patterns–they do not provide direct causal evidence regarding the specific function of miRNAs. Consequently, there is limited evidence as to how a miRNA's up- or down-regulation may initiate or perpetuate the complex post-injury inflammatory state that is thought to lead to poor clinical outcomes and the development of multiple organ failure. Inflammation and immune activation associated with injury is widely recognized to be essential for physiological initiation of repair and activation of immune surveillance following traumatic injury to tissues[2,4,33,115], however, overwhelming injury (i.e. "trauma load") to the host can precipitate significant morbidity from overzealous and inappropriate activation of the immune system leading to

a systemic inflammatory response (SIRS) and subsequent multiple organ dysfunction (MODS)[8,116]. While there has been a recognition of secondary post-traumatic hyperinflammatory state that significantly increases mortality[2,68] and correlates with the severity of injury[117], the immunopathology behind the processes that lead to an inappropriately high inflammatory response remains unclear.

4.1.3 Inflammatory Responses in Trauma Occur via miRNA-mediated TLR7-dependent Immune Activation

As alluded to earlier, our efforts to identify the unique role of circulating miRNAs in modulating the inflammatory response following traumatic injury stems from previous studies that observed that certain nucleic acids released during tissue and cellular damage trigger immune responses like cytokine or complement factor production[76–78,109]. These studies have also demonstrated that systemic RNase (but not DNase) administration reduces the burden of miRNA-induced injury in murine models of myocardial injury[106] and sepsis[77], and that genetic deletion of TLR7, the ssRNA sensor, improves sepsis outcomes. These data, along with our own observations in this study, support the notion that miRNAs released into circulation as a result of cellular damage, apoptosis, or necrosis, are key pro-inflammatory damage-associated molecular patterns that have an unique ability to initiate intracellular signaling pathways via TLR7, thereby leading to a robust activation of the immune system and the production of inflammatory cytokines.

To address to the paucity of evidence in defining the role of extracellular miRNA in trauma, we turned to explore the putative miRNA→TLR7-mediated immune activation cascade. Our initial observations demonstrated that the polytrauma model generated a

massive acute inflammatory response, which reflects the expected course of innate immune activation following a traumatic insult.

Through our investigations into the role of miRNA in trauma-induced immune activation, we first were able to establish that miRNAs are abundantly found in circulation following trauma. Our experiments then demonstrated that polytrauma-derived miRNAs are highly immunostimulatory insofar as their ability to induce strong pro-inflammatory responses as compared to sham-derived miRNAs. Subsequent testing of a subset of miRNAs abundantly found in polytrauma led to the finding that certain miRNAs exhibit unique immunostimulatory properties that appear to be governed in part by their nucleotide content: namely, % uridine. Finally, to establish putative mechanisms by which extracellular miRNA interact with the immune system, we showed that miRNA induce proinflammatory effects via a TLR7-dependent mechanism by using an *in vitro* TLR7 genetic knockout approach.

4.1.4 Insights Into TLR7 to Ligand Interactions: Uridine Ribonucleotide Content Predicts a miRNA's Immunogenicity

Among the many sensors located on immune cells serving pathogen- and damage-sensing functions, we focused on TLR7 as a key candidate for our study due to its established purpose of recognizing single-stranded RNA molecules[52,58,107,118,119]. Despite the exact mechanism of RNA recognition by TLR7 not being known, prior groups have established that TLR7 is uniquely a dual receptor for ssRNA and guanosine[51,107,120]. Specifically, Zhang et al. elegantly demonstrated that TLR7 dimerization initiated by ligand-protein interactions of guanosine or guanosine-like chemical analogues was synergistically activated by poly-UUU oligonucleotides at a spatially distinct uridine-sensing site[107],

suggesting that ssRNA containing uridine is not sufficient to induce the activation of TLR7 but can enhance the affinity of TLR7 for guanosine and thus its activation. Furthermore, the sequence specific recognition by TLR7 is supported our observations that ssRNAs containing uridine are an important feature for recognition by immune cells. We[79] and others[58,121,122] have previously demonstrated that the effect of substituting uridine bases for adenosines (U→A) in a miRNA sequence will nearly completely abrogate the immunostimulatory properties of a particular miRNA. Importantly, these data are supported by the landmark structural analysis revealing that the recognition of uridine by TLR7 occurs at the dimerization interface between the two monomer subunits within a "uridine pocket" that involves a total of **nine** (9) hydrogen bonds, including four (4) specific to uridine and five (5) specific to ribonucleic acids [107]. Correspondingly, the clearly defined importance of uridine binding to TLR7 directly reflects our observations that the pro-inflammatory properties of miRNAs are reflected by their uridine content (AUROC = 0.844). Indeed, quantitative measures of test performance indicated that maximum accuracy is achieved by choosing a %U cutoff of 28-30% (Sensitivity 94%, specificity 71%, Accuracy 83%, MCC 0.673).

4.1.5 Antagonism of miRNA-TLR7 Interactions Effectively Inhibits Immune Activation

One of the most interesting observations derived from our study was the finding that miRNA induced TLR7 activation is suppressed by the novel TLR7 antagonist, MD1. This compound, developed based on inferences of the miRNA-TLR7 binding dynamics, was designed to obstruct the miRNA-TLR7 binding interaction. To our amazement, MD1

potently abrogated the proinflammatory immune response to several highly proinflammatory miRNA.

Caveat lector: as development of MD1 currently remains in preliminary stages, the following discussion will primarily examine the rationale and approaches taken in developing MD1; the reader is cautioned that only an incomplete picture is provided since further data is forthcoming.

Several other groups have investigated the incorporation of 2'-O-methylation into the sense strand of small interfering RNAs (siRNAs) and have observed that 2'-O-methyl-modified RNA act as potent antagonists of immunostimulatory RNAs[122–124]. Despite these interesting observations, a recent search of the literature failed to uncover any follow-up studies that have further investigated the antagonist-like properties of these modified siRNA. Perhaps owing to the fact that the primary aims of their studies was to reduce the immunogenicity of siRNA compounds under development, these groups ultimately concede that the mechanism behind these antagonistic effects remain incompletely understood.

In our hands, our approach to developing a novel TLR7 antagonist originated from several key findings. First, in this study and several others, we observed that miRNA with higher uridine content exhibit greater immunostimulatory potential. Secondly, we previously reported that uridine to adenine nucleobase substitution (U→A) completely abrogated a miRNA's proinflammatory properties[77]. Finally, recent structural analyses of TLR7 revealed the presence of uridine recognition pockets located upon the TLR7 receptor[107,111]. Based on these data, several inferences were made regarding the likely

ligand-receptor interactions, from which we generated a novel ribonucleotide-based compound–MD1–that targeted each of these features.

The inhibitory capacity of the resultant compound (MD1) was demonstrated by coadministration of MD1 with various immunostimulatory miRNA. We observed a potent reduction in cytokine production using both fixed- and varying- dose-response curves (EC_{50}, Figure 38; IC_{50}, Figure 39; respectively). Additionally, we also observed that MD1 abolished the cytokine response in BMDMs to the TLR7 agonist compound R837 in a dose-dependent manner (Figure 40). These same experiments also revealed that the cytokine response is spared when MD1 is co-administered alongside TLR2/4/9 agonists, indicating the preservation of common downstream TLR signaling pathways. Together, these data, while incomplete, suggest that MD1 is a highly effective and potent antagonist of TLR7 as it produces dose-dependent decreases in inflammatory responses induced by TLR7-directed immunostimulatory agents such as miRNA.

While these results strongly suggest that MD1 acts as an inhibitor of TLR7, it must be noted that the use of MD1 as an immunomodulatory compound is highly speculative. Several defining pharmacological attributes of MD1 remain undetermined, such as the mechanism of action and the ligand-receptor binding affinity. These features are partially addressed by careful analysis of the shift and shape of the EC_{50} dose response curve, which inconclusively suggests a mixed competitive and non-competitive antagonism: both the magnitude of the maximal response is depressed while the EC_{50} is shifted (Figure 38). In fact, this is generally consistent with the expected *in vitro* behaviour predicted from *a priori* biochemical structural design considerations of MD1, however, additional experiments are needed to define these characteristics. Nevertheless, the lack

of comprehensive data currently precludes a definitive assertion regarding the mechanism of action. For example, two possibilities to explain the observed inhibitory effects of MD1 include orthosteric and allosteric antagonism; defined, respectively, as competitive antagonism via binding either directly at the ligand-binding site or at a remote site on the receptor.

Ultimately, these final experiments–culminating in the development of a TLR7 antagonist derived from a synthesis of results arising from an enquiry of the interplay between polytrauma-associated miRNA and TLR7–conclude the investigation into the role of endogenous circulating miRNA in trauma-associated immune system activation.

4.2 Significance of Findings

We evaluated the hypothesis that traumatic injury leads to a rise in a group of miRNAs in the blood that play key roles in trauma-induced systemic inflammatory injury. Our study revealed that trauma induces a massive release of miRNA into circulation, and that the single strand nucleic acid recognition receptor TLR7 is robustly stimulated by miRNAs upregulated in trauma, particularly by those with a high uridine content.

The importance of our findings are twofold: they clarify the roles of miRNA in the activation of the immune system following traumatic injury, and they suggest a means by which activation of the immune system can be modulated by antagonism of the cellular receptor of miRNA.

4.2.1 Modifying Immune System Responses to miRNA

The finding that circulating miRNA is found in abundant quantities following trauma along with the evidence that extracellular miRNA are strong drivers of a proinflammatory response implies that the hyperinflammatory immune response seen following traumatic injury is due, in part, to activation of the immune system in response to cellular and tissue injury. As the extracellular presence of substantial quantities of nucleic acids, including miRNA, is not normally seen in non-injured individuals, this suggests that in the process of extracellular release of miRNA following injury, these miRNAs can be trafficked to and act on immune cells in an endocrine fashion. This has the effect of generating remote immune activation and thus injury far from the original site of inflammatory response.

While the concept that remote organ injury occurring far from where the primary injury has occurred is not new, our findings suggest an additional mechanism by which organ injury may be due to the sequelae of the hyperinflammatory response to circulating miRNAs.

It seems clear that an excessive hyperinflammatory response can generally be viewed as being pathognomonic of a dysregulated immune system, which is known to precipitate multiple organ dysfunction and failure[2]. Thus, it follows that the ability to modulate the immune response and avoid an unrestrained hyperinflammatory response can clearly be seen as being a valuable tool in the prevention of immune-mediated sequelae to injury. To this end, the discovery that MD1 diminishes that miRNA-mediated TLR7 activation potentially provides an alternative approach to modulating–i.e. reducing–the impact of miRNA-induced inflammatory injury. While admittedly the development of a truly useful TLR7 inhibitor will require significant additional work, that we have procured preliminary data demonstrating nearly complete abrogation of miRNA-induced cytokine

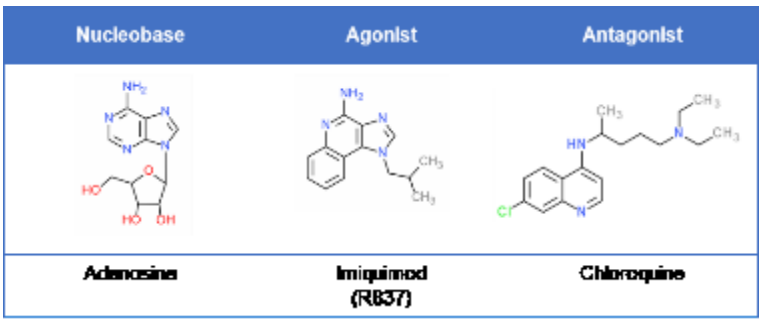

Figure 42. Selected nucleotide-based (Adenosine analogues) agonists (Imiquimod) and antagonists (Chloroquine) of TLR7

production indicates an enormous potential for MD1 stands to become a key therapy in minimizing the hyperinflammatory syndrome that undoubtedly would arise from with elevated RNA & miRNA extracellular.

Interestingly, several groups have developed similar ribonucleotide-based TLR7/8/9 immunomodulators in a pursuit to develop drugs that manipulate TLR signaling in various infectious, chronic inflammatory, and autoimmune disease states. Despite seemingly antithetical pharmacological strategies, both nucleobase analogue agonists and antagonists of TLR7 have successfully been used therapeutically as immune-directed medications (Figure 42). For example, chloroquine (and its analogue hydroxychloroquine of COVID-19 fame) has antitumoral and antiviral properties via inhibition of TLR7 & TLR9[125] signaling in addition to its antimalarial use, while Imiquimod (otherwise known as R837–used in this study) is in fact an TLR7 agonist that is an FDA approved drug prescribed as treatment of genital warts[126]. This historically successful development from nucleobase-derived immunomodulatory compounds into prescription drugs strongly conveys a sense of validity in the adoption of an immune modulation strategy, while also highlighting its marketability and feasibility.

As evidenced by the clinically efficacious use of TLR modulators such as chloroquine and Imiquimod, there is similarly potential for the use of novel TLR7 modulating compounds such as MD1 that target hyperinflammatory responses to injury. More importantly, recent developments during a global pandemic have highlighted the paucity of treatment options for a devastating viral infection that has wreaked havoc across nations. Early reports of this infection, termed the severe acute respiratory syndrome coronavirus 2 (SARS-CoV-2), have described a characteristic inflammatory storm seemingly caused by an amplified immune release and a massive release of inflammatory mediators and cytokines such as IL-6. Interestingly, coronaviruses belong to the phylogenetic family of single strand RNA viruses, which coincidentally are detected by the TLR7–the primary receptor of interest discussed in this work. This observation, while circumstantial and most certainly merely hypothesis generating, underscores the curious possibility that TLR7-directed immunotherapies may address the mounting public health issue at hand. Thus, our findings with respect to the roles of miRNA in TLR7 receptor activation as well our development of a TLR7 antagonist may be more appreciably applicable as the natural history of the SARS-CoV-2 cytokine storm is increasingly well defined; if not, at minimum, these findings may be useful in revealing clues as to the mechanisms of this deadly disease process.

4.3 Closing Remarks

We hope that this work provides a clear account of a novel experimental murine polytrauma model, characterization of miRNAs released following polytrauma, investigation into the putative mechanism of immune activation *in vitro* and *in vivo*,

preliminary evidence of a novel immunomodulatory TLR7 antagonist, and a sampling of potential areas to explore.

BIBLIOGRAPHY

1. Tremoleda JL, Watts SA, Reynolds PS, Thiemermann C, Brohi K. Modelling Acute Traumatic Haemorrhagic Shock Injury. *Shock*. 2017;48(6):610-623. doi:10.1097/SHK.0000000000000901

2. Hietbrink F, Koenderman L, Rijkers G, Leenen L. Trauma: the role of the innate immune system. *World J Emerg Surg*. 2006;1(15):1-1. doi:10.1186/1749-7922-1-15

3. DepartmentofDefense. Overall Casualties in OIF, OND, and OEF. 2017. https://www.defense.gov/casualty.pdf.

4. Keel M, Trentz O. Pathophysiology of polytrauma. *Injury*. 2005;36(6):691-709. doi:10.1016/j.injury.2004.12.037

5. Jagodzinski NA, Weerasinghe C, Porter K. Crush injuries and crush syndrome - a review. Part 2: the local injury. *Trauma*. 2010;12:133-148. doi:10.1177/1460408610372441

6. Simmons JW, Powell MF. Acute traumatic coagulopathy: Pathophysiology and resuscitation. *Br J Anaesth*. 2016;117:iii31-iii43. doi:10.1093/bja/aew328

7. Foëx BA. Systemic responses to trauma. *Br Med Bull*. 1999;55(4):726-743. doi:10.1258/0007142991902745

8. Manson J, Thiemermann C, Brohi K. Trauma alarmins as activators of damage-induced inflammation. *Br J Surg*. 2012;99(SUPPL. 1):12-20. doi:10.1002/bjs.7717

9. Kimura F, Shimizu H, Yoshidome H, Ohtsuka M, Miyazaki M. Immunosuppression following surgical and traumatic injury. *Surg Today*. 2010;40(9):793-808. doi:10.1007/s00595-010-4323-z

10. World Health Organization (WHO). *World Health Statistics 2019: Monitoring Health for the SDGs, Sustainable Development Goals.* Geneva; 2019.

11. Florence C, Haegerich T, Simon T, Zhou C, Luo F. Estimated lifetime medical and work-loss costs of emergency department–treated nonfatal injuries — United States, 2013. *Morb Mortal Wkly Rep*. 2015;64(38):1078-1082. doi:10.15585/mmwr.mm6438a5

12. National Trauma Institute. https://www.nattrauma.org/. Published 2018. Accessed May 24, 2018.

13. Centers for Disease Control and Prevention NC for IP and C. Years of Potential Life Lost (YPLL) Before Age 65. Web-based Injury Statistics Query and Reporting System (WISQARS). https://webappa.cdc.gov/sasweb/ncipc/ypll.html. Published 2017. Accessed February 22, 2020.

14. GBD 2017 Causes of Death Collaborators, Roth GA, Abate D, et al. Global, regional, and national age-sex-specific mortality for 282 causes of death in 195 countries and territories, 1980-2017: a systematic analysis for the Global Burden of Disease Study 2017. *Lancet*. 2018;392:1736-1788. doi:10.1016/S0140-6736(18)32203-7

15. MacLean M, Campbel l L, O'Connor T, et al. *Profile of Personnel Deployed to Afghanistan.* Veterans Affairs Canada; 2015.

16. U.S. Department of Defense. *Casualty Status*.; 2020.

17. Huber-Lang M, Lambris JD, Ward PA. Innate immune responses to trauma. *Nat Immunol*. 2018;19(4):327-341. doi:10.1038/s41590-018-0064-8

18. Mira JC, Cuschieri J, Ozrazgat-Baslanti T, et al. The epidemiology of chronic critical illness after severe traumatic injury at two level-one trauma centers. *Crit Care Med*. 2017;45(12):1989-1996. doi:10.1097/CCM.0000000000002697

19. Jacobsen J, Sofelt S, Sheikh S, Warberg J, Secher NH. Cardiovascular and endocrine responses to hemorrhage in the pig. *Acta Physiol Scand*. 1990;138(2):167-173. doi:10.1111/j.1748-1716.1990.tb08829.x

20. Barcroft H, Edholm O, McMichael J, Sharpey-Schafer E. Posthaemorrhagic fainting study by cardiac output and forearm flow. *Lancet*. 1944;243(6294):489-491.

21. Geerdes BP, Frederick KL, Brunner MJ. Carotid baroreflex control during hemorrhage in conscious and anesthetized dogs. *Am J Physiol - Regul Integr Comp Physiol*. 1993;265(1 34-1). doi:10.1152/ajpregu.1993.265.1.r195

22. Kirkman E, Watts S. Haemodynamic changes in trauma. *Br J Anaesth*. 2014;113(2):266-275. doi:10.1093/bja/aeu232

23. Little RA, Marshall HW, Kirkman E. Attenuation of the acute cardiovascular responses to haemorrhage by tissue injury in the conscious rat. *Q J Exp Physiol*. 1989;74:825-833.

24. Lenz A, Franklin GA, Cheadle WG. Systemic inflammation after trauma. *Injury*. 2007;38(12):1336-1345. doi:10.1016/j.injury.2007.10.003

25. Fry DE, Pearlstein L, Fulton RL, Polk HC. Multiple System Organ Failure: The Role of Uncontrolled Infection. *Arch Surg*. 1980;115(2):136-140. doi:10.1001/archsurg.1980.01380020006003

26. Moore FA, Sauaia A, Moore EE, Haenel JB, Burch JM, Lezotte DC. Postinjury Multiple Organ Failure: A Bimodal Phenomenon. *J Trauma - Inj Infect Crit Care*. 1996;40(4):501-510. doi:10.1097/00005373-199604000-00001

27. Nast-Kolb D, Aufmkolk M, Rucholtz S, Obertacke U, Waydhas C. Multiple organ failure still a major cause of morbidity but not mortality in blunt multiple trauma. *J Trauma - Inj Infect Crit Care*. 2001;51(5):835-842. doi:10.1097/00005373-200111000-00003

28. Durham R, Moran J, Mazuski J, Shapiro M, Baue A, Flint L. Multiple organ failure in trauma patients. *J Trauma*. 2003;55:608-616.

29. Jastrow KM, Gonzalez EA, McGuire MF, et al. Early Cytokine Production Risk Stratifies Trauma Patients for Multiple Organ Failure. *J Am Coll Surg*. 2009;209(3):320-331. doi:10.1016/j.jamcollsurg.2009.05.002

30. Hranjec T, Swenson BR, Dossett LA, et al. Diagnosis-Dependent Relationships between Cytokine Levels and Survival in Patients Admitted for Surgical Critical Care. *J Am Coll Surg*. 2010;210(5):833-844. doi:10.1016/j.jamcollsurg.2009.12.042

31. Kawai T, Akira S. The role of pattern-recognition receptors in innate immunity: update on Toll-like receptors. *Nat Immunol*. 2010;11(5):373-384. doi:10.1038/ni.1863

32. Kumar H, Kawai T, Akira S. Pathogen recognition by the innate immune system. *Int Rev Immunol*. 2011;30(1):16-34. doi:10.3109/08830185.2010.529976

33. Zedler S, Faist E. The impact of endogenous triggers on trauma-associated inflammation. *Curr Opin Crit Care*. 2006;12(6):595-601. doi:10.1097/MCC.0b013e3280106806

34. Roers A, Hiller B, Hornung V. Recognition of Endogenous Nucleic Acids by the Innate Immune System. *Immunity*. 2016;44(4):739-754. doi:10.1016/j.immuni.2016.04.002

35. Chao W. Inflammation and Heart Diseases: Role of Toll-Like Receptor Signaling. *J Anesth Perioper Med*. 2014;1:104-117.

36. Geijtenbeek TBH, Gringhuis SI. Signalling through C-type lectin receptors: Shaping immune responses. *Nat Rev Immunol*. 2009;9(7):465-479. doi:10.1038/nri2569

37. Heguy A, Baldarig CT, Macchias G, Telfords JL, Mellis M. Amino Acids Conserved in Interleukin-1 Receptors (IL-1Rs) and the Drosophila Toll Protein Are Essential for IL-1R Signal Transduction*. *J Biol Chem*. 1992;267(4):2605-2609.

38. Gay NJ, Keith FJ. Drosophila Toll and IL-1 receptor. *Nature*. 1991;351(6325):355-356.

39. Lemaitre B. The road to Toll. *Nature*. 2004;4:521. www.nature.com/reviews/immunol. Accessed February 23, 2020.

40. Medzhitov R, Preston-Hurlburt P, Janeway CA. A human homologue of the Drosophila Toll protein signals activation of adaptive immunity. *Nature*. 1997;388:394-397.

41. Lemaitre B, Nicolas E, Michaut L, Reichhart JM, Hoffmann JA. The dorsoventral regulatory gene cassette spatzle/Toll/Cactus controls the potent antifungal response in Drosophila adults. *Cell*. 1996;86(6):973-983. doi:10.1016/S0092-8674(00)80172-5

42. Poltorak A, He X, Smirnova I, et al. Defective LPS signaling in C3H/HeJ and C57BL/10ScCr mice: Mutations in Tlr4 gene. *Science (80-)*. 1998;282(5396):2085-2088. doi:10.1126/science.282.5396.2085

43. Alexopoulou L, Holt A, Medzhitov R, Flavell R. Recognition of double-stranded RNA and activation of NF-kB by Toll-like receptor 3. *Nature*. 2001;413:732-738.

44. Kumar H, Kawai T, Akira S. Pathogen recognition in the innate immune response. *Biochem J*. 2009;420(1):1-16. doi:10.1042/bj20090272

45. Botos I, David M. S, Davies DR. Structural biology of TLRs. *Structure*. 2011;19(4):447-459. doi:10.1016/j.str.2011.02.004.The

46. Kawasaki T, Kawai T. Toll-like receptor signaling pathways. *Front Immunol*. 2014;5(September):1-8. doi:10.1126/science.1085536

47. Miggin SM, O'Neill L. New insights into the regulation of TLR signaling. *J Leukoc Biol*. 2006;80(2):220-226. doi:10.1189/jlb.1105672

48. Leifer CA, Medvedev AE. Molecular mechanisms of regulation of Toll-like receptor signaling. *J Leukoc Biol*. 2016;100(5):927-941. doi:10.1189/jlb.2mr0316-117rr

49. Bell JK, Mullen GEDD, Leifer CA, Mazzoni A, Davies DR, Segal DM. Leucine-rich repeats and pathogen recognition in Toll-like receptors. *Trends Immunol*. 2003;24(10):528-533. doi:10.1016/S1471-4906(03)00242-4

50. Matsushima N, Tanaka T, Enkhbayar P, et al. Comparative sequence analysis of leucine-rich repeats (LRRs) within vertebrate toll-like receptors. *BMC Genomics*. 2007;8:1-20. doi:10.1186/1471-2164-8-124

51. Shibata T, Ohto U, Nomura S, et al. Guanosine and its modified derivatives are endogenous ligands for TLR7. *Int Immunol*. 2016;28(5):211-222. doi:10.1093/intimm/dxv062

52. Song W, Wang J, Han Z, et al. Structural basis for specific recognition of single-stranded RNA by Toll-like receptor 13. *Nat Struct Mol Biol*. 2015;22(10):782-787. doi:10.1038/nsmb.3080

53. Liu L, Botos I, Wang Y, et al. Structural basis of toll-like receptor 3 signaling with double-stranded RNA. *Science (80-)*. 2008;320(5874):379-381. doi:10.1126/science.1155406

54. Kang JY, Nan X, Jin MS, et al. Recognition of Lipopeptide Patterns by Toll-like Receptor 2-Toll-like Receptor 6 Heterodimer. *Immunity*. 2009;31(6):873-884. doi:10.1016/j.immuni.2009.09.018

55. Jin MS, Kim SE, Heo JY, et al. Crystal Structure of the TLR1-TLR2 Heterodimer Induced by Binding of a Tri-Acylated Lipopeptide. *Cell*. 2007;130(6):1071-1082. doi:10.1016/j.cell.2007.09.008

56. Botos I, Segal DM, Davies DR. The Structural biology of Toll-Like Receptors. *Structure*. 2011;19(4):447-459. doi:10.1016/j.str.2011.02.004.The

57. Takeda K, Kaisho T, Akira S. Toll-Like Receptors. *Annu Rev Immunol*. 2003;21(1):335-376. doi:10.1146/annurev.immunol.21.120601.141126

58. Diebold SS, Massacrier C, Akira S, Paturel C, Morel Y, Reis e Sousa C. Nucleic acid agonists for Toll-like receptor 7 are defined by the presence of uridine ribonucleotides. *Eur J Immunol*. 2006;36(12):3256-3267. doi:10.1002/eji.200636617

59. Barton GM, Kagan JC, Medzhitov R. Intracellular localization of Toll-like receptor 9 prevents recognition of self DNA but facilitates access to viral DNA. *Nat Immunol*. 2006;7(1):49-56. doi:10.1038/ni1280

60. Sarvestani ST, Tate MD, Moffat JM, et al. Inosine-Mediated Modulation of RNA Sensing by Toll-Like Receptor 7 (TLR7) and TLR8. *J Virol*. 2014;88(2):799-810. doi:10.1128/JVI.01571-13

61. Lund J, Sato A, Akira S, Medzhitov R, Iwasaki A. Toll-like receptor 9-mediated recognition of Herpes simplex virus-2 by plasmacytoid dendritic cells. *J Exp Med*. 2003;198(3):513-520. doi:10.1084/jem.20030162

62. Heil F, Hemmi H, Hochrein H, et al. Species-Specific Recognition of Single-Stranded RNA via Toll-like Receptor 7 and 8. *Science (80-)*. 2004;303(5663):1526-1529. doi:10.1126/science.1093620

63. Diebold SS, Kaisho T, Hemmi H, Akira S, Reis E Sousa C. Innate Antiviral Responses by Means of TLR7-Mediated Recognition of Single-Stranded RNA. *Science (80-)*. 2004;303(5663):1529-1531. doi:10.1126/science.1093616

64. Diebold SS, Massacrier C, Akira S, Paturel C, Morel Y, Sousa CR e. Nucleic acid agonists for Toll-like receptor 7 are defined by the presence of uridine ribonucleotides suppl. 2006. doi:10.1002/eji.201090071

65. Sioud M. Induction of inflammatory cytokines and interferon responses by double-stranded and single-stranded siRNAs is sequence-dependent and requires endosomal localization. *J Mol Biol*. 2005;348(5):1079-1090. doi:10.1016/j.jmb.2005.03.013

66. Yang J, Han H, Zhao Y, Qin H. Specific miRNA and its target in neutrophils after traumatic injury. *Acta Biochim Biophys Sin (Shanghai)*. 2015;47(9):749-754. doi:10.1093/abbs/gmv072

67. Uhlich RM, Konie JA, Davis JW, et al. Novel microRNA correlations in the severely injured. *Surgery*. 2014;156(4):834-841. doi:10.1016/j.surg.2014.06.017

68. Bedreag OH, Rogobete AF, Dumache R, et al. Use of circulating microRNAs as biomarkers in critically ill polytrauma patients. *Biomarkers Genomic Med*. 2015;7(4):131-138. doi:10.1016/j.bgm.2015.11.002

69. Yeri A, Courtright A, Reiman R, et al. Total extracellular small RNA profiles from plasma, saliva, and urine of healthy subjects. *Sci Rep*. 2017;7(October 2016):1-13. doi:10.1038/srep44061

70. Glinge C, Clauss S, Boddum K, et al. Stability of circulating blood-based microRNAs-Pre-Analytic methodological considerations. *PLoS One*. 2017;12(2). doi:10.1371/journal.pone.0167969

71. Pritchard CC, Cheng HH, Tewari M. MicroRNA profiling: Approaches and considerations. *Nat Rev Genet*. 2012;13(5):358-369. doi:10.1038/nrg3198

72. Mall C, Rocke DM, Durbin-Johnson B, Weiss RH. Stability of miRNA in human urine supports its biomarker potential. *Biomark Med*. 2013;7(4):623-631. doi:10.2217/bmm.13.44

73. Mitchell PS, Parkin RK, Kroh EM, et al. Circulating microRNAs as stable blood-based markers for cancer detection. *Proc Natl Acad Sci U S A*. 2008;105(30):10513-10518. doi:10.1073/pnas.0804549105

74. Caserta S, Kern F, Cohen J, Drage S, Newbury SF, Llewelyn MJ. Circulating Plasma microRNAs can differentiate Human Sepsis and Systemic Inflammatory Response Syndrome (SIRS). *Sci Rep*. 2016;6(December 2015):1-13. doi:10.1038/srep28006

75. Zhou SS, Jin JP, Wang JQ, et al. MiRNAS in cardiovascular diseases: Potential biomarkers, therapeutic targets and challenges review-article. *Acta Pharmacol Sin*. 2018;39(7):1073-1084. doi:10.1038/aps.2018.30

76. Xu J, Feng Y, Jeyaram A, Jay SM, Zou L, Chao W. Circulating Plasma Extracellular Vesicles from Septic Mice Induce Inflammation via MicroRNA- and TLR7-Dependent Mechanisms. *J Immunol*. 2018;201(11):ji1801008. doi:10.4049/jimmunol.1801008

77. Zou L, Feng Y, Xu G, Jian W, Chao W. Splenic RNA and MicroRNA Mimics Promote Complement Factor B Production and Alternative Pathway Activation via Innate Immune Signaling. *J Immunol*. 2016;196(6):2788-2798. doi:10.4049/jimmunol.1502106

78. Chen C, Feng Y, Zou L, et al. Role of extracellular RNA and TLR3-Trif signaling in myocardial ischemia-reperfusion injury. *J Am Heart Assoc*. 2014;3(1). doi:10.1161/JAHA.113.000683

79. Feng Y, Zou L, Yan D, et al. Extracellular MicroRNAs Induce Potent Innate Immune Responses via TLR7/MyD88-Dependent Mechanisms. *J Immunol*. 2017;199:2106-2117. doi:10.4049/jimmunol.1700730

80. Whiting D, Dinardo JA. TEG and ROTEM: Technology and clinical applications. *Am J Hematol*. 2014;89(2):228-232. doi:10.1002/ajh.23599

81. Schipor S, Vladoiu S, Baciu AE, et al. A comparative analysis of three methods used for RNA quantitation. *Rom Reports Phys*. 2016;68(3):1078-1088.

82. Hartmann RK, Bindereif A, Westhof A, Eric S. Appendix: UV Spectroscopy for the Quantitation of RNA. In: Hartmann RK, Bindereif A, Westhof A, Eric S, eds. *Handbook of RNA Biochemistry*. ; 2005:910-913. doi:10.1002/9783527647064.app1

83. Duarte DB, Vasko MR, Fehrenbacher JC. Models of Inflammation: Carrageenan Air Pouch. *Curr Protoc Pharmacol*. 2012;March:Chapter 5: Unit 5.6. doi:10.1002/0471141755.ph0506s56.Models

84. Yoshino S, Bacon PA, Blake DR, Scott DL, Wainwright AC, Walton KW. A model of persistent antigen-induced chronic inflammation in the rat air pouch. *Br J Exp Pathol*. 1984;65(2):201-214.

85. Sedgwick AD, Moore AR, Al-Duaij AY, Edwards JC, Willoughby DA. The immune response to pertussis in the 6-day air pouch: a model of chronic synovitis. *Br J Exp Pathol*. 1985;66(4):455-464. http://www.ncbi.nlm.nih.gov/pubmed/4027178.

86. Turégano-Fuentes F, Pérez-Diaz D, Sanz-Sánchez M, Alfici R, Ashkenazi I. Abdominal blast injuries: Different patterns, severity, management, and prognosis according to the main mechanism of injury. *Eur J Trauma Emerg Surg*. 2014;40(4):451-460. doi:10.1007/s00068-014-0397-4

87. Gonzalez LM, Moeser AJ, Blikslager AT. Animal models of ischemia-reperfusion-induced intestinal injury: progress and promise for translational research. *Am J Physiol - Gastrointest Liver Physiol*. 2015;308(2):G63-G75. doi:10.1152/ajpgi.00112.2013

88. Chiu C-J, McArdle A, Rea B, Scott H, Gurd F. Intestinal Mucosal Lesion in Low-Flow States. *Arch Surg*. 1970;101(4):478. doi:10.1001/archsurg.1970.01340280030009

89. Del Corso F, Coniglio C, Giugni A, et al. Multiple organ failure in trauma patients. *Trauma Surg Vol 1 Trauma Manag Trauma Crit Care, Orthop Trauma Neuro-Trauma*. 2014;(October):191-204. doi:10.1007/978-88-470-5403-5_14

90. Vanholder R, Sever M, Erek E, Lamiere N. Rhabdomyolysis. *J Am Soc Nephrol*. 2000;8(11):1553-1561. http://jasn.asnjournals.org/content/11/8/1553.full.

91. Jagodzinski NA, Weerasinghe C, Porter K. Crush injuries and crush syndrome - a review. Part 1: the systemic injury. *Trauma*. 2010;12(2):69-88. doi:10.1177/1460408610372440

92. Petejova N, Martinek A. Acute kidney injury due to rhabdomyolysis and renal replacement therapy: A critical review. *Crit Care*. 2014;18(3):1-8. doi:10.1186/cc13897

93. Giannini EG, Testa R, Savarino V. Liver Enzyme Alterations. *CMAJ*. 2005;172(3):367-379. doi:10.1503/cmaj.1040752

94. Yang X, Schnackenberg LK, Shi Q, Salminen WF. Chapter 13: Hepatic toxicity biomarkers. In: Gupta R, ed. *Biomarkers in Toxicology*. Academic Press; 2014:241-259. doi:10.1016/B978-0-12-404630-6.00013-0

95. LeSage G, Glaser S, Alpini G. Regulators of cholangiocyte proliferation. *Liver*. 2001;21(2):73-80. doi:10.3727/105221616X692568

96. Yoshioka K, Mori A, Taniguchi K, Mutoh K. Cell proliferation activity of proliferating bile duct after bile duct ligation in rats. *Vet Pathol*. 2005;42(3):382-385. doi:10.1354/vp.42-3-382

97. Morton J, Snider TA. Guidelines for collection and processing of lungs from aged mice for histological studies. *Pathobiol Aging Age-related Dis*. 2017;7(1):1313676. doi:10.1080/20010001.2017.1313676

98. Matute-Bello G, Downey G, Moore BB, et al. An official american thoracic society workshop report: Features and measurements of experimental acute lung injury in animals. *Am J Respir Cell Mol Biol*. 2011;44(5):725-738. doi:10.1165/rcmb.2009-0210ST

99. Feng Y, Zou L, Chen C, Li D, Chao W. Role of Cardiac- and Myeloid-MyD88 Signaling in Endotoxin Shock. *Anesthesiology*. 2014;121(6):1258-1269. doi:10.1097/ALN.0000000000000398

100. Vasilescu C, Dragomir M, Tanase M, et al. Circulating miRNAs in sepsis - A network under attack: An in-silico prediction of the potential existence of miRNA sponges in sepsis. *PLoS One*. 2017;12(8):1-21. doi:10.1371/journal.pone.0183334

101. Benz F, Roy S, Trautwein C, Roderburg C, Luedde T. Circulating MicroRNAs as biomarkers for sepsis. *Int J Mol Sci*. 2016;17(1). doi:10.3390/ijms17010078

102. Lorenzen JM, Kielstein JT, Hafer C, et al. Circulating miR-210 predicts survival in critically ill patients with acute kidney injury. *Clin J Am Soc Nephrol*. 2011;6(7):1540-1546. doi:10.2215/CJN.00430111

103. Wang HJ, Zhang PJ, Chen WJ, Feng D, Jia YH, Xie LX. Four serum microRNAs identified as diagnostic biomarkers of sepsis. *J Trauma Acute Care Surg*. 2012;73(4):850-854. doi:10.1097/TA.0b013e31825a7560

104. Benjamini Y, Hochberg Y. Controlling the False Discovery Rate: A Practical and Powerful Approach to Multiple Testing. *J R Stat Soc Ser B*. 1995;57(1):289-300. doi:10.2307/2346101

105. NCBI, NLM, NIH. BLAST Results: mmu-let-7b-5p vs. mmu-let-7j. https://blast.ncbi.nlm.nih.gov/Blast.cgi. Published 2019. Accessed May 1, 2019.

106. Feng Y, Chen H, Cai J, et al. Cardiac RNA induces inflammatory responses in cardiomyocytes and immune cells via Toll-like receptor 7 signaling. *J Biol Chem*. 2015;290(44):26688-26698. doi:10.1074/jbc.M115.661835

107. Zhang Z, Ohto U, Shibata T, et al. Structural Analysis Reveals that Toll-like Receptor 7 Is a Dual Receptor for Guanosine and Single-Stranded RNA. *Immunity*. 2016;45(4):737-748. doi:10.1016/j.immuni.2016.09.011

108. Gantier MP, Tong S, Behlke MA, et al. TLR7 Is Involved in Sequence-Specific Sensing of Single-Stranded RNAs in Human Macrophages. *J Immunol*. 2008;180(4):2117-2124. doi:10.4049/jimmunol.180.4.2117

109. Zou L, Feng Y, Li Y, et al. Complement Factor B Is the Downstream Effector of TLRs and Plays an Important Role in a Mouse Model of Severe Sepsis. *J Immunol*. 2013;191(11):5625-5635. doi:10.4049/jimmunol.1301903

110. Colak E, Leslie A, Zausmer K, et al. RNA and Imidazoquinolines Are Sensed by Distinct TLR7/8 Ectodomain Sites Resulting in Functionally Disparate Signaling Events. *J Immunol*. 2014;192(12):5963-5973. doi:10.4049/jimmunol.1303058

111. Zhang Z, Ohto U, Shibata T, et al. Structural Analyses of Toll-like Receptor 7 Reveal Detailed RNA Sequence Specificity and Recognition Mechanism of Agonistic Ligands. *Cell Rep*. 2018;25(12):3371-3381.e5. doi:10.1016/j.celrep.2018.11.081

112. Edwards J, Sedgwick A, Willoughby D. The formation of a structure with the features of synovial lining by subcutaneous injection of air: An in vivo tissue culture system. *J Pathol*. 1981;134(2):147-156. doi:https://doi.org/10.1002/path.1711340205

113. Essandoh K, Fan GC. Role of extracellular and intracellular microRNAs in sepsis. *Biochim Biophys Acta - Mol Basis Dis*. 2014;1842(11):2155-2162. doi:10.1016/j.bbadis.2014.07.021

114. Darrabie MD, Cheeseman J, Limkakeng AT, et al. Toll-like receptor activation as a biomarker in traumatically injured patients. *J Surg Res*. 2018;231:270-277. doi:10.1016/j.jss.2018.05.059

115. Medzhitov R. Origin and physiological roles of inflammation. *Nature*. 2008;454(7203):428-435. doi:10.1038/nature07201

116. Pfeifer R, Tarkin IS, Rocos B, Pape HC. Patterns of mortality and causes of death in polytrauma patients-Has anything changed? *Injury*. 2009;40(9):907-911. doi:10.1016/j.injury.2009.05.006

117. Pasquale MD, Cipolle MD, Monaco JA, Simon N. Early inflammatory response correlates with the severity of injury. *Crit Care Med*. 1996;24(7):1238-1242. doi:10.1097/00003246-199607000-00029

118. Kaiser S, Rimbach K, Eigenbrod T, Dalpke AH, Helm M. A modified dinucleotide motif specifies tRNA recognition by TLR7. *Rna*. 2014;20(9):1351-1355. doi:10.1261/rna.044024.113

119. Shimizu T. Structural insights into ligand recognition and regulation of nucleic acid-sensing Toll-like receptors. *Curr Opin Struct Biol*. 2017;47:52-59. doi:10.1016/j.sbi.2017.05.010

120. Lee J, Chuang T-H, Redecke V, et al. Molecular basis for the immunostimulatory activity of guanine nucleoside analogs: Activation of Toll-like receptor 7. *Proc Natl Acad Sci*. 2003;100(11):6646-6651. doi:10.1073/pnas.0631696100

121. Sioud M. Single-stranded small interfering RNA are more immunostimulatory than their double-stranded counterparts: A central role for 2'-hyroxyl uridines in immune responses. *Eur J Immunol*. 2006;36(5):1222-1230. doi:10.1002/eji.200535708

122. Sioud M, Furset G, Cekaite L. Suppression of immunostimulatory siRNA-driven innate immune activation by 2′-modified RNAs. *Biochem Biophys Res Commun*. 2007;361(1):122-126. doi:10.1016/j.bbrc.2007.06.177

123. Hamm S, Latz E, Hangel D, et al. Alternating 2'-O-ribose methylation is a universal approach for generating non-stimulatory siRNA by acting as TLR7 antagonist. *Immunobiology*. 2010;215(7):559-569. doi:10.1016/j.imbio.2009.09.003

124. Robbins M, Judge A, Liang L, McClintock K, Yaworski E, MacLachlan I. 2′-O-methyl-modified RNAs act as TLR7 antagonists. *Mol Ther*. 2007;15(9):1663-1669. doi:10.1038/sj.mt.6300240

125. Mohamed FE, Al-Jehani RM, Minogue SS, et al. Effect of toll-like receptor 7 and 9 targeted therapy to prevent the development of hepatocellular carcinoma. *Liver Int*. 2015;35(3):1063-1076. doi:10.1111/liv.12626

126. Adams JL, Smothers J, Srinivasan R, Hoos A. Big opportunities for small molecules in immuno-oncology. *Nat Rev Drug Discov*. 2015;14(9):603-621. doi:10.1038/nrd4596

127. Schmitt FCF, Freund I, Weigand MA, Helm M, Dalpke AH, Eigenbrod T. Identification of an optimized 2′-O-methylated trinucleotide RNA motif inhibiting Toll-like receptors 7 and 8. *Rna*. 2017;23(9):1344-1351. doi:10.1261/rna.061952.117

128. Forsbach A, Nemorin J-G, Montino C, et al. Identification of RNA Sequence Motifs Stimulating Sequence-Specific TLR8-Dependent Immune Responses. *J Immunol*. 2008;180(6):3729-3738. doi:10.4049/jimmunol.180.6.3729

129. Gao W, Xiong Y, Li Q, Yang H. Inhibition of toll-like receptor signaling as a promising therapy for inflammatory diseases: A journey from molecular to nano therapeutics. *Front Physiol*. 2017;8(JUL). doi:10.3389/fphys.2017.00508

130. Vandooren J, Berghmans N, Dillen C, et al. Intradermal air pouch leukocytosis as an in vivo test for nanoparticles. *Int J Nanomedicine*. 2013;8(December):4745-4755. doi:10.2147/IJN.S51628

APPENDIX A: PUBLICATIONS

Portions of this thesis have been published as follows:

ORAL PRESENTATIONS

- Suen A et al. Circulating Plasma miRNAs Trigger Innate Immune Activation in a Mouse Model of Polytraumatic Injury? Dalhousie Anesthesia Annual Research Day. Halifax, NS, Canada. April 10, 2019.
- Suen A et al. Extracellular miRNAs and Innate Immune Activation Following Polytraumatic Injury in Mice. Association of University Anesthesiologists (AUA) Annual Meeting. Chicago, IL, USA. April 26, 2018.
- Suen A et al. Innate Immune Activation and Organ Injury in a Mouse Model of Polytrauma: Role of Extracellular (Ex-) microRNAs? Presented by A Suen at the Dalhousie Anesthesia Annual Research Day. Halifax, NS, Canada. April 13, 2018.

ABSTRACTS & POSTER PRESENTATIONS

- Lopez K, Suen A et al. Impact of hypobaric exposure on inflammation and organ injury in a non-hemorrhagic mouse model of polytrauma. Shock Society Annual Meeting. Toronto, ON, Canada. June 6-9, 2020.
- Suen A et al. Circulating plasma miRNAs trigger innate immune activation in a mouse model of polytraumatic injury. Military Health Systems Research Symposium, Kissimmee, FL, USA. August 20, 2019.
- Suen A et al. Circulating plasma miRNAs trigger innate immune activation in a mouse model of polytraumatic injury. Association of University Anesthesiologists (AUA) Annual Meeting & International Anesthesia Research Society (IARS). Montreal, QC, Canada. May 16&19, 2019.
- Suen A et al. Circulating plasma miRNAs trigger innate immune activation in a mouse model of polytraumatic injury. University of Maryland Anesthesiology Spring Research Retreat. Baltimore, MD, USA. April 4, 2019.
- Suen A et al. Extracellular (ex-) micro-RNA and Innate Immune Activation Following Polytraumatic Injury in Mice. Military Health System Research Symposium. Kissimmee, FL, USA. August 22, 2018.
- Suen A et al. Extracellular (ex-) micro-RNA and Innate Immune Activation Following Polytraumatic Injury in Mice. Shock Society Annual Meeting. Scottsdale, AZ, USA. June 10, 2018.
- Suen A et al. Extracellular miRNAs and Innate Immune Activation Following Polytraumatic Injury in Mice. Association of University Anesthesiologists (AUA) Annual Meeting. Chicago, IL, USA. April 26, 2018.

APPENDIX B: APPROVALS.

1. University of Maryland School of Medicine

Office of Animal Welfare Assurance

Institutional Animal Care and Use Committee

IACUC Protocol #0916003

"Extracellular RNA: Novel Biomarker and Potential Therapeutic Target in Trauma"

Description	**Review Date**
Initial Approval	05-Jan-2017
Amendment #1 – Tibia # & Muscle Crush	27-Apr-2017
Amendment #2 – Hypobaria & Exosomes	12-Mar-2018
Amendment #3 – TLR7KO	17-Sep-2018
Amendment #4 – Air Pouch	07-Feb-2019
Amendment #5 – Neuro-Behavioural study	

2. Department of the Air Force

AFMSA/SGE-C

Office of Research Oversight and Compliance

Animal Research Protocol, AFOSR-2017-009A

"Extracellular RNA: Novel Biomarker and Potential Therapeutic Target in Trauma"

Description	**Review Date**
Initial Approval	25-Apr-2017
Amendment #1	19-Jun-2017
Amendment #2	
Amendment #3	21-Sep-2018
Amendment #4	08-Feb-2019

3. University of Maryland, Baltimore

Human Research Protections Office (HRPO)

Institutional Review Board (IRB)

Institutional Biosafety Committee (IBC)

General Clinical Research Center (GCRC)

"Extracellular RNA: Novel Biomarker and Potential Therapeutic Target in Trauma"

Description (Protocol number)	**Review Date**
Initial Approval – IBC-00004691	13-Jul-2018
Initial Approval – GCRC-0079925	18-Jul-2018
Initial Approval – HRPO-00079925	11-Jan-2019